SOLID ACID AND SUPPORTED METAL CATALYST FOR BIOMASS CONVERSION INTO VALUE ADDED CHEMICALS

A THESIS

SUBMITTED TO THE

UNIVERSITY OF PUNE

FOR THE DEGREE OF

DOCTOR OF PHILOSOPHY

IN

CHEMISTRY

BY

Ramakanta Sahu

UNDER THE GUIDANCE OF

Dr. D. Srinivas

CATALYSIS & INORGANIC CHEMISTRY DIVISION
NATIONAL CHEMICAL LABORATORY
PUNE-411 008
INDIA

JANUARY 2011

CERTIFICATE

Certified that the work incorporated in the thesis entitled:" **Solid Acid and Supported Metal Catalyst for Biomass Conversion into Value Added Chemicals**", submitted by **Mr. Ramakanta Sahu**, for the degree of ***Doctor of Philosophy in Chemistry***, was carried out by the candidate under my supervision at Catalysis & Inorganic Chemistry Division, National Chemical Laboratory, Pune-411 008, India. Such materials as has been obtained from other sources have been duly acknowledged in the thesis.

Date: **Dr. D. Srinivas**

Place: Pune Research Guide

DECLARATION BY RESEARCH SCHOLAR

I hereby declare that the thesis entitled "**Solid Acid and Supported Metal Catalyst for Biomass Conversion into Value Added Chemicals**", submitted for the degree of ***Doctor of Philosophy in Chemistry*** to the University of Pune, has been carried out by me at Catalysis & Inorganic Chemistry Division, National Chemical Laboratory, Pune-411 008, India, under the supervision of **Dr. D. Srinivas**. The work is original and has not been submitted in part or full by me for any other degree or diploma to this or any other University.

Date: **Ramakanta Sahu**

Place: Pune Research Scholar

I dedicate this work, with deep respect and great love, to my parents. You not only gave me the gift of life but an unrelenting passion to live it fully. For that I am so very grateful.

ACKNOWLEDGEMENTS

I find it difficult to write something in short to acknowledge my research supervisor, Dr. D. Srinivas. His constant inspiration, invaluable guidance and constructive criticism helped me a lot to focus my views in the proper perspective. I take this opportunity to express my intense reverence towards him for the extensive scientific discussions and giving me the liberty to carry out my research work independently. Although, this eulogy is insufficient, I preserve an everlasting gratitude for him.

I am deeply indebted to Dr. Paresh L. Dhepe who was my mentor in understanding the essence of biomass conversion. His tireless attitute has been an impetus for me throughouot the course of study. My deepest personal regards are due for him forever for his timely help and strong support, both scientific and personal, at all stages of my research. I am thankful to Dr. A. P. Singh and Dr. Nandini Devi for the stimulating discussions, valuable suggestions and constant encouragement and support. I convey my sincere gratitude to Dr. N. M. Gupta, Dr. C. V. V. Satyanarayana and Dr. A. K. Kinage for helping me in every possible way. I duly acknowlege the constant help provided by Dr. T. Raja and Dr. Shubhangi Umbarkar for TPD and FTIR study.

I wish to convey my sincere gratitude to Dr. Rajiv kumar, former Head, Catalysis Dvision for not only providing the divisional facilities for use but also for helpful stimulating discussion and personal help whenever required.

My heartful thanks are due to Dr. M. K. Dongare, Dr. (Mrs.) A. A. Belhekar*, Dr. S. B. Halligudi, Dr. B. Biswonathan, Dr. A. V. Ramaswamy, Dr. S. P. Mirajkar, Dr. (Mrs) S. Deshpande, Dr. (Mrs) K. kalaraj, Dr. Selvaraj, Dr. Bokade, Ms. Samuel Violet, Dr. R. Patil, Dr. S. Ganpathy, Mr. R. K. Jha, Mr. Gholap, Mr. Gaikwad, Mr. Jagtap, Mr. Akhbar, Mr. Purushottaman, Mr. Madhu and all other scientific and non-scientific staff of the division and NCL for their valuable help and cooperation.*

It gives me great pleasure to thank my labmates, Dr. P. Kalita, Dr. S. Senapati, Dr. A. Deshmukh, Puja, Binu, Pravin, Aparna, Tushar, Deepa, Manoj, Pranalee, Nilofer, Lasitha, Anuja, Aysha, Hifsudin, Gauri, Christy, Anup, Prasenjit, Rajanikant, Jitesh, Rakesh, Anupam, Jijil, Sumona, Sheetal, Leena, Rajesh, Shoy, Dr. S. Selvakumar and Jutika for listening my woes and making me feel comfortable all the time when I was depressed with the outcomes and lively atmosphere in the lab. Without their support it would not have been possible to complete this task. I would like to express my gratefulness to colleagues in the division- Dr. Surendran, Dr. Shrikant, Prinson, Bala, Rajesh, Priti, Shital, Mehe Jabeen, Trupti, Ankush, Sanyo, Neelam, Aany, Hari, Anu, Dr. Shanbhag, Dr. Suman, Dr. Ankur, Dr. Surekha, Dr. Devu, Ganesh, Nishita, Santosh,

Dr. L. Saikia, Sangita, Tejas, Jetendra Kumar Satyarthi, Anuj Kumar, Bhogesh, Joby, Nagaraj, Maitri, Tushara and Niphadkar.

I would like to convey my appreciation to my collegues from NCL (oriya) Dr. Gokhaneswar, Pitamber, Jeetendra, Chakadola, Raju, Mandakini, Dr. Rosy, Puspanjali, Manaswin, Dr. Shitaram, Dr. (Mrs) Sabita and all other research scholars for such a friendly and cheerful working atmosphere, for their constant support, love and care throughout my stay at NCL.

I should not forget my beloved friends- Dr. Mahesh, Dr. Debasish, Tamas and Pradeep. Special thanks to Atul Kumar for kind support and calm listening to me. It has been great pleasure to share a cup of tea and spend time with Atul and my labmates.

I take this opportunity to express my profound respect to my teachers throughout my carrier, who are the key inspiration and help to build up my research career in science.

It gives me immense pleasure to thank my parents and family members for their love, unfailing support, tremendous patience, trust and encouragement during many years of studies that they have shown in their own special way. They have been a constant source of strength and determination, and have brought a great deal of happiness to my life.

I would like to confess that even though I tried my best, it is not possible for me to acknowledge and thank all the known and unknown faces individually for their direct and indirect help for the completion of this work. I am grateful to all of them for their kind cooperation throughout the course of my study.

Words are not enough to express my love and gratitude to my family members. It is their love, blessings and prayers that helped me throughout my life. I am very much indebted to them. Above all, I thank God for his blessings, for forgiving my mistakes, for leading me in the right path and for being there whenever I needed.

Finally, I thank the Council of Scientific and Industrial Research, Government of India, for awarding research fellowship and Dr. S. Sivaram, Ex-director, Dr. S. Pal Director and Dr. B. D. Kulkarni, Deputy Director, National Chemical Laboratory for allowing me to carry out my research work, extending all infrastructural facilities and to submit this work in the form of a thesis for the award of Ph. D. degree.

January, 2011 *Ramakanta Sahu*

3. CATALYTIC CONVERSION OF HEMICELLULOSE INTO CHEMICALS

List of Figures

List of Schemes

List of Tables

List of Abbreviations

AC	Activated Carbon
Al- MCM-41	Al- Mobil Composite Material-41
Al- SBA-15	Al- Santa Barbara Amorphous-15
BET	Brauner, Emmett And Teller
BHF	2,5-Bis(Hydroxymethyl)-Furan
Cs-HPA	Cesium-exchange Heteropoly Acid
CTMABr	Cetyl Trimethylammonium Bromide
DMSO-d_6	Deuterated Dimethyl Sulfoxide
DEPT	Distortionless Enhancement by Polarization Transfer
DFF	2,5-Diformylfuran
DMF	2,5-Dimethylfuran
DOE	Department Of Energy
FAU	Faujasite
FDCA	2,5-Furandicarboxylic Acid
FFCA	5-Formyl Furan Carboxylic Acid
GC	Gas Chromatography
Gtons	Giga Tons
Hβ	Beta Zeolite (H form)
HCW	Hot Compressed Water
HK	Horvath-Kawazoe
HMF	5-Hydroxymethyl Furfural
HMFC	5-Hydroxymethyl Furfural Carboxylic Acid
HMOR	Mordenite Zeolite (H form)
HPLC	High Performance Liquid Chromatography
HUSY	Ultra Stable Y Zeolite (H form)
ICP-OES	Inductively Coupled Plasma-Optical Emission Spectroscopy
LC-MS	Liquid Chromatography-Mass Spectroscopy
MAS NMR	Magic-Angle Spinning Nuclear Magnetic Resonance Spectroscopy
MIBK	Methyl Isobutyl Ketone
MMT	Million Metric Tonne
TPD-NH_3	Temperature-Programmed Desorption of Ammonia
NREL	National Renewable Energy Laboratory

PerBU	Periodic Building Unit
PNNL	Pacific Northwest National Laboratory
RID	Refractive Index Detector
SEM	Scanning Electron Microscopy
TCD	Thermal Conductivity Detector
TEM	Transmission Electron Microscopy
TEOS	Tetraethylorthosilicate
TOF	Turn over Frequency
TLC	Thin Layer Chromatography
TMAOH	Trimethylammonium Hydroxide
US	United States
XPS	X-Ray Photoelectron Spectroscopy
XRD	X-Ray Powder Diffraction
HZSM-5	Zeolite Synthesize Material-5 (H form)

CHAPTER-1
GENERAL INTRODUCTION

1.1. Introduction

In the vision 2020 catalysis report prepared by the US chemical industry, one of the recommendations was to use renewable feedstocks - especially cellulose and carbohydrates, as sources for the production of valuable chemicals by sustainable means. It was stated in the report that the use of renewable raw materials should be increased by 13% until 2020 [1]. The European Union has established a platform for sustainable chemistry demanding that 30% of the chemicals should be produced from renewable resources by 2025. Heterogeneous catalysis plays an important role in the synthesis of chemicals in a sustainable way. Currently, 90% of the chemical processes, in particular for the production of fine and bulk chemicals, use catalysts. Replacement of homogeneous catalysts and stoichiometric reagents by solid catalysts make the chemical manufacturing processes environmentally benign [2]. Moreover, the benefits in using solid catalysts are associated with their easy separation and reuse. The use of biomass instead of petroleum products diminishes the negative impact on the environment caused by fossil fuels. Moreover, use of biomass could lead to new type of chemistry in chemicals synthesis and products with a tag of green and biodegradability [3-5]. In view of all these above points, the present work is designed in exploring efficient solid catalysts for the conversion of biomass into chemicals.

The major drives for biomass utilization are: (1) depletion of fossil fuels (at the present rate of consumption, the fossil fuel resources can be available only up to 25 years) [6-8] and (2) more and more concerns about environmental pollution and global warming [9]. In power sector there are various options for alternative sources like wind, solar, nuclear, hydroelectric, tidal, geothermal and biomass. However, such choices are limited for the chemicals sector. Biomass is the only renewable resource for the production of chemicals [10]. At present, only a small fraction of biomass is used in chemicals synthesis, in industry. Greater efforts are needed to intensify this program and to preserve the environment from polluting. Catalysis and, in particular, heterogeneous catalysis, is expected to play a major role in this endeavor [11]. The first generation technology for the production of fuels and chemicals (from sugars and vegetable oils) is competing with food for their feedstocks. Hence, it doesn’t provide a long term solution. The second generation of technology of their production utilizes the abundant, less expensive, lignocellulosic biomass feedstock and therefore, is more attractive [13].

1.2. Biomass

The material, which is derived from the living matter, is called Biomass**.** It is defined as the organic component of crops, crop waste, wood, grass, fast growing plants, short rotation crops, animal wastes, garbage, alcohol fuels, landfill gas, food processing by-products, municipality solid wastes, aquatic plant or algae and ocean biomass [14]. Biomass is broadly classified into two categories as plant- and animal-derived biomass. Their sub-classifications are given below.

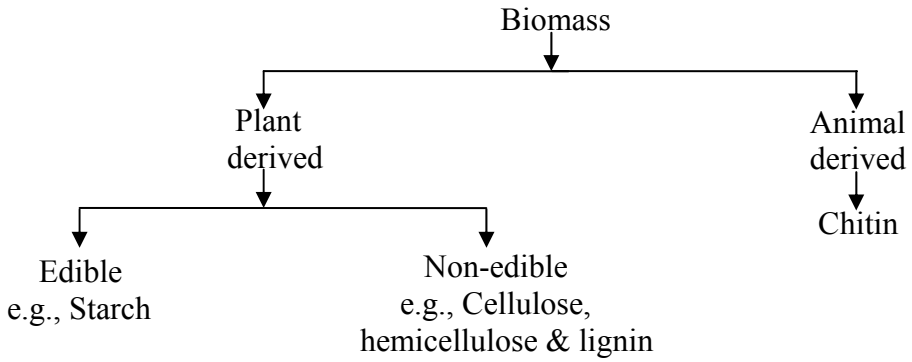

Woody biomass consists of cellulose (40-50%), hemicellulose (20-30%), lignin (20-28%) and some percentage of other substances (amino acids, minerals - K, Na, Ca, Mg, etc.) and organic extractives (fats, waxes, alkaloids, proteins, phenolics, pectins, mucilages, gums, resins, terpenes, starches, simple sugars, etc.) [15-18].

1.2.1. Plant-derived Biomass and its Structure

Plants synthesize the lignocellulosic material by the photosynthetic process. Typically, in the presence of chlorophyll, plants generate biomass by utilizing carbon dioxide, water and sunlight producing oxygen as the by-product. The primary products are C_6 and C_5 sugars. They are further polymerized to form carbohydrates (starch, cellulose and hemicellulose), lignin (aromatic alcohol), pectin and proteins [19]. These materials give mechanical strength to the plant, store energy, and protect the plant against microbial and insects attack. Biomass is the most abundant renewable feedstock for the synthesis of chemicals. Annually, nature produces 170 billion metric tons of biomass by the photosynthesis process, out of which 75% is carbohydrates. Only 3-4% is used for food, shelter, cloth, pulp and paper. The rest is unutilized [20].

1.2.1.1. Edible Biomass

The biomass which is used as food by human being is called edible biomass. The edible biomass is mainly carbohydrates such as monosaccharides (glucose, fructose, xylose, etc.), disaccharides (sucrose, lactose, etc.) and polysaccharides (starch).

Monosaccharides. The common monosaccharides are C_5 (xylose, arabinose, etc.) and C_6 (glucose, fructose, etc.) sugars. Glucose or dextrose is an aldohexose (C_6 sugar), which is the monomer unit of starch, cellulose, sucrose, and lactose. Industrially, glucose is synthesized from starch by an enzymatic and mineral acid hydrolysis process. Depending on the position of the –OH group present at the anomeric center (C_1), glucose is of two types: α-D-glucose if, –OH at C_1 center is axial and β-D-glucose if, -OH at C_1 center is equatorial in position (Fig. 1.1 A and B). The β anomer is more stable than the α anomer. Fructose is a ketohexose (Fig. 1.1 C) naturally found in honey, sucrose, and fruit juice. Xylose is a pentose sugar found in embryo and major monomer unit of hemicellulose (Fig.1.1 D).

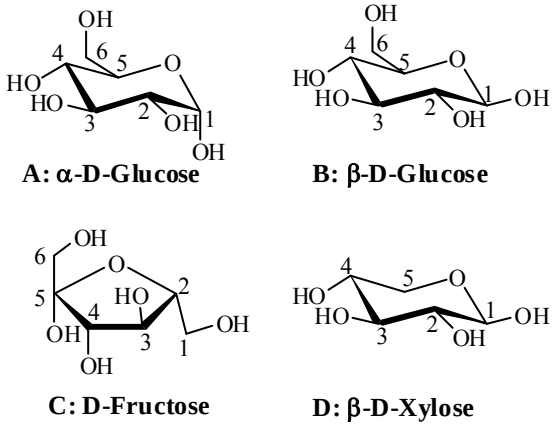

Fig. 1.1. Structure of monosaccharides.

Disaccharides. The common disaccharides are the dihexoses ($C_{12}H_{22}O_{11}$). There are two types of disaccharides: (a) sucrose (two monosaccharide molecules linked through their reducing group) (Fig. 1.2 A) and (b) lactose (Fig. 1.2 B) and maltose (Fig.1.2 C) (C_1 of one molecule is linked to C_4 of the other). They are found in natural compounds.

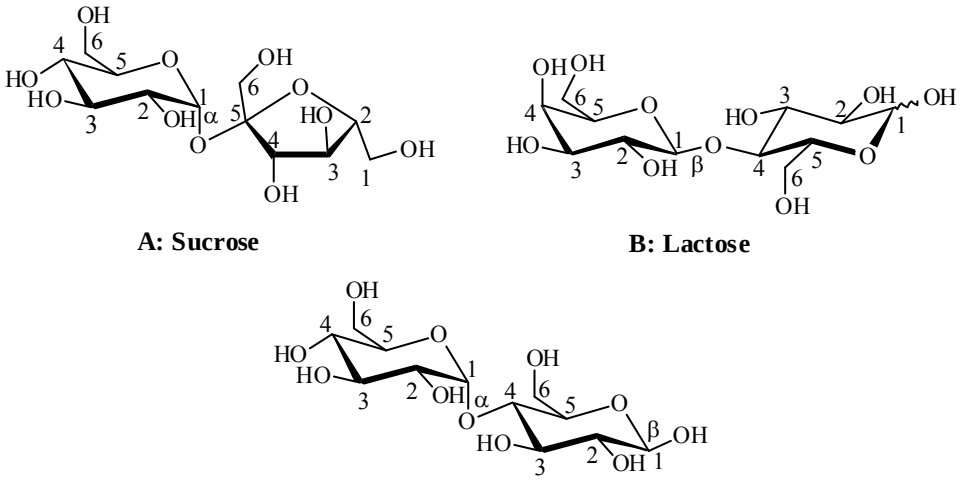

Fig. 1.2. Structure of disaccharides.

Polysaccharides. The main edible polysaccharide is starch. It is a non-structural component of the softwood and hardwood. It is also the major carbohydrate reserve in tubers, fruits and seeds.

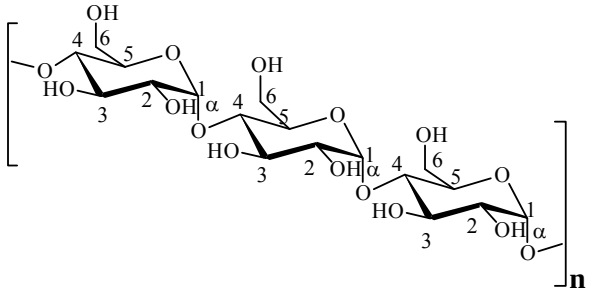

Fig. 1.3. Structure of amylose.

Starch consists of two types of molecules, amylose (Fig. 1.3, 20-30%) and amylopectin (Fig. 1.4, 70-80%). Both consist of polymers of α-D-glucose units. In amylase, glucose is linked at α-(1→4), with the ring oxygen atoms all on the same side, whereas in amylopectin about one residue is linked in the α-(1→6) manner. Therefore, amylopectin is a non-linear polymer whereas amylase is a linear polymer. Amylopectin is water insoluble and gives violet color with iodine but amylose is water soluble and gives blue color with iodine. The relative proportions of amylose to amylopectin and the α-(1→6) branch-points, both depend on the source of the starch, for example, amylomaizes contain over 50% of amylose whereas 'waxy' maize has almost none (~3%).

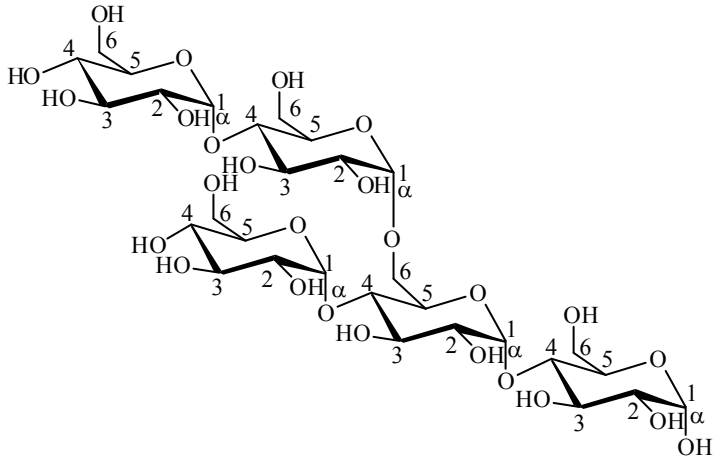

Fig. 1.4. Structure of amylopectin.

1.2.1.2. Non-edible Biomass

The biomass, which cannot be digested by human being is called non-edible biomass. They are plant derived disaccharides (cellobiose and xylobiose), polysaccharides (cellulose and hemicellulose), phenolics (lignin) and other components. Chitin is a non-edible, animal-derived polysaccharide found in nature.

Disaccharide. The common non-edible disaccarides are cellobiose (Fig. 1.5 A) and xylobiose (Fig. 1.5 B). Cellobiose is a reducing sugar which is synthesized from the condensation of two glucose molecules or by the hydrolysis of cellulose. Each glucose molecule is linked via a β-(1→4) linkage. It has free alcoholic groups which give rise to strong inter and intra-molecular hydrogen bonds. Xylose is the monomer unit of xylobiose having a β-(1→4) linkage. It is synthesized from hemicellulose or by the condensation of two xylose units. It is also a reducing sugar.

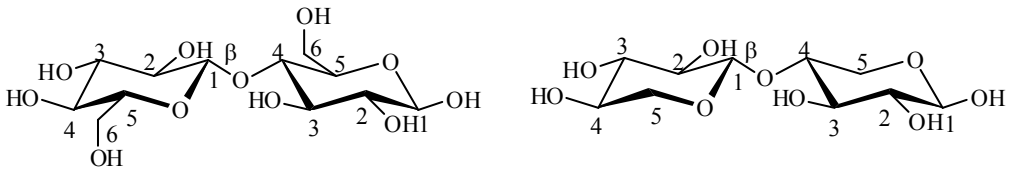

A: Cellobiose **B: Xylobiose**

Fig. 1.5. Structure of non-edible disaccharides.

Polysaccharide. The non-edible, plant-derived polysaccharides are cellulose and hemicellulose. Chitin is the animal-derived polysaccharide.

Cellulose. It is the main polysaccharide in wood having a general formula $(C_6H_{10}O_5)_n$. It is a homopolysaccharide composed of D-glucopyranose or the anhydrous form of glucopyranose units having β-(1→4) glycosidic linkage (Fig. 1.6).

Cellobiose is the repeating unit of cellulose. The molecules are completely linear and have a strong tendency to form intra- and intermolecular hydrogen bonds. This leads to bundling of cellulose molecules into micro-fibrils and definite crystalline structure. Hence, the cellulose fibers are insoluble in water or in common organic solvent. The portion which is insoluble in strong alkalis is called α-cellulose. β-Cellulose partially precipitates in neutral medium while γ-cellulose is soluble in water. Annually, 50 billion ton of cellulose is produced by nature.

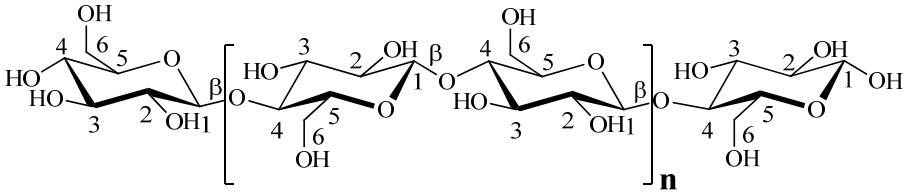

Fig. 1.6. Structure of cellulose.

Hemicellulose. This is the third most common polysaccharides in nature. These are the heterogeneous polymers of pentoses (xylose, arabinose, etc.), hexoses (mannose, glucose, galactose, etc.) and sugar acids. Unlike cellulose, hemicellulose is not chemically homogeneous. The hemicelluloses contain mainly xylans (polymer of xylose), which are heteropolysaccharides with homopolymeric backbone chains of D-xylopyranose units linked in β-(1→4) manner (Fig. 1.7). Besides xylose, xylans may contain arabinose, glucuronic acid or its 4-O-methyl ether. The frequency and composition of branches are dependent on the source of xylan.

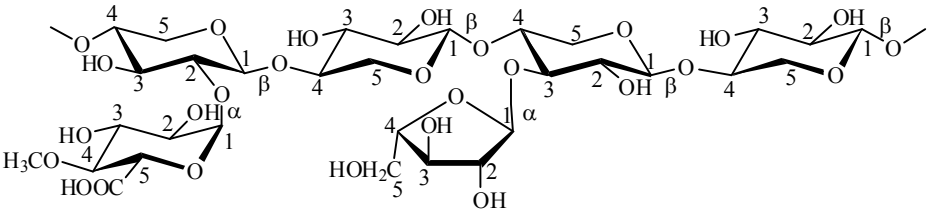

Fig. 1.7. Structure of hemicellulose.

Chitin. It is a white, hard, second most abundant, natural nitrogenous mucopolysaccharide, and the supporting material of crustacean's insects. It is highly hydrophobic and insoluble in water as well as in most of the organic solvents. It is soluble in hexafluoro-isopropanol, hexafluoroacetone, chloroalcohols in conjugation with aqueous solutions of mineral acids [21] and dimethylacetamide containing 5% lithium chloride. 10 Gtons of chitin are constantly present in the biosphere [22]. It is a major source of surface pollution in coastal area. Industrially, chitin is prepared from

the shells of crabs, shrimps, prawns, and lobsters. Isolated chitin is a highly ordered copolymer of 2-acetamido-2-deoxy-β-D-glucose connected through β-(1→4) linkages (Fig. 1.8). Depending upon sources, chitin is of two types. α-Chitin occurs in the calyces of hydrozoa, the egg shells of nematodes and rotifers, the radulae of mollusks, and the cuticles of arthropods. β-Chitin is the part of the shells of brachiopods and mollusks, the cuttlefish bone, the squid pen, and the pogonophora tubes.

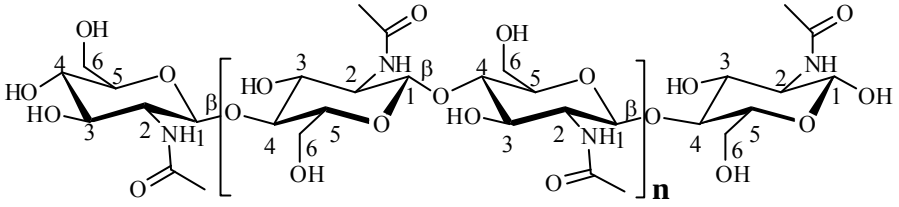

Fig. 1.8. Structure of chitin.

Lignin. The term "lignin" came from the Latin word "lignum" which means wood. It is the abundant renewable source of aromatic polymers [23]. Three general monomer phenyl propane units (sinapyl alcohol, coniferyl, and *p*-coumaryl alcohols) are present in the structure of lignin (Fig. 1.9). Typically, lignin is a three-dimensional, highly branched, polyphenolic substance that consists of an irregular array of variously bonded "phenolic hydroxyl, benzyl alcohol carbonyl and methoxy-substituted phenylpropane units [24, 25]. These subunits are bonded via ether bonds or carbon-carbon bonds. The structure of lignin is also described in terms of the frequency of functional groups which interlink between individual units and forms an amorphous structure.

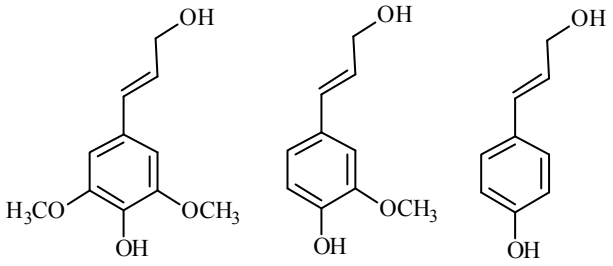

Sinapyl alcohol Coniferyl alcohol Coumaryl alcohol

Fig. 1.9. Structure of lignin monomer units.

Other Components. Biomass may contain a wide range of organic extractives, such as fats, waxes, alkaloids, proteins, phenolics, sugars, pectins, mucilages, gums, resins, terpenes, starches, glycosides, saponins, and essential oils. Extractives function as intermediates in the metabolism, energy reserve and as protective agents against

microbial and insect attack. Biomass also contains a small content of inorganic species (K, Na, Mg, B, Cl, P, Ca, S, etc.) for nutrient uptake during its growth [26].

1.3. Present Scenario and Motivation of Work

1.3.1. Production of Chemicals, Fuels and Energy from Fossil Feedstock

Currently, more than 90% of transportation fuels, energy and chemicals are derived from fossil fuel resources (petroleum, coal, and natural gas). Fig. 1.10 gives an estimate of the global fossil feedstock reserves [27]. These feedstocks are used for the synthesis of common fuels and for the production of energy, heat and hydrogen as potential energy carriers. In the production of gasoline, coal is converted into synthesis gas, which is then transformed into fuel via Fischer-Tropsch synthesis [28]. Methane is reacted with air or oxygen to get methanol and formaldehyde at 430°C with low conversion [29]. Hydrogen which is an energy carrier is produced by the steam reforming process [30, 31]. The olefins (ethylene, propylene and butadiene) and aromatics (benzene, toluene, *p*-xylene and *o*-xylene) are synthesized from the petrochemicals (gas or petroleum).

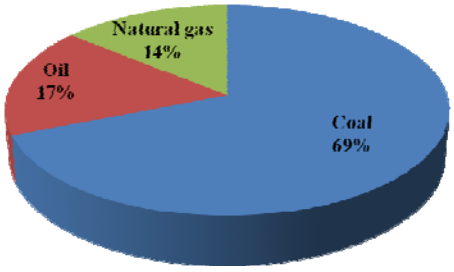

Fig. 1.10. Estimation of fossil reserves.

1.3.2. Alternative Sources for Fuels and Energy

Today's society depends on fossil feedstocks for fuel and energy. However, the use of fossil feedstock for the generation of energy and fuels is associated with several important issues. First, fossil feedstocks are finite. Their current consumption rate is increasing because of the high demand of energy and fuels which will lead to inevitable depletion within a few decades. Hence, the crude oil price is increasing day by day (petroleum oil $70-90/barrel). Second, the consumption of fossil fuels leads to CO_2 emissions in the atmosphere, which contributes to global warming and climatic issues. Third, the heterogeneous distribution of the fossil fuel reserves on the earth. Fourth, it is the origin of political, economic and security issues worldwide. These

important concerns make the society to look for renewable sources of energy which are sustainably available in the environment. It should be emphasized that these sources release significantly lower levels of environmental pollutants than the conventional sources of energy. Ideally, they emit no greenhouse gases (carbon dioxide, nitrogen oxides, etc.). New and renewable energies provide new challenges for the humankind. There are many avenues open to the development of these energy sources.

There are alternate sources for production of fuels and energy to create a clean environment. But no other alternative source (except fossil feedstocks) exits for the production of chemicals. The theme of this thesis is to synthesize chemicals from biomass, being renewable as well as sustainable source. Biomass provides the organic carbon for our industrial society [32].

1.3.3. Synthesis of Chemicals from Biomass

Because of the availability and sustainability of renewable feedstock, the biomass conversion technologies are expected to make significant impact on the production of bulk chemicals in the near future. There is a substitution potential of 10-15% of fossil oil-based bulk chemicals, especially for oxygenated bulk chemicals, such as ethylene glycol and propylene glycol, iso-propanol and acetone [33]. Glycerin, a by-product of biodiesel production, is a very favorable short-term option for the production of propylene glycols. There is clear potential for a bio-based production of ethylene, acrylic acid and N-containing bulk chemicals such as acrylonitrile, acrylamide and caprolactam [34-36]. Technologies involving the conversion of polysaccharides (cellulose, hemicellulose) or sugars for the synthesis of platform chemicals are still in their infancy [37, 38].

One example for chemical production from biomass is cellulose conversion to glucose by the hydrolysis process [39, 40]. The cellulose is hydrolyzed and then hydrogenated to form sorbitol and mannitol using supported noble metal catalysts [41-43]. Glucose and fructose can be dehydrated using solid acid catalysts to form 5-hydroxymethyl furfural (HMF) in water and organic media [44, 45]. Other innovative chemical methods are to convert fatty acids into polymer building blocks. Kansas Polymer Research Center has developed a bio-derived polyol (BiOH) process by the chemical conversion of triglycerides [35, 36]. Despite these achievements, the

transition of industrial chemical production from petrochemical to biomass feedstock still faces real hurdles.

1.4. Biorefinery Concept

Biorefinery is multidisciplinary in nature. It requires various operators with different skills and expertise (e.g. agriculturalists, chemists and biotechnologists). Biorefinery is a facility that integrates biomass conversion processes and equipment to produce fuels, energy and chemicals. It aims for a complete valorization of biomass source by performing the overall processes [46-48]. The biorefinery concept is quite similar to petroleum refineries, which produce fuels and petroleum products. The biorefinery may include thermal, chemical and biological processes and its development. For the multiple product formation, the biorefineries can take advantage of the differences in biomass components and intermediates and maximize the value derived from the biomass feedstock [10, 49]. The lignocellulosic biorefinery typically uses 'dry' lignocellulose such as wood, straw, bagasse, etc. These raw materials (consisting primarily of polysaccharides and lignin) will enter the biorefinery and through an array of processes, will be fractionated and converted into a variety of energy, chemicals and bio-derived products. However, a biorefinery requires a large throughput to be economical. Biomass is a low density feedstock that is expensive to transport. There are three types of biorefineries published in the literature:

Type I biorefineries: They use of one feedstock and one process producing a single major product. For example, biodiesel is produced from oils or fats through transesterification.

Type II biorefineries: Many chemicals, energy and bio-materials are produced using a single feedstock through many processes. One example is the chemical industry producing a multitude of carbohydrate derivatives, including native and modified starches, sweeteners, polyol and bio-ethanol from cereal grains.

Type III biorefineries: These are the most developed type of biorefinery. They are able to produce a variety of industrial products using various types of feedstocks and processing technologies. During the multiple product formation some by-products are also formed which might become a key product in the future. In this approach, there is a possibility to select the most profitable combination of raw materials and processes to produce multiple products.

Currently, there are three stages of type III biorefinery systems being pursued in research and development:

1. Separation of the biomass into its components (cellulose, hemicellulose, lignin, proteins, amino acids, pure plant oil (PPO), minerals, fine chemicals and pharmaceutical compounds) in a primary fractionation/de-polymerization unit. Typical technologies applied in this stage are traditional separation processes like filtration, solvent extraction and distillation. However, novel concepts like supercritical CO_2 extractions and catalytic de-polymerization may also be explored. Really, some of biorefinery technologies are already at a stage of commercialization, while others require further research and technological development.

2. Conversion of the intermediate fractions to valuable end products (e.g. bio-fuels) and chemical intermediates is performed in a secondary refinery process. Examples of the chemical intermediates are conventional intermediates, such as alcohols or acids, and platform chemicals like xylose, glucose or HMF compounds. The secondary conversion processes may be distinguished into thermo-chemical processes (e.g. gasification, liquefaction, etc.) and biochemical processes (e.g., fermentation).

3. Further (catalytic) processing of the chemical intermediates to high value-added end-products.

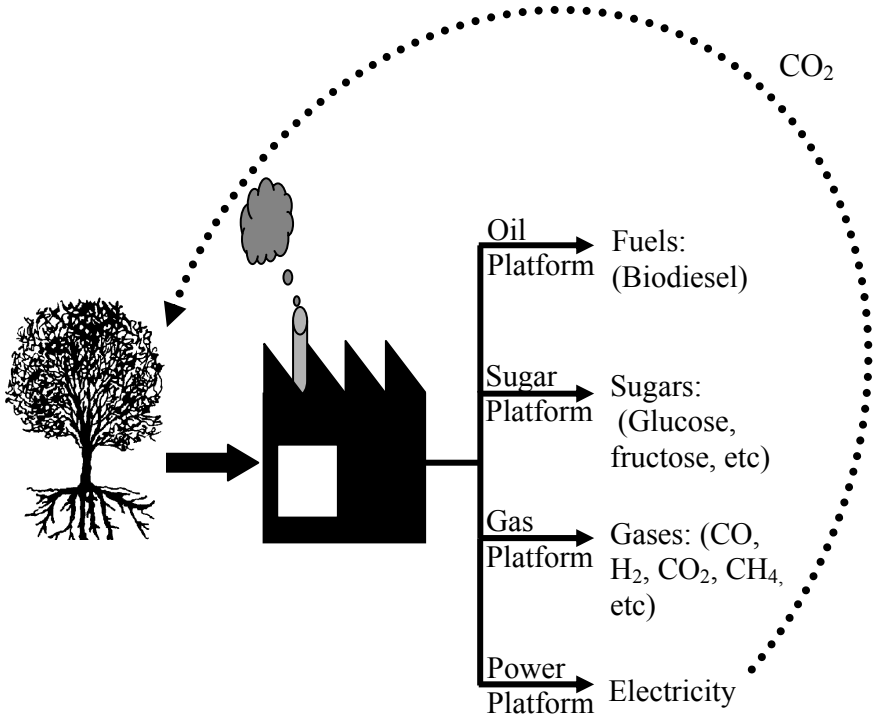

Fig. 1.11. Biomass utilization for the production of chemicals, fuels and energy.

'NREL' biorefinery concept is built on two different platforms to promote different product slates. The 'sugar platform' is based on biochemical conversion processes and focuses on the fermentation of sugars extracted from biomass feedstocks by hydrolysis and chemo-catalytic routes. The 'syngas platform' is based on thermochemical conversion processes and focusses on the gasification (syngas and hydrogen) and pyrolysis (bio-oil) of biomass feedstocks and by-products from the conversion processes. The systematic biorefinery operation scheme is given in Fig. 1.11 [50]. The conceptual outline of a biorefinery is that it takes in raw biomass from the field, extracts food and feed from it, and uses the remaining lignocelluloses to produce fuels, energy and chemicals.

1.5. Biomass Conversion Technologies

The first step in any biomass conversion process is the decomposition of the solid lignocellulosic biomass into its building blocks or its precursors. Depending upon the raw material characteristics and the type of products desired, biomass can be converted into various forms of energy by numerous technical processes. The various technologies adopted in biomass conversion are divided into three typical categories as shown below. Among them, the thermochemical conversion and biochemical conversion are the major routes for biomass decomposition.

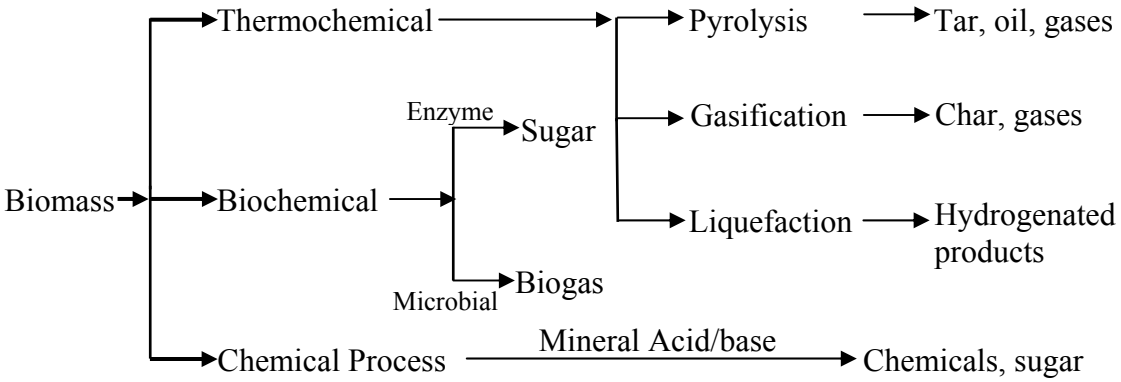

1.5.1. Thermochemical Process

Thermochemical conversion includes three sub-categories: pyrolysis, gasification and direct liquefaction.

1.5.1.1. Pyrolysis

Pyrolysis is the thermal decomposition of organic matter occurring in the absence of air or oxygen. Thermal decomposition in an oxygen deficient environment

can also be considered to be true pyrolysis. The products of the pyrolysis process can be gases (CO_2, CO and H_2), liquids (bio-oils) and/or solids (char) [51, 52]. During pyrolysis, moisture is first evaporated (at ~110°C). Then, hemicellulose is decomposed (at 200-260°C), followed by cellulose (at 240-380°C) and lignin (at 280-500°C). Pyrolysis can be further divided into conventional pyrolysis and flash pyrolysis. Conventional pyrolysis is characterized by a relatively slow heating rate (<10°C/s) compared to that of fast pyrolysis. Flash pyrolysis describes the rapid moderate temperature (400-600°C) pyrolysis that produces quantities of the liquid. The feedstock of pyrolysis is usually a dry matter.

1.5.1.2. Gasification

Gasification describes the process in which oxygen-deficient thermal decomposition (750-850°C) of organic matter produces non-condensable fuel or synthesis gases. Gasification generally involves pyrolysis as well as combustion to provide heat for the endothermic pyrolysis reactions. However, indirectly heated gasification is often used to describe the process in which heat is brought from outside the reaction chamber to drive the pyrolysis in the absence of combustion. The gasification process falls between pyrolysis and complete combustion. Some of the benefits of gasification compared to combustion include: more flexibility in terms of energy applications, more economical and thermodynamic efficiency at a small scale and potentially lower environmental impact when combined with gas cleaning [53, 54].

1.5.1.3. Liquefaction

Liquefaction is hydrogenation or high-pressure thermal decomposition of biomass or decomposition of organic materials at moderate temperature (300-400°C). Liquefaction can be divided into two categories viz., direct and indirect liquefaction. The direct liquefaction involves rapid pyrolysis to produce liquid tars, oils and condensable organic vapors. Indirect liquefaction involves the use of a catalyst to convert non-condensable, gaseous products of pyrolysis or gasification into liquid products. Liquefaction contains various processes such as solvolysis, depolymerization, decarboxylation, hydrogenolysis and hydrogenation. In solvolysis, the biomass forms micelle like structure, while depolymerization leads to form smaller molecules followed by dehydration and decarboxylation. When biomass is treated with hydrogen, hydrogenolysis and hydrogenation of functional groups occur.

The main purpose of this process is to decrease the C:O ratio and increase in C:H ratio for getting higher calorific value gaseous products [55, 56].

1.5.2. Biochemical Process

Bacteria, enzymes and yeasts are capable of breaking down the carbohydrates of biomass into sugars by hydrolysis process. Wine or alcohol is produced in the fermentation process where biomass is converted into alcohol which is used as combustible fuel. Bacteria or microorganism break down the biomass to produce methane and carbon dioxide. Methane thus produced from sewage treatment plants and landfills can be used for heating and generation of power. Biochemical process is broadly classified into two categories as enzymatic degradation process and fermentation process. Before biocatalytic action, the biomass is pretreated using various techniques such as physical pretreatment (irradiation, hydrothermolysis, steam explosion and other mechanical treatment), biological pretreatment (microbe), chemical pretreatment (acid, alkaline, gas, oxidant, organic solvent, extraction of lignin) [57, 58]. By this process, the rigid structure gets destructed and hence, large surface area material is formed for easy access by microorganisms to act on it.

1.5.2.1. Enzymatic Process

Lignocellulosic materials can be degraded by various microorganisms. The cellulose is hydrolyzed by enzymes called cellulases which consist of three different enzymes such as endo-glucanases, exo-glucanases (cellobiohydrolases) and *β*-glucosidases. The endoglucanases catalyze random cleavage of internal bonds of the cellulose chain, while exoglucanases attack the chain ends releasing cellobiose. *β*-glucosidases are only active on cello-oligosaccharides and cellobiose to release glucose monomer units [59]. Hemicellulose is hydrolyzed by various enzymes and microorganisms. Endo-xylanase, exo-xylanase, *β*-xylosidase and other enzymes, such as *α*-L-arabinofuranosidase, *α*-glucuronidase, acetylxylan esterase, ferulic acid esterase, and *p*-coumaric acid esterase are responsible to hydrolyse various substitutions of xylans [60, 61]. The endo-xylanase attacks the main chains of xylans. Exo-xylanase attacks the interior part of xylan to form xylobioses whereas *β*-xylosidase hydrolyzes xylooligosaccharides to xylose. The α-arabinofuranosidase and *α*-glucuronidase attack the arabinose and 4-O-methyl glucuronic acid substituents, respectively, from the xylan backbone. The esterase (acetylxylan esterase) hydrolyzes the ester linkages between xylose units of the xylan and acetic acid or between

arabinose side chain residues and phenolic acids, such as ferulic acid (ferulic acid esterase) and *p*-coumaric acid (*p*-coumaric acid esterase). Many microorganisms such as *penicillium capsulatum*, *thermomonospora fusca* and *talaromyces emersonii* also perform complete hydrolysis of hemicellulose. Pectins are another main structural polysaccharide group of plant cell walls. Many enzymes are involved in pectin degradation. They may be acting either by hydrolysis or by trans-elimination (performed by lyases). Pectin degrading enzymes i.e., polymethylgalacturonase, (endo-) polygalacturonase pectin depolymerase, pectinase, exopolygalacturonase and exopolygalacturanosidase, hydrolyse the polygalacturonic acid chain of the pectin polymer by the addition of a water molecule.

1.5.2.2. Fermentation

Depending on the feedstock, biomass is converted into monosaccharides by various routes. These monosaccharides are fermented by yeast. *Saccharomyces cerevisiae* and *zymomonas mobilis* ferment glucose to ethanol rapidly and efficiently. They cannot ferment other sugars such as xylose and arabinose to ethanol. The yeasts - *pachysolen tannophilus*, *pichia stipitis*, and *candida shehate* have the capability to ferment xylose to ethanol but with low ethanol tolerance.

Bio-methane has the potential application in energy and fuels like bio-fuel (e.g. bio-diesel, bio-ethanol). Bio-methane can be produced by the fermentation process from a wide range of conventional lignocellulosic biomass [62, 63] such as maize, wheat, rye, sunflower and other varieties. Biogas is also produced from kitchen garbage and sewage sludge, maintaining temperature at 5-70°C and neutral pH under anaerobic conditions.

1.5.3. Mineral Acid and Base Treatment Processes

Both dilute and concentrated mineral acids (HCl, H_2SO_4, H_3PO_4, etc.) and bases (NaOH, KOH, $Ca(OH)_2$, etc.) are used to convert cellulose, hemicellulose and lignin into monomer sugars, aromatic alcohols and their derivatives. The dilute acid process requires high temperature, pressure and short time to form maximum products while the concentrated acid processes require relatively mild conditions with much longer reaction time [64]. During dilute acid treatment of biomass, it forms sugars, which may be further degraded into other products in this reaction. Typically, cellulose can be degraded with 50% glucose yield using 1% dilute acid at 240°C. This yield is increased by decreasing reaction time and increasing temperature [65].

Concentrated acid treatment gives about 100% sugar yields [66]. Biomass is very much sensitive towards bases. The base degradation rate is higher than the acid degradation but it is difficult to obtain high yield of sugars because the monomer and dimer carbohydrates are severely attacked by alkalis and form salts of monomer sugars below 100°C [15].

1.6. Overview of Preparation of Sugars from Biomass

Commonly, monomer sugars are synthesized via hydrolysis of biomass. Table 1.1 gives an overview of sugar synthesis using various types of feedstock and catalysts.

Table 1.1. Overview of sugar formation from lignocellulosic materials

Feedstock	Catalyst	Reaction conditions			Products	Ref
		T (°C)	P (bar)	t (h)		
Bagasse	No catalyst	200	-	0.14	7-13% xylose	[67]
Bagasse (125 g/L)	H_3PO_4 (4%)	122	-	5	55% conv.	[68]
Corn stover (150 g/L)	H_2SO_4	170	-	0.25	55% xylose	[69]
Pin chips	H_2SO_4 (1.1%)	190	-	0.04	85% xylose, 46% glucose, etc.	[70]
Rice straw	H_2SO_4 (0.5%)	210	15	0.14	80% xylose and 26% glucose	[71]
Corn stover (77 g/L)	(22 FPU/g)	49	-	38	70% glucose	[72]
Rice straw	H_2SO_4 (1%)	121	-	0.45	77% xylose	[73]
Bagasse	HCl (4%)	90	-	10	80% xylose	[74]
Bagasse	HCl (0.1%)	140	-	0.66	74% xylose	[75]
Cellulose	C-SO_3H	150	-	24	90% glucose	[76]
Cellulose	NaOH (18%)	100	-	1	30% glucose	[26]
Cellulose	HCW#	250	250	0.33	40% glucose	[26]
corn stalk, rice straw, pine wood, bagasse	Ionic liquid† (7 wt% HCl)	100	-	1	66%, 74%, 81% 68% sugar	[77]
Straw and filter paper	Celluclast Novozyme 188	50	-	24	65% hydrolysis products	[78]
Wheat straw	Pulpzyme HA 1 mL/g)	121		24	64% conv. and 12% xylose	[79]
Delignified bagasse	Crude enzyme*	50		48	90% xylose	[80]

#Hot compressed water, † C_4mimCl, *Penicillium Janthinellum

1.7. Drawbacks of Conventional Processes

All aforementioned processes (except heterogeneous catalytic process) have several drawbacks. Direct combustion of biomass gives lot of ash and low heat production. The enzymatic processes operate at ambient temperatures but at a slow rate. The rate also decreases with time due to irreversible adsorption of end products on the enzyme. Moreover, the enzymatic processes are expensive. Separation of the catalyst is an issue with the homogeneous acids or bases. It generates lot of neutralization wastes. The acid or base catalyzed processes require a special reactor set-up because of the corrosiveness of the catalysts. In thermal degradation processes (pyrolysis, gasification and liquefaction) there is no good selectivity for the products. High capital costs for the separation of desired products are needed. However, solid catalysts (heterogeneous process) offer several advantages and overcome the above-said drawbacks of the other processes. The process using solid catalysts could be more selective and environmentally benign.

1.8. Advantages of Heterogeneous Catalytic Process

According to phase separation there are two kinds of catalysts i.e. homogeneous and heterogeneous. Heterogeneous catalysts are insoluble in the medium in which the reaction is taking place, while homogeneous catalysts dissolve in the reaction medium. Table 1.2 presents the main relative differences between these two types of catalytic processes.

Table 1.2. Differences between homogeneous and heterogeneous catalyst processes

Mode of action	Heterogeneous	Homogeneous
Mode of use	Fixed-bed or slurry	Dissolved in reaction medium
Toxicity	Usually non-toxic	Toxic
Handle	Easy to handle	Difficult to handle
Storage	Easy to store	Difficult to store
Regenerability	Easy	Difficult
Separation	Easy	Difficult
Stability	Tolerate a wide range of temperatures and pressures	Short range of temperature tolerance
Recyclability	Easy	Can be very difficult
Selectivity	Usually poor	Good
Reaction rate	Slower	Faster
Deactivation	Deactivated	No deactivation

1.9. Solid Acid Catalysts

Solid acids are widely studied due to their vast applications [81-83]. Based on texture, they are categorized into two types: porous and non-porous. Typically, porous solid acids are zeolites, clays, surface modified or hetero-atom incorporated in mesoporous silicas, sulfonated carbon, ion-exchange resins, etc. Non-porous solid acids are heteropoly acids, metal oxides, etc. The porous materials are further divided into three types: microporous (pore size ca. 2-20 Å), mesoporous (pore size ca. 20-500 Å) and macroporous (pore size >500 Å) solids. Microporous materials including zeolites and clays are both academically and industrially interesting because they are stable and shape selective. The mesoporous materials are hydrothermally less stable than zeolites. Based on acid type, the solid acids are categorized into Brönsted and Lewis acids. The strength and number of these sites available, depend on the surface area, pore size, amount of aluminum, etc. of the catalysts.

1.9.1. Zeolites

Zeolite (in Greek "zeos" and "lithos", meaning "boiling stones") group of minerals were discovered in 1756 and named by the Swedish mineralogist Baron Cronstedt [84]. Traditionally, zeolites are defined as "tri-dimensional microporous crystalline inorganic polymer material of aluminum and silicon oxide, in which both are tetrahedrally coordinated by oxygen atom.'' The general empirical formula of zeolites is: $(M^{n+})_{x/n}[(AlO_2)_x(SiO_2)_y]^{x-}\bullet mH_2O$, where, 'M' is a cation, 'm' is the number of moles of water of crystallization, x and y are the number of $[AlO_4]^{5-}$ and $[SiO_4]^{4-}$ tetrahedron in the unit cell. Table 1.3 presents the pore dimensions of some zeolites.

Table 1.3. Classification of zeolites on the basis of pore diameter

Pore size	Typical material	Ring membered	Pore diameter (Å)
Ultra-large pore	Cloverite	20	6.0 x 13.2
	JDF-20	20	6.2 x 14.5
	$AlPO_4$-8	14	7.9 x 8.7
Large pore	HY	12	7.4 x 7.4
	Hβ	12	6.8 x 7.3
	HMOR	12	6.7 x 7.0
	$AlPO_4$-5	12	7.3
	HZSM-12	12	5.5 x 5.9
Medium pore	HZSM-48	10	5.3 x 5.6
	HZSM-5	10	5.3 x 5.6; 5.1 x 5.5
Small pore	CaA	8	4.2
	SAPO-34	8	4.3

Zeolites contain both Lewis and Brönsted acid sites. Pure siliceous materials are electrically neutral. By replacing silicon (tetrahedrally coordinated with oxygen atoms) having a formal charge of +4 in the frame work lattice with aluminum **(**formal charge +3), a negative charge on the tetrahedron is created (Fig.1.12). This negative charge is balanced by a cation (NH_4^+ and alkali/alkaline cations like Na^+, K^+, and Ca^{2+} or H^+). In zeolites, the protons are formally assigned as bonded to the bridging oxygen of a Si-O-Al bond to form hydroxyl groups that act as strong Brönsted acids. The overwhelming evidence is that the hydroxyl groups within the zeolite channels provide the active Brönsted sites [85, 86]. These are usually prepared via ammonium ion exchange:

$$NaZ + NH_4^+(aq) \rightleftharpoons NH_4Z + Na^+(aq)$$

$$NH_4Z \xrightleftharpoons{\Delta} NH_3(g) + HZ$$

Lewis acid sites are related to the formation of positively charged oxide clusters or ions within the structures of the zeolites (Fig. 1.12). The cationic species present in the catalyst framework can act as a Lewis acid site, because of their electron acceptor properties. These species are typically alumina or silica/alumina, formed by extraction of aluminum from the lattice or metal ions exchanged for the protons of acid sites. The former type of Lewis acidity, i.e. aluminum oxide clusters containing alumina in octahedral and tetrahedral coordination will usually be a stronger Lewis acid than the exchangeable metal cations [87, 88].

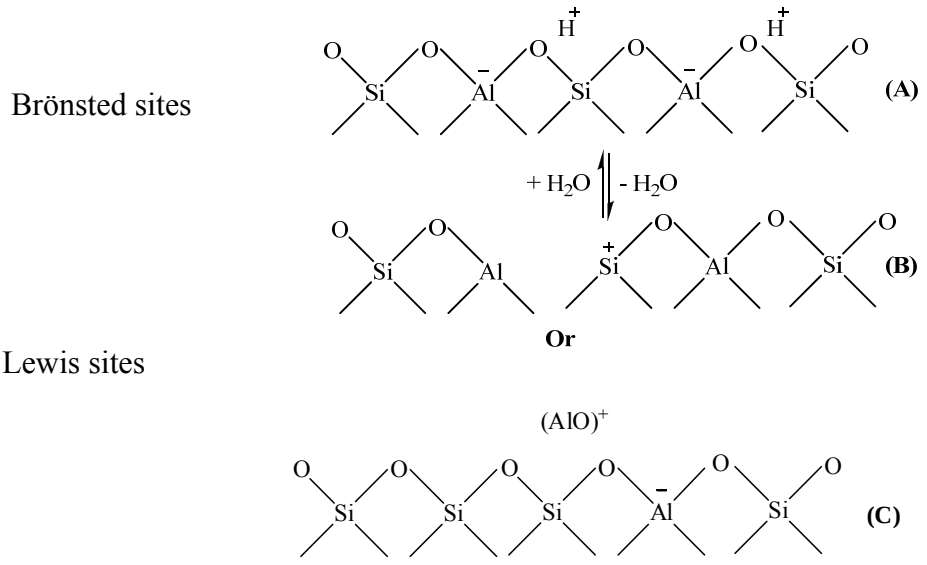

Fig. 1.12. Formation of Brönsted and Lewis acid sites in zeolites.

1.9.2. Super Acids

The presence of sulfur in oxide species plays a good role for the generation of acid sites. The Hammett acidity value of SO_4^{2-}/ZrO_2 is -16.1. From this point of view, the acid strength stronger than that of 100% H_2SO_4 (Hammett acidity function <-12), could be classified as 'super acid'. Solid super acids such as sulfated zirconia, titania, tin oxide, etc., have been reported [89-91]. In these catalysts, the S=O groups have a high double bond nature. The strength of super acids depends on the extent of losing the double bond character by an electron shift from an adsorbed basic molecule to the sulfur complex [92]. The larger the shift, the higher is the acid strength. The generation of super acidity is independent of the sulfur source such as $(NH_4)_2SO_4$, SO_3, SO_2 or H_2S, provided that the oxidation state of sulfur is brought to its highest one [93, 94]. The surface sulfur complex in the highly active catalysts or highly acidic catalysts has a strong tendency of reducing the bond order of S=O from a highly covalent double-bond character to a lesser double-bond character when a basic molecule is adsorbed on its central metal cation (Fig. 1.13). The strong ability of the sulfur complex with structure to accommodate electrons from a basic molecule is the driving force to generate highly acidic properties. The structure of sulfated zirconia collapses above 130°C and in the presence of water,. Hence, it cannot be used for aqueous phase reaction at higher temperature.

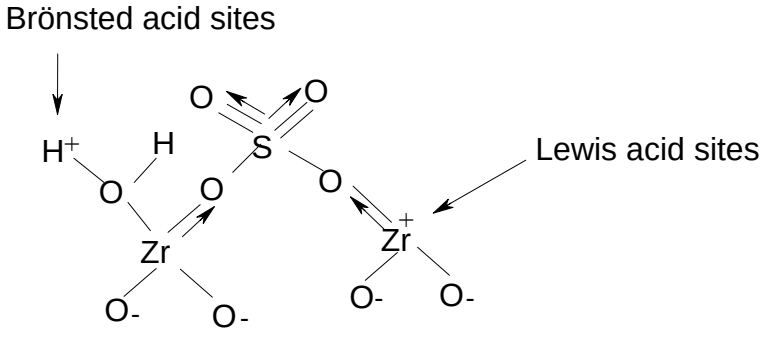

Fig. 1.13. Brönsted and Lewis Acid sites in solid super acids.

1.9.3. Clays

Clays are defined as phylosilicate consisting of two-dimensional tetrahedral sheet (T) fused with octahedral sheet (O) having charge balancing cations for charge neutrality. The basic units of clays are SiO_4 or $Si(OH)_4$ and MO_6 or $M(OH)_6$ where M is Al^{3+}, Mg^{2+}, Fe^{3+}, etc. On the basis of layer arrangement, the phylosilicates are classified into eight main groups [95].

(1) Serpentine-kaolinite (layer type = 1:1, example: chrysolite)
(2) Talc-pyrophylite (layer type = 2:1, example: talc)
(3) Smectite (layer type = 2:1, example: montmorillonite)
(4) Vermiculite (layer type = 2:1, example: vermiculite)
(5) Mica (layer type = 2:1, example: biotite)
(6) Brittle mica (layer type = 2:1, example: clintonite)
(7) Chlorite (layer type = 2:1, example: clinochlore)
(8) Sepiolitie (example: sepiolite)

In clays, the alkali and alkaline cations (Na^+, K^+ and Mg^{2+}) are located in the interlayer sites. These can be exchanged and the acidic properties of clays can be enhanced.

1.9.4. Heteropoly Acids

Heteropoly acids are polymeric oxoacids composed of more than two different metal ions. $H_3PW_{12}O_{40}$ is the example of heteropolyacids. Heteropoly acids (HPA) and their salts are interesting catalysts due to their controllable acidity and redox properties [96]. It is an efficient catalyst used in a variety of reactions such as alkylation and acylation of hydrocarbons. The order of the acidity of HPA determined by using Hammett scale is as follows: $H_3PW_{12}O_{40} > H_4PW_{12}VO_{40} > H_3SiW_{12}O_{40} > H_4PMo_{11}MoO_{40} > H_3PW_{12}O_{40} > H_3PMo_{12}O_{40} > H_4SiMo_{12}O_{40}$. HPAs are highly soluble in water. Water insoluble HPA are synthesized by the precipitation method from aqueous solutions of $H_3PW_{12}O_{40}$ with Cs_2CO_3 [97].

1.10. Heterogeneous Catalysts in Biomass Conversion

Recently, many heterogeneous catalysts (solid acids and supported metals) have been reported for the conversion of biomass into chemicals. Cellulose and sucrose were hydrolyzed into glucose using sulfonated activated carbon [98, 99], zeolites, ion exchange resin [100], transition metal oxide and lanthanum salts [101]. Similarly, sucrose and starch have been hydrolyzed by various solid acids (grafted mesoporous materials) [102] to glucose and fructose. It has also been reported that cellulose can be directly converted to sugar alcohol (~25% sorbitol and ~6% mannitol yield) using ruthenium or platinum supported on silica or metal oxides [41, 42]. Cellobiose has also been converted over solid catalysts [103]. The solid catalyst-based processes were found to be advantageous and selective.

1.11. Objective and Scope of the Thesis

Conversion of biomass into value-added chemicals and fuels is an area of considerable current interest. Catalyst plays a crucial role in such transformations. Use of solid catalysts make the biomass conversion processes environmental friendly and sustainable. Although there have been some reports on the application of solid catalysts in the conversion of starch and cellulose, similar such studies on the conversion of hemicellulose into its constituent sugars are scarce. Hence, it is the objective of the present study to undertake such investigation and identify suitable catalysts that could yield higher amounts of sugars and their derivatives at optimized conditions. Accordingly, hemicellulose derived from softwood (oat spelt) and hardwood (birch wood) has been chosen for the hydrolysis over several solid acid catalysts including zeolites, Al-containing mesoporous silica, clay, Cs-exchanged heteropolyacid and metal oxide catalysts. The acid catalysts used in the present study are chosen in such a way that they are already in commercial use. Their acidity and strength could be fine tuned. They are different in their pore architecture so that pore size effects on the hydrolysis could be understood. Part of C_5 (xylose and arabinose) sugars produced on hydrolysis gets converted into furfural via dehydration. Furfural is a high value chemical and finds applications in the preparation of specialty polymers and pharmaceuticals. Therefore, another objective of this study is to identify reaction conditions to optimize the yields of furfural. Yet another objective of the study is the direct conversion of hemicellulose in bagasse to sugars/furfural.

Oxidation bio-derived furans (furfural and 5-hydroxymethylfurfural) into furan carboxylic acid are an important transformation. Presently, such oxidations are carried out using stoichiometric oxidants which generate significant amount of waste. Oxidation with molecular oxygen or air in the presence of solid supported metal catalysts makes the process green. In view of this, Pt and Au supported on reducible and non-reducible oxides have been prepared and their application in the oxidation reactions has been investigated. By and large, the main objective is to develop green and sustainable catalytic processes for the conversion of hemicellulose (biomass) into several valuable chemicals. .

1.12. Outline of the Thesis

The thesis is divided into **six** chapters. Brief contents of each chapter are given below.

Chapter 1 provides a brief introduction to the importance of biomass and its conversion to chemicals and fuels. It emphasizes the various technologies for the conversation of biomass. The concept of biorefinery and an overview of literature survey on biomass conversion using homogeneous and heterogeneous solid catalysts are also presented. Finally, the scope and objectives of the present work are outlined.

Chapter 2 deals with materials and characterization procedures. The synthesis and various sources of procurement of zeolites, Al-containing mesoporous silicas, clay, supported metal catalysts and Cs-exchange heteropoly acid used in this work are presented. These catalysts are characterized by various physicochemical techniques including X-ray powder diffraction (XRD), N_2 sorption, elemental analysis, temperature-programmed desorption of ammonia, scanning electron microscopy and transmission electron microscopy.

Chapter 3 describes the conversion of hemicellulose into chemicals over solid acid catalysts (zeolites: HUSY (Si/Al = 15 and 40), HY (Si/Al = 2.6), Hβ (Si/Al = 19), HMOR (Si/Al = 10) and HZSM-5 (Si/Al = 10); Al-containing mesoporous silica: Al-MCM-41(Si/Al = 50) and Al-SBA-15 (Si/Al = 50); acid treated clay K-10; cesium exchanged heteropolyacid (HPA) and metal oxides ($Nb_2O_5 \cdot H_2O$ and γ-Al_2O_3). The effect of various reaction parameters including reaction temperature, pressure (N_2 gas) and substrate to catalyst mole ratio on product yield is studied. Both softwood and hardwood-derived hemicelluloses are used as substrates. Reusability of the catalyst is also investigated. Finally, structure-function correlations are made. To the best of knowledge this is the first study reporting the hydrolysis of hemicellulose over solid acid catalysts.

Chapter 4 presents the conversion of hemicellulose in bagasse into sugars and furfural. Catalytic activities of HUSY (Si/Al = 15), Hβ (Si/Al = 19) and HMOR (Si/Al = 10) for this reaction are investigated. The influence of different reaction parameters such as temperature, pressure and reactants mole ratio on product yield is examined. Possible means for enhancing the yield of furfural is probed using co-solvents. Reusability of the solid catalysts is probed.

Chapter 5 discusses the selective oxidation of HMF and furfural over supported metal catalysts (Pt/γ-Al_2O_3, Pt/AC, Pt/ZrO_2, Pt/CeO_2, Pt/TiO_2 and Au/γ-Al_2O_3). Molecular oxygen and air are used as oxidants. The influence of base on product carboxylic acid yield is studied. Tentative reaction mechanism is proposed. The catalysts are characterized and structure-activity correlations are made.

Chapter 6 presents an overall summary and conclusions of the work.

In general, the work presented in this thesis contributes to the green and sustainable catalytic processes and the catalytic conversion of non-edible biomass into value-added chemicals.

1.13. References

[1] P. M. Arvela, B. Holmbom, T. Salmi, D. Y. Murzin, *Catal. Rev.* **2007** 49, 197.

[2] J. W. Geus, A. J. Dillen, *Fine Chemicals Through Heterogeneous Catalysis,* Wiley-VCH, Weinheim **2001**.

[3] C. Okkerse, H. V. Bekkum, *Green Chem*. **1999**, 4, 107.

[4] P. T. Anastas, J. C. Warner, *In Green Chemistry Theory and Practice*, Oxford University Press, New York **1998**.

[5] A. L. Marshall, P. J. Alaimo, *Chem. Eur. J.* **2010**, DOI:10.1002/ Chem.200903028

[6] C. Briens, J. Piskorz, F. Berruti, *Int. J. Chem. React. Eng.* **2008**, 6, 1.

[7] P. McKendry, *Bioresour. Technol.* **2002**, 83, 37.

[8] P. McKendry, *Bioresour. Technol.* **2002**, 83, 47.

[9] A. Corma, S. Iborra, A. Velty, *Chem. Rev.* **2007**, 107, 2411.

[10] B. Kamm, M. Kamm, *Appl. Microbiol. Biotechnol*. **2004**, 64, 137.

[11] B. E. Dale, S. Kim, *Biorefineries Industrial Process and Products,* Vol. 1, Wiley-VCH, Weinheim **2006**.

[12] R. H. Whittaker, G. E. Likens, *In Primary Productivity of The Biosphere,* Springer-Verlag, New York **1975**.

[13] C. Liao, Y. Yan, C. Wu, H. Huang, *Biomass Bioenergy* **2004**, 27, 111.

[14] C. Lewis, *Biological Fuels*, Hodder Education, London **1998**.

[15] Y. Sun, J. Cheng, *Bioresour. Technol.* **2002**, 83, 1.

[16] B. Kamm, M. Kamm, P. R. Gruber, S. Kromus, *In Biorefineries-Industrial Processes and Products: Status Quo and Future Directions,*

Vol. 1, Wiley-VCH, Weinheim **2006**.

[17] H. Zoebelin, *Dictionary of Renewable Resources,* Wiley-VCH, Weinheim **2001**.

[18] C. E. Wyman, *Appl. Biochem. Biotechnol*. **1994**, 46, 897.

[19] J. D. Murphy, K. M. Carthy, *Appl. Energy* **2005**, 82, 148.

[20] H. Roper, *Starch* **2002**, 54, 89.

[21] P. Madhavan*, Chitin, Chitosan and their Novel Application*, Science Lecture Series, CIFT, Kochi **1983**, 28, 189.

[22] C. Jeuniaux, M. F. Voss-Foucart, *Biochem. Syst. Ecol.* **1991**, 19, 347.

[23] A. V. Bridgwater, *Therm. Sci.* **2004**, 8, 21.

[24] J. M. Carthy, A. Islam, *Lignin Chemistry, Technology and Utilization In Lignin: Historical, Biological and Materials Perspectives,* ACS, symposium series, Washington **2000**, 742, 2.

[25] H. H. Nimz, *Tappi J.* **1973**, 56, 124.

[26] Y. Yun, L. Xia, W. Hongwei, *Energy & Fuels* **2008**, 22*,* 46.

[27] F. H. Myhr, Oxford University Press, *Definition: Renewable Energy Resource*, www.cpast.org/articles/fetch3.adp

[28] Ullmann's, *Encyclopedia of Industrial Chemistry* (6 ed. electronic release), dimethylether **2002**.

[29] K. Jopp, *Volkswagen Magazine* **2003**.

[30] H. Jacobsen, *Angew. Chem. Int. Ed.* **2004**, 43, 1912.

[31] R. D. Davda, R. R. Dumesic, J. A. N. Cortright, *Nature* **2002**, 418, 964.

[32] S. Quo, *Biorefineries Industrial Process and Products*, Wiley-VCH, Weinheim **2005**.

[33] J. V. Haveren, E. L. Scott, P. M. Sanders, *J. Biofuels Bioproducts and Biorefining* **2007**, 2, 41.

[34] M. Fukuda, K. Mikoshiba, *BioEssays* **1997**, 19, 593.

[35] R. D. Burgoyne, A. Morgan, *Phsiol. Rev*. **2003**, 83, 581.

[36] D. R. Dodds, R. A. Gross, *Science* **2007**, 318, 250.

[37] D. A. Simonetti, J. A. Dumesic, *ChemSusChem.* **2008**, 1, 725.

[38] D. Y. Goswami, F. Kreith, *In Handbook of Energy Efficiency and Renewable Energy*, Vol.1, Taylor & Francis, London **2007**.

[39] D. Yamaguchi, M. Kitano, S. Suganuma, K. Nakajima, H. Kato, M. Har, *J. Phys. Chem. C* **2009,** 113*,* 3181.

[40] A. Takagaki, C. Tagusagawa, K. Domen*, Chem. Commun*. **2008**, 42, 5363.

[41] A. Fukuoka, P. L. Dhepe, *Angew. Chem. Int. Ed*. **2006**, 45, 516.

[42] C. Luo, S. Wang, H. Liu, *Angew. Chem. Int. Ed.* **2007**, 46, 7636.

[43] R. Rinaldi, R. Palkovits, F. Schüth, *Angew. Chem. Int. Ed.* **2008**, 47, 8047.

[44] C. Moreau, R. Durand, D. Peyron, J. Duhamet, P. Rivalier, *Ind. Crops Prod.* **1998**, **7**, 95.

[45] S. Lima, M. Pillinger, A. A. Valente, *Catal. Commun.* **2008**, 9, 2144.

[46] R. D. Perlack, L. L. Wright, A. F. Turhollow, R. L. Graham, *Biomass as Feedstock for a Bioenergy and Bioproducts Industry: the Technical Feasibility of a Billion-ton Annual Supply,* www.eere.gov/biomass

[47] J. J. Bozel, M. K. Patel, *Feed Stocks for Future*, ACS, Symposium Series, Washington **2006**, 921, 1.

[48] U. S. Department of Energy, *Energy Efficiency and Renewable Energy*, *Biomass Program*, www.nrel.gov/biomass/biorefinery.html

[49] S. Fernando, S. Adhikari, C. Chandrapal, N. Murali, *Energy & Fuels* **2006**, 20, 1727.

[50] G. Centi, R. A. V. Santen, *Catalysis for Renewable,* Wiley-VCH, Verelag GmbH &Co. KGaA, Weinheim **2006**.

[51] A. V. Bridgwater, G. V. C. Peacocke, *Renewable and Sustainable Energy Rev*. **2000**, 4, 1.

[52] S. C. Zernik, A. V. Bridgwater**,** *Energy & Fuels* **2004**, 18, 590.

[53] S. R. Akersten, B. V. Drift, W. Prins, W. P. M. V. Swaaij, *Ind. Eng. Chem. Res.* **2003**, 42, 6755.

[54] S. C. Zernik, R. Evans, R. French, *Ind. Eng. Chem. Res.* **2002**, 41, 4209.

[55] A. D. Nelson, P. M. Molton, J. A. Russell, *Ind. Eng. Chem. Res.* **1984**, 23, 471.

[56] T. Minowa, M. Murakami, Y. Dote, T. Ogi, S. Yokoyama, *Biomass Bioenergy* **1995**, 8, 117.

[57] T. Amon, B. Amon, V. Kryvoruchko, A. Machmuller, K. Hopfner-Sixt, V. Bodiroza, R. Hrbek, J. Friedel, E. Potsch, H. Wagentristl, M. Schreiner, W. Zollitsch, *Bioresour. Technol.* **2007**, 98, 3204.

[58] D. Antoni, V. V. Zverlov, W. H. Schwarz, *Appl. Microbiol. Biotechnol*. **2007**, 77, 23.

[59] R. Kumar, S. Singh, O. V. Singh, *J. Ind. Microbiol. Biotechnol.* **2008**, 35, 377.

[60] F. Niehaus, C. Bertoldo, M. Kahler, G. Antranikian*, Appl. Microbiol. Biotechnol.* **1999**, 51, 711.

[61] B. C. Saha, *J. Ind. Microbiol. Technol.* **2003**, 30, 279.

[62] M. Hutnan, M. Drtil, L. Mrafkova, *Biodegradation* **2000**, 11, 203.

[63] J. Turner, G. Sverdrup, M. K. Mann, P. Maness, B. Kroposki, M. Ghirardi, R. J. Evans, D. Blake, *Int. J. Energy Res*. **2008**, 32, 379.

[64] A. O. Converse, *Bioresour. Technol.* **2002**, 81, 109.

[65] Y. Y. Lee, Z. Wu, R. W. Torget, *Bioresour. Technol.* **2000**, 71, 29.

[66] S. J. B. Duff, W. D. Murray, *Bioresour. Technol.* **1996**, 55, 1.

[67] S. E. Jacobsen, C. E. Wyman, *Ind. Eng. Chem. Res*. **2002**, 41, 1454.

[68] S. Gameza, J. J. Gonzalez-Cabriales, J. A. Ramirez, G. Garrote, M. Vazquez, *J. Food Eng.* **2006**, 74, 78.

[69] Y. Lu, N. S. Mosier, *Biotechnol. Prog*. **2007**, 23, 116.

[70] K. H. Kim, M. Tucker, Q. Nguyen, *Bioresour. Technol*. **2005**, 96, 1249.

[71] K. Karimia, S. Kheradmandiniaa, M. J. Taherzadeh, *Biomass Bioenergy* **2006**, 30, 247.

[72] X. B. Lu, Y. M. Zhang, J. Yang, Y. Liang, *Chem. Eng. Technol.* **2007**, 30, 938.

[73] I. C. Roberto, S. I. Mussatto, R. C. L. B. Rodrigues, *Ind. Crops Prod.* **2003**, 17, 171.

[74] B. P. Lavaracka, G. J. Gri, D. Rodman, *Biomass Bioenergy* **2002**, 23, 367.

[75] P. Jr, I. M. Mancilha, S. Sato, *Braz. J. Chem. Eng*. **1997**, 14, 3.

[76] A. Herrera, S. J. T. Luis, J. J. G. A. Cabriales, J. A. Ram, M. V. Azquez, *J. Food Eng.* **2004**, 63, 103.

[77] C. Liab, Q. Wanga, Z. K. Zhao, *Green Chem.* **2008**, 10, 177.

[78] J. B. Kristensen, C. Felby, H. Jørgensen, *Appl. Biochem. Biotechnol*. **2009**, 156, 557.

[79] S. Sirisansaneeyakull, M. Rizzi, *J. Nat. Sci.* **1998**, 32, 224.

[80] M. G. Adsula, J. E. Ghuleb, H. Shaikhb, R. Singhb, K. B. Bastawdea, D. V. Gokhalea, A. J. Varmab, *Carbohydr. Poly.* **2005**, 62, 6.

[81] A. Corma, A. Martinez, *Catal. Rev. Sci. Eng.* **1993**, 35, 483.

[82] K. Gaare, D. Akporiaye, *J. Mol. Catal.* **1989**, 49, 109.

[83] E. Houdry, A. Joseph, *Bull. Assoc. Fr. Tech. Pet.* **1956**, 117, 177.

[84] A. F. Cronstedt, *Kongi. Svenska Vetenskaps Acad. Handlinger* **1756**, 17, 120.

[85] R. S. Hansford, *Ind. Eng. Chem.* **1947**, 39, 849.

[86] D. Barthomeuf, *Mater. Chem. Phys.* **1987**, 17, 49.

[87] A. Baranski, S. Ceckiewicz, *J. Chem. Soc. Farad. Trans.* **1978**, 74, 146.

[88] H. G. Karge, *Stud. Surf. Sci. Catal.* **1991**, 65, 133.

[89] K. Tanabe, T. Yamaguchi, K. Akiyama, A. Mitoh, K. Awabuchi, K. Isogai, *Proc. 8th Inter. Cong. Catal.*, Verlag Chemie, Berlin, **1984**.

[90] K. Arata, M. Hino, *Bull. Chem. Soc. Jpn.* **1980**, 53, 446.

[91] K. Tanabe, T. Yamaguchi, *Successful Design of Catalysts,* Elsevier,

Amsterdam **1992**.

[92] T. Jin, T. Yamaguchi, K. Tanabe, *J. Phys. Chem.* **1986**, 90, 4794.

[93] T. Yamaguchi, T. Jin, K. Tanabe, *J. Phys. Chem.* **1986**, 90, 31.

[94] Y. Nagase, T. Jin, H. Hattori, T. Yamaguchi, K. Tanabe, *Bull. Chem. Soc. Jpn.* **1985**, 58, 916.

[95] B. J. B. Mott, *Catal. Today* **1988**, 2, 199.

[96] S. Shikata, S. Nakata, T. Okuhara, M. Misono, *J. Catal*. **1997**, 166, 263.

[97] S. Tatemestsu, T. Hibi, T. Okuhara, M. Misono, *Chem. Lett*. **1984**, 865, 56.

[98] A. Onda, T. Ochi, K. Yanagisawa, *Green Chem.* **2008**, 10, 1033.

[99] S. Suganuma, K. Nakajima, M. Kitano, D. Yamaguchi, H. Kato, S. Hayashi, M. Hara, *J. Am. Chem. Soc.* **2008**, 130, 12787.

[100] B. Satyanarayana, Y. B. G. Varma, *Indian J. Technol.* **1970**, 8, 58.

[101] K. Seri, T. Sakaki, M. Shibata, Y. Inoue, H. Ishida*, Bioresour. Technol.* **2002**, 81, 257.

[102] P. L. Dhepe, M. Ohashi, S. Inagaki, M. Ichikawa, A. Fukuoka, *Catal. Lett.* **2005**, 102, 163.

[103] N. Yan, C. Zhao, Chen Luo, P. J. Dyson, H. Liu, Y. Kou, *J. Am. Chem. Soc.* **2006**, 128 , 27.

CHAPTER-2

MATERIALS AND CHARACTERIZATION METHODS

2.1. Introduction

Catalytic conversion of biomass into chemicals and fuels is area of considerable contemporary importance [1]. Lignocellulose (derived from plant kingdom) is the abundant class of biomass. It is composed of lignin and cellulosic compounds – cellulose and hemicellulose. While cellulose is a homopolymer of β-D-glucose, hemicellulose is a heteropolymer of C_5 and C_6 sugars. Hydrolysis and further transformation of hemicellulose lead to several value-added chemicals. As mentioned in Chapter 1 (section 1.11), the objective of this thesis is to develop methods for (1) the one-pot hydrolysis of hemicellulose into corresponding monomeric sugars (C_5 and C_6) and (2) oxidation of furfural and 5-hydroxymethyl furfural, HMF (both derived from C_5 and C_6 sugars via dehydration) to furoic acid and 2, 5-furandicarboxylic acid (FDCA), respectively (Scheme 2.1). Accordingly, two categories of solid acid catalysts have been examined for these two transformations: (i) solid acid catalysts - for hydrolysis of hemicellulose and (ii) supported noble metal catalysts - for oxidation of furfural and HMF. The various solid acid catalysts investigated in this work include: (a) zeolites with varying Si/Al ratio and 3-dimensional structural topology (HY, HUSY, HMOR, HZSM-5 and Hβ), (b) aluminium-incorporated two-dimensional mesoporous silica (Al-MCM-41 and Al-SBA-15), (c) montmorillonite clay (K10) with layered structure (d) cesium-exchanged heteropolyacid (Cs-HPA) with Keggin structure and (e) metal oxides ($Nb_2O_5•H_2O$, γ-Al_2O_3 and sulphated zirconia). The various supported noble metal (2 and 3.5 wt%) catalysts investigated include: Pt/γ-Al_2O_3, Pt/activated carbon, Pt/ZrO_2, Pt/CeO_2, Pt/TiO_2 and Au/γ-Al_2O_3. This chapter describes the catalyst materials, their source of procurement and any further modifications made and their characterization by various physicochemical techniques.

2.2. Materials

2.2.1. Zeolites

Zeolites in protonated or ammonium ion forms (CAS No. 1318-02-1) as white powders [HY (Si/Al molar ratio = 2.6), HUSY (Si/Al = 15), HUSY (Si/Al = 40), HMOR (Si/Al = 10), Hβ (Si/Al = 19), HZSM-5 (Si/Al = 11.5)]

were procured from Zeolyst International, USA. Physicochemical characteristics of these materials as quoted by the supplier are listed in Table 2.1. These as-received forms were calcined at 550°C for 12 h and stored in a desiccator over silica gel.

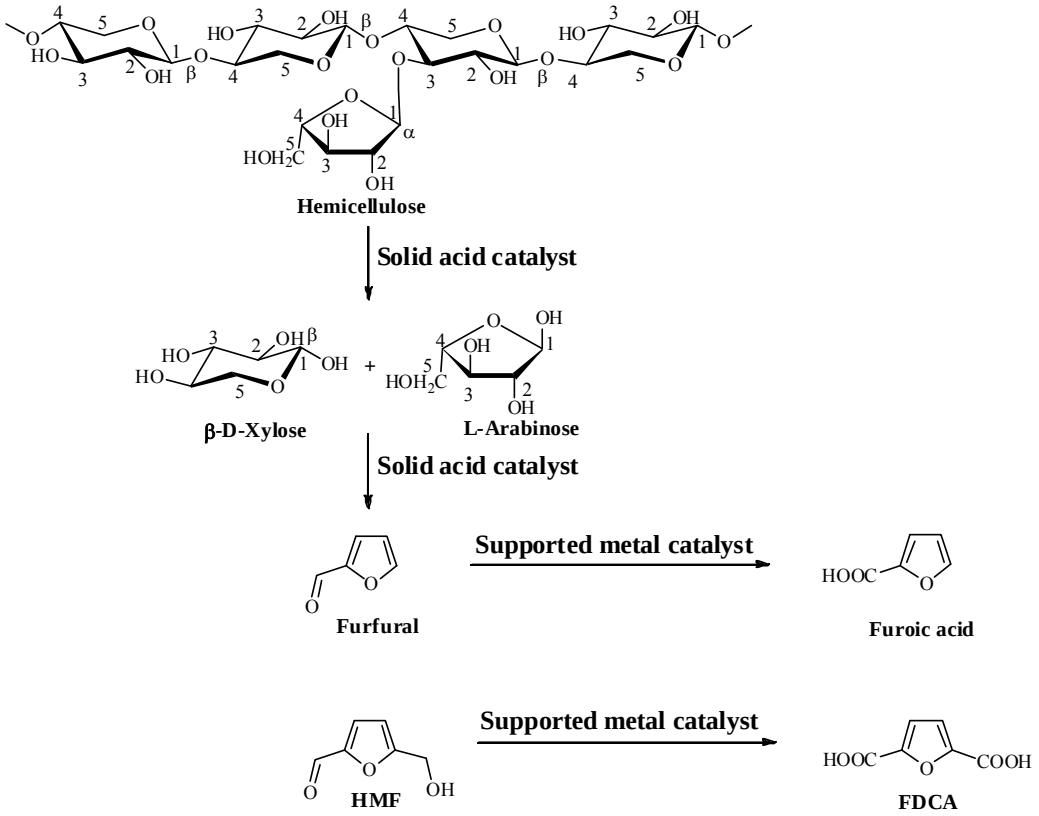

Scheme 2.1. Conversion of hemicellulose into value-added chemicals.

Table 2.1. Physicochemical characteristics of zeolites

Name	Code No.	SiO_2/Al_2O_3 mole ratio	Na_2O wt%	Unit cell size (Å)	Surface area (m^2/g)	Appea-rance
HY	CBV500	5.2	0.20	24.53	750	White powder
HUSY	CBV720	30	0.03	24.28	780	White powder
HUSY	CBV780	80	0.03	24.24	780	White powder
HZSM-5	CBV2314	23	0.05	-	425	White powder
HMOR	CBV21A (NH_4^+ form)	20	0.08	-	500	White powder
Hβ	CP814C*	38	0.05	-	710	White powder

2.2.2. Synthesis of Aluminum-incorporated Mesoporous Silica

2.2.2.1. Al-MCM-41

The Al-MCM-41 sample was prepared using a molar gel composition: 1 SiO_2 : 0.33 TMAOH : 0.55 CTMABr : 60 H_2O : 0.01 Al_2O_3 [2]. In a typical preparation, 10 g of cetyl trimethylammonium bromide (CTMABr; LOBA Chemie, CAS No 57-09-0, 99% purity) and 40 g of distilled water were taken in a 100 mL polypropylene beaker and stirred for 0.5 h at 600 rpm. To it, 10.42 g of tetraethylorthosilicate (TEOS; Aldrich, CAS No. 78-10-4, 99.999% purity) was added dropwise with continuous stirring. After complete addition, the gel formed was stirred for another 15 min. Then, 6 g of trimethylammonium hydroxide (TMAOH; 25% solution, Aldrich, CAS No. 75-59-2, 99% purity) was added dropwise while stirring. The gel was stirred for another 10 min. In another beaker, 0.166 g of $Al_2(SO_4)_3 \cdot 18H_2O$ (Aldrich, CAS No. 10043-01-3, 99% purity) was dissolved in 14 g of water. This solution was added dropwise to the above-gel with constant stirring. After this addition, the gel was stirred for 5 h. The contents of the beaker were transferred to a Teflon-lined autoclave and heated at 110°C under autogenous pressure for 5 days. The obtained material was filtered, washed with water, later by acetone and dried at 60°C. The as-synthesized material was calcined in the presence of nitrogen gas (raising the temperature at a rate of 0.8°C/min and keeping for 1 h after reaching 500°C) followed by air (at 550°C) for 12 h. The white solid, thus, obtained was labeled as Al-MCM-41 (Si/Al = 50).

2.2.2.2. Al-SBA-15

Al-SBA-15 was prepared using a molar gel composition: 0.0007 mol P123 : 0. 041 mol TEOS : 0.24 mol HCl : 0.45 Al(*i*-pr)$_3$: 6.67 mol H_2O [3]. In a typical preparation, 4 g of triblock co-polymer (P123; Aldrich, CAS No. 9003-11-6, 99% purity) and 30 g of distilled water were taken in a polypropylene beaker and stirred for 2 h. Then, 120 g of 2 M HCl (LOBA, CAS No. 7664-93-9, 37% HCl) was added under stirring at 25°C. In another beaker, 8.46 g of TEOS and 0.92 g of aluminium isopropoxide (Al(*i*-pr)$_3$; MERCK, CAS No. 555-31-7, 99.99% purity) were taken and 10 g of 2 M HCl was added. The solution was stirred for 3 h. This solution was slowly

added to the polymer solution under stirring at 40°C for 20 h. Finally, the gel formed was transferred into a polypropylene bottle and kept at 100°C for 48 h. The solid product formed was filtered, washed with water, latter with acetone and dried at 60°C. It was then calcined in the presence of nitrogen and air as described below. The calcined, white solid thus, formed was labeled as Al-SBA-15 (Si/Al = 50). The following scheme gives the details of calcination procedure adopted in the preparation of Al-MCM-41 and Al-SBA-15.

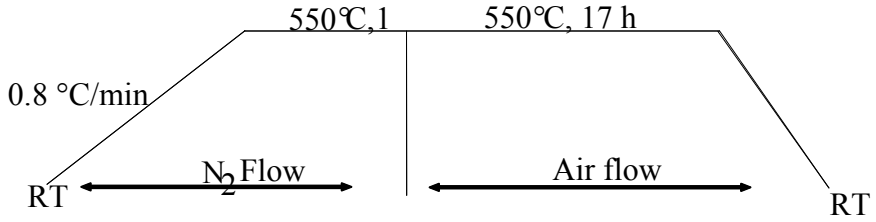

2.2.3. Preparation of Cesium-exchanged Phosphotungstic Acid

In general, the heteropoly salts of small cations and of many transition metals (Ce^{3+}, La^{3+}, Fe^{3+}, etc.) are highly soluble in water and in several organic solvents [4, 5]. However, their salts with large size counter cations are less soluble. For example, Cs^+, Ag^+, Tl^+, Hg^{2+}, Pb^{2+} and the larger alkaline earth metal salts are often insoluble. NH_4^+, K^+ and Rb^+ salts of some of the important series of heteropoly anions are also insoluble. Solubility of the heteropoly compounds in water must be attributed to very low lattice energies and solvation of cations. Solubility is governed by packing patterns in the crystals. The counter cations are fitted in between the large negative anions. When large cations like Rb^+, Cs^+ are present they allow stable packing in the large interstices, causing sufficient increase in lattice energy to produce insolubility [6].

The cesium-exchanged heteropoly acid, $Cs_{2.5}H_{0.5}[PW_{12}O_{40}]$, was synthesized by the ion-exchange method. Stoichiometric amounts of Cs_2CO_3 (Sigma-Aldrich, CAS No. 534-17-8, 99.99% purity) and $H_3PW_{12}O_{40}$ (Sigma-Aldrich, CAS No. 12501-23-4, 99.99% purity) were used for the synthesis of cesium-exchanged heteropoly acid (Cs-HPA). In a typical synthesis, 1 g of phosphotungstic acid ($H_3PW_{12}O_{40}$; 0.347 mmol)) dissolved in 20 g of water was added drop-wise to 0.1407 g (0.432 mmol) of cesium carbonate dissolved in 10 g of water taken in a round bottom flask. The reaction mixture was stirred at 25°C for 1 h. A white precipitate obtained was

separated out by centrifuging the reaction mixture at 8000 rpm. The precipitate was dried at 60°C for 16 h in an air-oven (Yield = 80%).

Montmorillonite clay (K10) and $Nb_2O_5•H_2O$ were procured from Aldrich and used as received. Sulphated zirconia was obtained from a commercial source.

2.2.4. Synthesis of Supported Metal Catalysts

All chemicals and supports used in this study were of analytical grade and used without any further purification. Details of the chemicals and supports used in the synthesis of supported metal catalysts are listed in Table 2.2.

Support zirconia was prepared from zirconyl nitrate. 55.05 g of zirconyl nitrate (LOBA, CAS No. 14985-18-3, 99% purity) was dissolved in 1082 g of distilled water taken in a beaker. To it, 5% ammonia solution (MERCK, CAS No. 7664-41-7, 99% purity) was added drop-wise while stirring vigorously. Addition was continued until the pH of the solution was 9.1. The final solution was stirred for 0.75 h at 25°C. The stirring was stopped and the precipitate was aged at room temperature (25°C) for overnight. The precipitate was filtered and washed with water till the pH of the filtrate was neutral. The filtered material was dried overnight in an oven at 120°C. It was then crushed and calcined at 500°C for 4 h.

All the supports were activated at 150°C for 6 h under vacuum (10^{-3} bar) and preserved in desiccators for further use.

Table 2.2. Details of chemicals and supports used in synthesis of supported metal catalysts

Chemical/Support	Chemical formula	Purity (%)	Source
Tetraammineplatinum nitrate	$(NH_3)_4\,Pt(NO_3)$	99.995	Aldrich
Tetrachloroauric acid	$H[AuCl_4]•3H_2O$	99.9	Aldrich
Gamma-alumina	γ-Al_2O_3	99	Aldrich
Activated carbon (AC)	C	-	Aldrich
Cerium dioxide	CeO_2	99.9	Aldrich
Titanium dioxide	TiO_2	99	LOBA
Zirconyl nitrate	$ZrO(NO_3)_2•xH_2O$	99	LOBA

2.2.4.1. Supported Pt Catalysts

2 g of activated γ-Al_2O_3 and 20 g of distilled water were taken in a 50 mL round-bottom flask and stirred for 0.5 h at 25°C. To it, 2.72 g of aq. tetraammine platinum nitrate (Aldrich, CAS No. 20634-12-2, 99.99% purity) solution (containing 26 mg of Pt/g) was added drop-wise under vigorous stirring. The stirring was continued for 16 h at 25°C. The solvent was removed by rotary evaporator. The content was then evacuated (10^{-3} bar) at 80°C for 6 h to make sure that the support was free of moisture. It was then subjected to calcination. Later, the material was reduced at 400°C for 2 h in the presence of hydrogen (flow rate = 30 mL/min). A grey colored material, Pt/γ-Al_2O_3 (Pt = 3.5 wt%), thus, obtained was stored in a desiccator.

A series of supported platinum metal (3.5 wt%) catalysts (Pt/AC, Pt/ZrO_2, Pt/CeO_2 and Pt/TiO_2) was prepared following the above procedure and by using appropriate supports [7].

2.2.4.2. Supported Au Catalysts

2 g of activated γ-Al_2O_3 and 10 g of water were taken in a 50 mL round-bottom flask. The contents were stirred for 0.5 h and 10 g of aq. chloroauric acid (Aldrich, CAS No. 16961-25-4, 99.9% purity) solution (containing 0.2 mg of Au/g of solution) was added drop-wise while stirring vigorously. The stirring was continued for 16 h at 25°C. The solvent was removed by rotary evaporator. The content was then evacuated (10^{-3} bar) at 80°C for 6 h. It was then subjected to calcination. Later, the material was reduced at 300°C for 2 h in the presence of hydrogen (flow rate = 30 mL/min). A blue colored material, Au/γ-Al_2O_3 (Au = 2 wt%), thus, obtained was stored in a desiccator. The following scheme provides the details of calcination and reduction program used in the preparation.

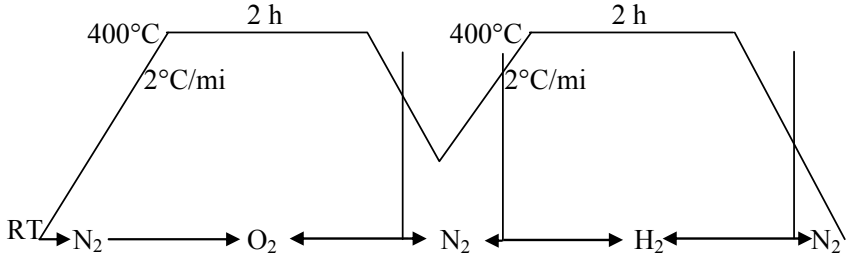

2.3. Characterization Methods

The catalysts were characterized by a number of physicochemical techniques including X-Ray powder diffraction (XRD), N_2 sorption, nuclear magnetic resonance (NMR), X-Ray photo electron spectroscopy (XPS), elemental analysis by inductively coupled plasma-optical emission spectroscopy (ICP-OES), temperature-programmed desorption of ammonia (TPD-NH_3), scanning electron microscopy (SEM) and transmission electron microscopy (TEM). Each technique is unique by itself and provides important information on the structural and textural features, metal concentration and acidity of the catalyst materials [8-13].

2.3.1. Inductively Coupled Plasma-Optical Emission Spectroscopy

Inductively coupled plasma-optical emission spectroscopy (ICP-OES) analysis was done on a Spectro Arcos instrument equipped with the winlab Software. Metals can be analysed by either a radial or an axial plasma configuration [15]. Standard solutions were used for the calibration purpose. In the case of zeolites, 0.05 g of solid acid was taken in the polypropylene bottle. 2 g of hydrofluoric acid, 2 g of water and ~0.01 g of conc. sulphuric acid were added to it. The mixture was heated at 80°C up to dryness. 5 g of water was added and the aqueous solution was collected. Then it was made to 50 mL and analyzed by using an ICP-OES instrument. In the case of supported metal catalyst, 0.05 g of the catalyst was taken in a beaker. About 5 g of aqua regia (conc. HNO_3 and conc. HCl in the molar ratio of 1:3) was added to it. Then, the contents were heated at 80°C till dryness. 20 g of water was added and the solution was recovered. Later, it was made up to 50 mL and then analyzed for metal content by ICP-OES.

2.3.2. X-Ray Powder Diffraction

XRD is the most important and commonly used technique to monitor the structure, phase purity, degree of crystallinity and unit cell parameters of crystalline materials. In this technique, the sample is prepared as a thin layer on a glass plate. The powder X-Ray diffractographs were recorded on a Rigaku Miniflex diffractometer using a Ni-filtered monochromatic Cu K_α radiation (λ = 1.5406 Å). The samples were scanned between a 2θ range of 5

and 90° at the scan rate of 2°/min. Silicon (2θ = 28.45°) was used as an external standard. The crystallite size was determined using the Scherrer equation, $L = k\lambda/\beta\cos\theta$, where L = crystallite size, k is a constant whose value is 0.9 -1.0, λ = wavelength of the X-Ray beam and β = full width at half maximum (FWHM) on the 2θ scale expressed in radians corrected for instrumental broadening as given: $\beta^2 = w_1^2 - w_2^2$ where w_1 and w_2 are the FWHM of the sample and silicon standard (111) line, respectively.

2.3.3. N_2 Sorption Study

The method for measuring the surface area of solids is based on the theory developed by Brauner, Emmett and Teller (BET) in 1938 considering the concept of multilayer adsorption. The general version of BET equation can be represented as [16]:

$$P/V\ (P_0-P) = 1/V_mC + [(C-1)/V_mC]\ (P/P_0)$$

where, P is the adsorption equilibrium pressure, P_0 is the saturation vapor pressure of the adsorbate at the experimental temperature, V is the volume of gas adsorbed at pressure P, V_m is the volume of adsorbate required for monolayer coverage and C is a constant that is related to the heat of adsorption and liquefaction. The specific surface areas of the catalysts were measured by N_2 sorption at liquid nitrogen temperature (-196°C) and at low pressure (10^{-7} bar) using a Nova 1200 and Autosorb 1C Quanta Chrome instruments, USA. Prior to measurements, the samples were dried under vacuum at 300°C for 2 h. The specific surface area was determined by using the BET method. The pore size distributions were calculated from both adsorption and desorption branches of the isotherms using HK method. Pore volume was determined by using the t-plot method [16].

2.3.4. Nuclear Magnetic Resonance Spectroscopy

Solid state NMR: Magic-angle spinning NMR is a powerful tool for structural elucidation of solid samples. The position of the NMR signal is sensitive to the nature and chemical environment of magnetic nuclei. The solid state ^{29}Si and ^{27}Al NMR spectra were recorded on a Bruker Avance-300MHz spectrometer, operated at a field of 7.06 tesla. A fine powder of the sample was placed in 4 mm zirconia rotor and spun at 10 kHz for both ^{29}Si

and ^{27}Al. The number of scans for ^{29}Si and ^{27}Al NMR were 5275 and 2800, respectively.

Liquid state NMR: Liquid state ^{1}H and ^{13}C NMR spectra were recorded on a Bruker DRX-300 NMR spectrometer with tetramethylsilane (TMS) as the internal standard. The distortionless enhancement polarization transfer (DEPT) spectrum was recorded under a Hartmann-Hahn match condition with a contact time of 1 sec and a relaxation delay of 4 sec.

2.3.5. X-Ray Photoelectron Spectroscopy

The binding energy (BE) from X-ray photoelectron spectroscopy (XPS) is often used to determine the oxidation state of the element. X-ray photoelectron spectra were recorded using an ESCA-3000 instrument (VG Scientific LTD, England) with a 9 channeltron CLAM4 analyzer under a vacuum better than $1x10^{-8}$ Torr, using Al-K_α (1486.6 eV) and constant pass energy of 50 eV. The binding energy value was charge-corrected to the C_{1s} signal (284.6 eV).

2.3.6. Scanning Electron Microscopy

Scanning electron microscopy (SEM) provides information on the morphology of the catalyst samples. It scans over a sample surface with a probe of electrons (5-50 eV) and detects the yield of either secondary or back-scattered electrons as a function of the position of the primary beam. Contrast is generally caused by the orientation of the surface. The surfaces facing the detector appear brighter than the surfaces that point away from the detector. The interaction between the electron beam and the sample produces different types of signals providing detailed information about the surface structure and morphology of the sample [17]. The SEM micrographs of the samples were obtained on a Leo Leica Cambridge UK Model Stereoscan 440 scanning electron microscope. The samples were loaded on stubs and sputtered with thin gold film to prevent surface charging and also to protect from thermal damage due to electron beam.

2.3.7. Transmission Electron Microscopy

Transmission electron microscopy (TEM) is typically used for high resolution (near atomic resolution) imaging of solid samples for

microstructural analysis. In addition to structural characterization, it can also be used to detect the location of metal clusters and its size. The technique involves: (i) irradiation of a very thin film of the sample by a high energy electron beam, which is diffracted by the lattices of a crystalline or semi-crystalline material and propagates along different directions, (ii) imaging and angular distribution analysis of the forward-scattered electrons (unlike in SEM where back scattered electrons are detected). TEM photographs were taken from a FEI TECNAI T20 Model instrument operated at an accelerating voltage of 200 kV. Samples for TEM measurements were prepared by placing droplets of homogeneously dispersion sample in iso-propanol on a polymer micro grid supported on a Cu grid.

2.3.8. Temperature-Programmed Desorption of Ammonia

Temperature-programmed desorption monitors the surface or bulk processes of solid catalysts in the presence of gaseous environment. Continuously, the gas phase composition is analyzed by thermal conductivity detector (TCD) as the temperature is raised linearly with time. The acidity of the catalysts was measured using NH_3 as a probe molecule. The TPD-NH_3 experiments were carried out on a Micromeritics AutoChem-2910 instrument. 0.1 g of the catalyst was activated at 600°C by raising the temperature at a rate of 4°C/min in helium flow (30 mL/min) for 1 h. The temperature was decreased to 50°C and NH_3 was adsorbed by exposing the samples to 10% NH_3 in helium for 1 h. It was then flushed with helium for another 1 h at 150°C to remove all the physisorbed NH_3. Desorption of NH_3 was carried out in helium flow (30 mL/min) by increasing the temperature from 150 to 600°C at the rate of 10°C/min. While desorption temperature can be related to the strength, the amount of ammonia desorbed gives an estimate of the concentration of acid sites.

2.4. Conclusions

The catalyst materials used in this work for the hydrolysis of hemicellulose and oxidation of furan chemicals were discussed. They were characterized by a range of physicochemical techniques including elemental analysis (ICP-OES), XRD, N_2 sorption, SEM, TEM and TPD-NH_3.

2.5. References

[1] R. Kumar, S. Singh, O. V. Singh, *J. Ind. Microbiol. Biotechnol.* **2008**, 35, 377.

[2] N. T. Mathew, S. Khaire, S. Mayadevi, R. Jha, S. Sivasanker, *J. Catal.* **2005**, 229, 105.

[3] P. T. Tanev, T. G. Pinnavaiva, *Science* **1995**, 267, 865.

[4] P. Souchay, *Ions Mineraux Condenses*, Masson Cie, Paris **1969**.

[5] M. T. Pope, *Heteropoly and Isopoly Oxometalates*, Springer, Berlin **1983**.

[6] I. V. Kozhevnikov, K. I. Matveev, *Russ. Chem. Rev.* **1982**, 51, 1075.

[7] G. Bergeret, *in Handbook of Heterogeneous Catalysis,* Vol. 2, Wiley-VCH, Weinheim **1997**.

[8] H. V. Bekkum, E. M. Flanigen, *Introduction to Zeolite Science and Practice,* Elsevier, Amsterdam **2001**.

[9] A. Corma, *Catal. Rev. Sci. Engg*. **1985**, 27, 29.

[10] A. Corma, H. Garcia, *Chem. Rev.* **2003**, 103, 4307.

[11] G. T. Kokotailo, C. A. Fyfe, *J. Phys. Chem.* **1989**, 50, 441.

[12] A. Corma, *Chem. Rev.* **1997**, 97, 2373.

[13] P. Ratnasamy, A. Kotasthane, V. Shiralkar, A. Thangaraj, S. Ganapathy, *in Zeolite Synthesis*, ACS, Symp. Series **1989**, 398, 405.

[14] S. Brunauer, P. H. Emmett, E. Teller, *J. Am. Chem. Soc*. **1938**, 60, 309.

[15] A. Montaser, D. W. Golightly, *Inductively Coupled Plasmas in Analytical Atomic Spectrometry*, VCH Inc., New York **1992**.

[16] J. M. Thomas, W. J. Thomas, *Principles and Practice of Heterogeneous Catalysis*, Wiley-VCH, Weinheim **1997**.

[17] J. I. Goldstein, H. Yakowitz, *Practical Scanning Electron Microscopy*, Plenum Press, New York **1975**.

CHAPTER-3

CATALYTIC CONVERSION OF HEMICELLULOSE INTO CHEMICALS

3.1. Introduction

In recent times, lignocellulose (a plant-derived biomass) is gaining more and more importance as a raw material for the synthesis of chemicals and fuels [1]. In 2004, the US Department of Energy (DOE) identified 12 chemicals, derived from biomass, which could be used as building block chemicals in a bio-based economy [2]. Shifting society's dependence from petroleum-based to renewable biomass-based resources is generally viewed as key to the development of a sustainable industrial society. The production of chemicals from biomass leads to lower greenhouse gas emissions. Further, many end-products and materials derived from biomass have no synthetic counterpart because they could not be produced economically by traditional methods (from the petroleum feedstock). Bio-based chemicals often have unique properties, for instance biodegradability, biocompatibility and the absence of eco- or human toxicity. Hemicellulose is the second largest component of the lignocellulosic biomass. The conversion of hemicellulose with high efficiency and low cost is a key issue in the industrial lignocellulosic biomass conversion processes [3, 4].

Typically, lignocellulose is composed of 40-50% of cellulose, 20-30% of hemicellulose, 20-28% of lignin and some percent of organic and inorganic materials (metals, terpenes, waxes, tannins and proteins) [5, 6]. Depending on the sources, the hemicellulose can be categorized into two types (i) softwood (coniferous)-derived hemicellulose and (ii) hardwood (deciduous)-derived hemicellulose. The chemical composition and structural aspects of these hemicelluloses are described below [7].

Softwood Hemicellulose. Softwood hemicellulose is a biopolymer containing a backbone having β-(1→4) linked xylopyranose units (Fig. 3.1). A α-D-glucose unit is attached to the backbone as a side chain via α-(1→2) linkage. L-Arabinose (on an average one unit per 5-12 xylose units) is also attached to the backbone through α-(1→3) linkages. Some branching is also observed at C_2 of the xylose units. Unlike in the case of hardwood hemicellulose, no substitution by acetyl groups is found in softwood hemicellulose [8-10]. Pruce, pine and oat spelt are the examples of softwood hemicellulose. In general, oat spelt hemicellulose is composed of ≥70% of

xylan, ≤ 10% of arabinose, and ≤ 15% of glucose. In this study, this material is taken as a substrate for the chemical synthesis.

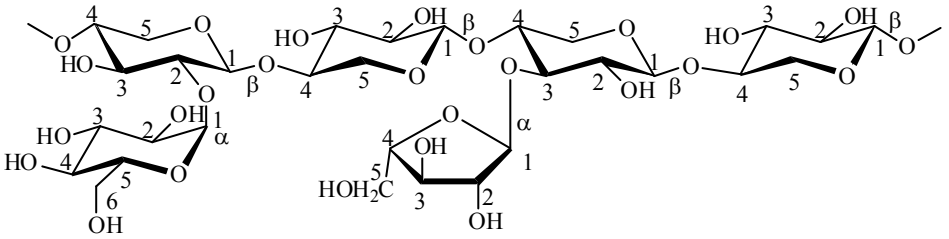

Fig. 3.1. Tentative structure of softwood hemicellulose.

Hardwood Hemicellulose. The backbone of hardwood hemicellulose consists of xylopyranose units connected via β-(1→4) linkages (Fig. 3.2). Most of the hydroxyl groups at C_2 and C_3 positions of the xylose units are substituted with acetyl groups. In addition, xylose units are also substituted with α-(1→2)-linked 4-O-methylglucuronic acid residues. In most of the hardwood xylans, on an average at every 10^{th} xylose unit there is one 4-O-methyl-D-glucuronic acid present. Hardwood hemicellulose does not contain arabinose side chains and is more symmetrical and has a high degree of polymerization. The xylan content is more than 90% in the hardwood (birch wood) hemicellulose [11].

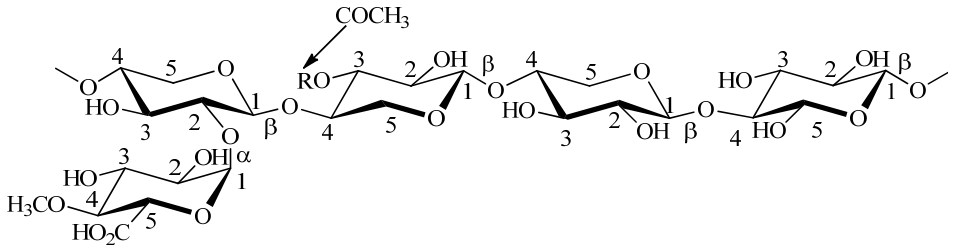

Fig. 3.2. Tentative structure of hardwood hemicellulose.

The percentage of hemicellulose and degree of polymerization (after isolation) can vary with the source. In hardwood-derived hemicellulose, the degree of polymerization is in the range of 100-200, whereas in softwood-derived hemicellulose this value is between 70 and 130 [12, 13]. Structurally, softwood hemicellulose is less symmetric in nature than hardwood hemicellulose.

3.2. Synthesis of Chemicals from Hemicellulose

Hemicellulose is a heteropolymer of C_5 and C_6 sugars (Scheme 3.1). When it is hydrolized, many sugars such as xylose, arabinose, mannose, glucose and galactose and acetic acid are liberated. Depending on the reaction

conditions, these sugars are converted into furan derivatives such as furfural and hydroxymeythyl furfural (HMF) [14, 15], formic acid and levulinic acids [16].

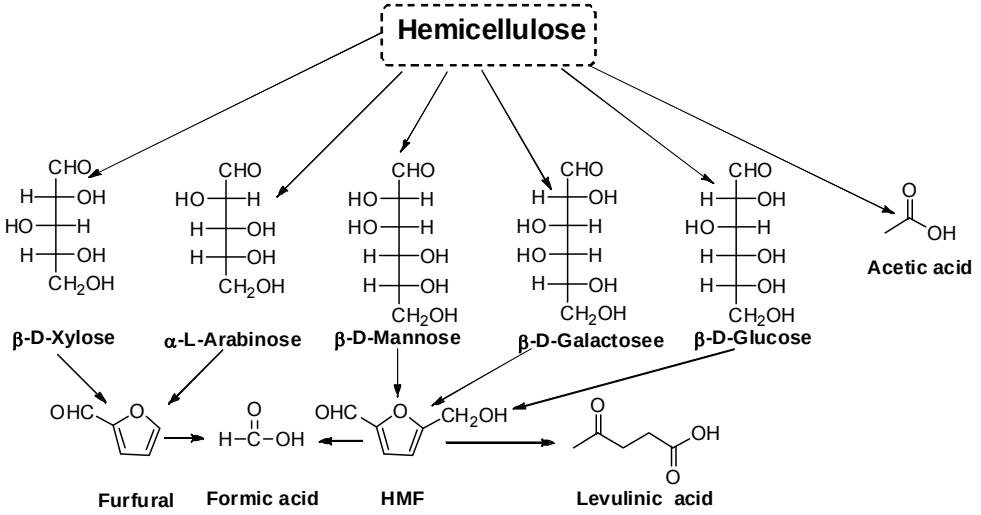

Scheme 3.1. Chemicals derived from hemicellulose.

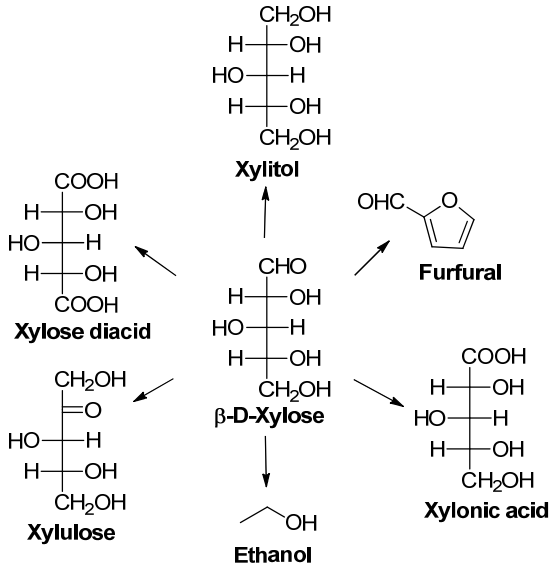

Fig. 3.3. Potential applications of xylose.

Xylose has been identified as an important platform chemical. Functional group transformations of xylose through oxidation and reduction are well-known. Xylose is also a very important raw material for the synthesis of xylitol which has several applications such as natural food sweetener, dental carries reducer and sugar substitute for diabetics (Fig. 3.3).

Hemicellulose can be hydrolyzed chemically or enzymatically. In chemical hydrolysis, the chemicals predominantly used are homogeneous mineral acids (H_2SO_4, HCl, H_3PO_4, etc.) [17-19] and alkali (NaOH) [7]. As

these chemicals are corrosive and special/expensive construction material (alloys or ceramic/carbon-brick material) has to be employed in the hydrolysis process. Acid recovery is also a high energy-demanding process. In addition, acid neutralization produces significant amount of hard water and salt by-product. Hence, the environmental impact strongly limits the application of this process. The enzymatic hydrolysis process can be carried out at mild operating conditions. Due to the complex nature of hemicellulose, its complete breakdown requires the action of a combination of several hydrolytic enzymes (endo-1, 4-β-xylanase, β-D-xylosidase, acetyl xylanesterase, α-glucoronidase and arabinase) with diverse modes of action and specificity [20-22]. Stability, recovery, pH control and long reaction times are issues with this enzymatic process. A two-step process for the conversion of hemicellulose into monomeric sugars is also reported [23], where in the first-step, hemicellulose is converted autocatalytically at 160°C into water-soluble oligomers, which are then, in the second-step, hydrolyzed to monomeric sugars in the presence of ion-exchange resins. An efficient solid-catalyst process for the conversion of hemicellulose in one-pot is desirable. This chapter reports the studies in this direction.

3.3. Materials and Methods

3.3.1. Chemicals

All the chemicals are of analytical grade and used without any further purification. Glucose, xylose, arabinose, formic acid and sugar alcohols were purchased from s.d. fine Chem., India. Levulinic acid, softwood (oat spelt) and hardwood (birch) hemicelluloses, furfural, HMF and various organic acids were purchased from Aldrich. All the chemicals procured have purity greater than 98%. The softwood-derived hemicellulose has the following chemical composition: ≥70% xylose, ≤10% arabinose and ≤15% glucose. The hardwood-derived hemicellulose has a xylose content of >90%. Deionised water was used in the reactions and in the preparation of various standard solutions.

3.3.2. Solid Acid Catalysts

Various solid acid catalysts including zeolites [HY (Si/Al = 2.6), HUSY (Si/Al = 15), HUSY (Si/Al = 40), HMOR (Si/Al = 10), Hβ (Si/Al = 19)

and HZSM-5 (Si/Al = 11.5)], Al-incorporated mesoporous silica [Al-MCM-41 (Si/Al = 50) and Al-SBA-15 (Si/Al = 50)], montmorillonite clay (K10), cesium-exchanged phosphotungstic acid (Cs-HPA) and metal oxides ($Nb_2O_5 \bullet H_2O$, γ-Al_2O_3 and sulphated zirconia) were used in the hydrolysis of hemicellulose. The preparation, procurement (in some cases) and physicochemical characterization of these catalysts are described in Chapter 2 (section 2.4). Prior to use in reactions, zeolites were pre-treated in air at 550°C for 12 h. The catalysts K10, $Nb_2O_5 \bullet H_2O$, Cs-HPA, γ-Al_2O_3 and sulphated zirconia were activated under vacuum (10^{-3} bar) at 80°C for 6 h.

Fig. 3.4. Experimental set-up (Parr reactor).

3.3.3. Experimental Set-up

All the reactions were carried out in a 100 mL Parr (USA) autoclave (Fig. 3.4). A known quantity of the substrate (softwood or hardwood-derived hemicellulose), catalyst (solid acid) and deionised water were charged into the reactor. It was purged three times with nitrogen gas to remove oxygen from the autoclave. Then, the reactor was pressurized with nitrogen (at 25°C) to 50 bar. The autoclave was heated to a desired temperature and the reaction was conducted for a desired period of time. Internal pressure was measured by means of a transducer. Reaction temperature was measured by means of a J-type thermocouple placed in contact with the reactants. The sample was withdrawn at desired time intervals. It was then centrifuged. Catalyst particles and any unconverted hemicellulose were separated. The liquid portion was

filtered through 0.22 µm syringe filter. It was then used for analysis by high performance liquid chromatography (HPLC). Mass balance was confirmed.

3.3.4. Analytical Procedure

The composition of the reaction mixture (liquid product) was determined using a Shimadzu HPLC system (Model No. CBM-102; Fig. 3.5) equipped with a syringe pump (Model No. LC-9A), carbohydrate Pb^{+2} column (length = 300 mm and I.D. = 7.8 mm) and refractive index detector (Model No. RID-6A). Degassed deionised water was used as the mobile phase and pumped at a flow rate of 0.6 mL/min. Oven (Model No. CTO-10ASVP) temperature was set at 80°C and the detector temperature was maintained at 40°C. The concentration of each compound in the reaction mixture was determined using standards and calibration curves. Further, the products (especially oligomers) were identified by using LC-MS.

Fig. 3.5. Shimadzu HPLC analytical system.

Product Estimation. Standard solutions (xylose, arabinose and furfural) were injected into a HPLC system. The slope was calculated and used to obtain total weight of xylose, arabinose and furfural in the product mixture. 0.6 g of softwood hemicellulose was taken as a substrate in the reactions. Softwood hemicellulose contains mainly (≥80%) the xylose and arabinose units. Glucose was present at ≤ 15 wt%. For simplicity, only the xylose + arabinose content was taken for the product yield calculations. Xylose and arabinose have a molecular formula of $C_5H_{10}O_5$ and molecular weight of 150. However, while forming a polymer, these units (xylose and arabinose) loose

water. Hence, the molecular weight of the repeating unit of hemicellulose polymer is 132. However, during hydrolysis, when hemicellulose is converted into xylose and arabinose, one molecule of water is added. Therefore, 0.6 g of hemicellulose will produce 0.6818 g of xylose and arabinose and 0.4363 g of furfural (molecular weight = 96). Glucose peak overlaps with that of oligomers. Hence, the glucose content in the product could not be calculated. Since no oligomer standards were available, the response factor of the oligomer was considered the same as that of xylose monomer. Conversion of hemicellulose was calculated by two methods: first based on the difference between total solid charged and that recovered after the reaction (weight basis) and secondly based on total products formed (as estimated from the HPLC analysis). Estimation from the latter method is always lower (by 5%) than the former method as certain oligomers (> pentamer) could not be detected by our HPLC system. The product yields were determined using the following equations.

$$\% \text{ Yield of oligomer} = \frac{\text{Weight of oligomer formed} \times 100}{\text{Weight of oligomer expected to form (0.6 g)}}$$

$$\% \text{ Yield of xylose + arabinose} = \frac{\text{Weight of xylose + arabinose formed} \times 100}{\text{Weight of xylose + arabinose expected to form (0.6818 g)}}$$

$$\% \text{ Yield of furfural} = \frac{\text{Weight of furfural formed} \times 100}{\text{Weight of furfural expected to form (0.4363g)}}$$

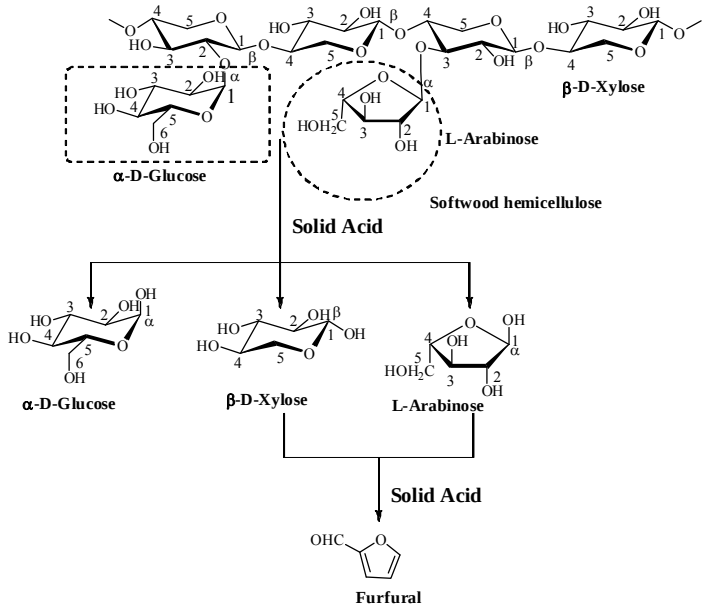

Scheme 3.2. Hydrolysis products of softwood hemicellulose.

3.4. Results and Discussion

3.4.1. Catalyst Characterization

3.4.1.1. X-Ray Powder Diffraction

Fig. 3.6 shows the XRD profiles of HY (Si/Al = 2.6), HUSY (Si/Al = 15) and HUSY (Si/Al = 40). All these three FAU (faujasite) materials are highly crystalline in nature and showed sharp reflections in the 2θ range of 5 - 50°. The following conclusions can be drawn from the XRD profiles:

(1) Upon dealumination, the overall intensity of the XRD peaks increased.

(2) The intensity of different peaks in HY (Si/Al = 2.6) decreased in the order: (533) > (311) > (111). However, for the dealuminated HUSY, intensity of these peaks decreased in the order: (111) > (331) > (533). This is possibly due to the change in the occupancy of exchangeable cations. Similar observations were found when HY was exchanged with different other transition or alkali metal ions [24].

(3) Crystallite size (CS) determined using Scherrer equation for different FAU samples decreased in the order: HY (Si/Al = 2.6; CS = 53.6 nm) > HUSY (Si/Al = 15; CS = 50.4 nm) > HUSY (Si/Al = 40; CS = 48.9 nm).

(4) A marginal shift of the peaks toward higher 2θ values (from 6.18 to 6.29°) was observed with an increase in Si/Al ratio.

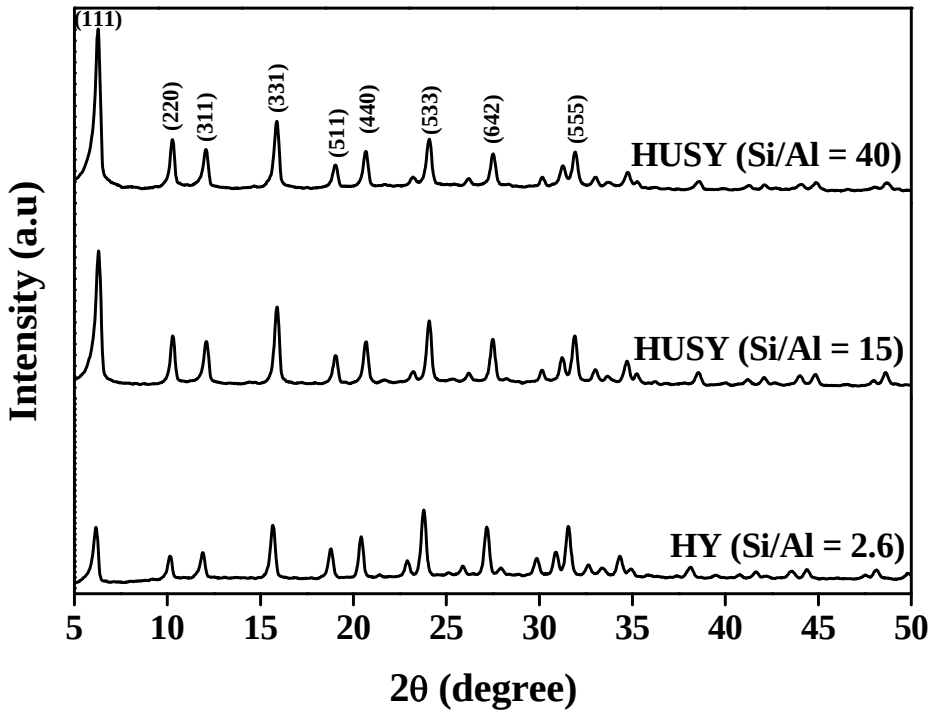

Fig. 3.6. XRD profiles of zeolites HY and HUSY.

Fig. 3.7 depicts the XRD pattern of zeolite Hβ (Si/Al = 19) which is characterized by a combination of sharp and broad (or diffuse) reflections suggesting that structural disorder pervades the framework. Higgins et al [19] determined the lattice geometry of Hβ based on electron and X-Ray diffraction data. It was reported that three ordered polytypes (A, B and C) are present in the structure of Hβ. The sharp reflections in the X-Ray pattern can be indexed based on a tetragonal lattice ($P4_122$) and two different monoclinic lattices (C2/c and P2) which correspond to the A, B and C ordered polytypes, respectively. The sample used in this study is composed of all these polytypes. The average crystallite size of zeolite Hβ was determined to be 37.6 nm.

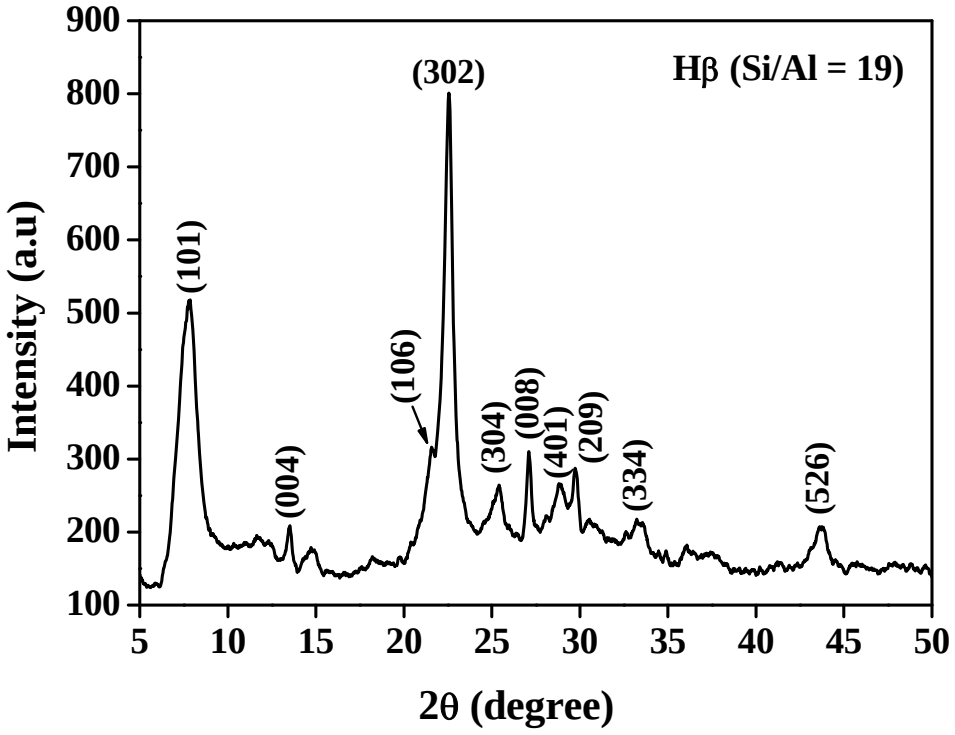

Fig. 3.7. XRD pattern of Hβ.

XRD pattern of HZSM-5 (Si/Al = 11.5) with MFI topology is shown in Fig. 3.8. The assignments of various peaks are also provided in the figure. The diffraction pattern can be interpreted based on an orthorhombic crystal system. The material is highly crystalline and the average crystallite size estimated based on the most intense peak is 37.6 nm.

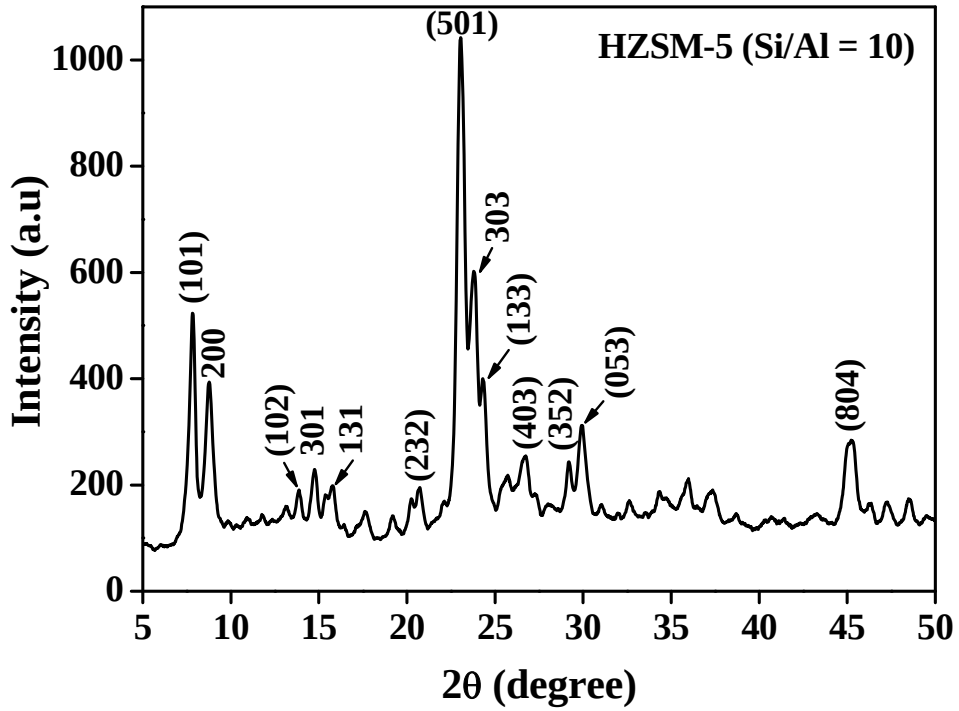

Fig. 3.8. XRD profile of HZSM-5.

Fig. 3.9 provides the XRD pattern of HMOR (Si/Al = 10). The material is highly crystalline and the crystallite size estimated from the (202) reflection based on Scherrer equation is 56.8 nm. K10 clay (Fig. 3.10) showed the first peak at 2θ = 8.9°, which is assigned to the basal reflection from (001). Several peaks were observed in the diffractogram of as-purchased K10. The peaks located at 20, 35, 54 and 62° were assigned to the diffraction peaks of (110), (105), (210) and (300) reflections of montmorillonite, respectively. The diffraction pattern totally agrees with that reported in the literature for the K10 clay [25, 26]. The XRD pattern of Cs-exchange heteropoly acid (Fig. 3.11) is similar to its parent sample. The crystallinity of the samples was not significantly affected during the cesium metal exchange process, the relative intensities of the prominent lines decreased by 10% compared to that of the parent sample. The average crystallite sizes of K10 and Cs-exchanged heteropoly acid were estimated to be 50.2 and 26.6 nm, respectively.

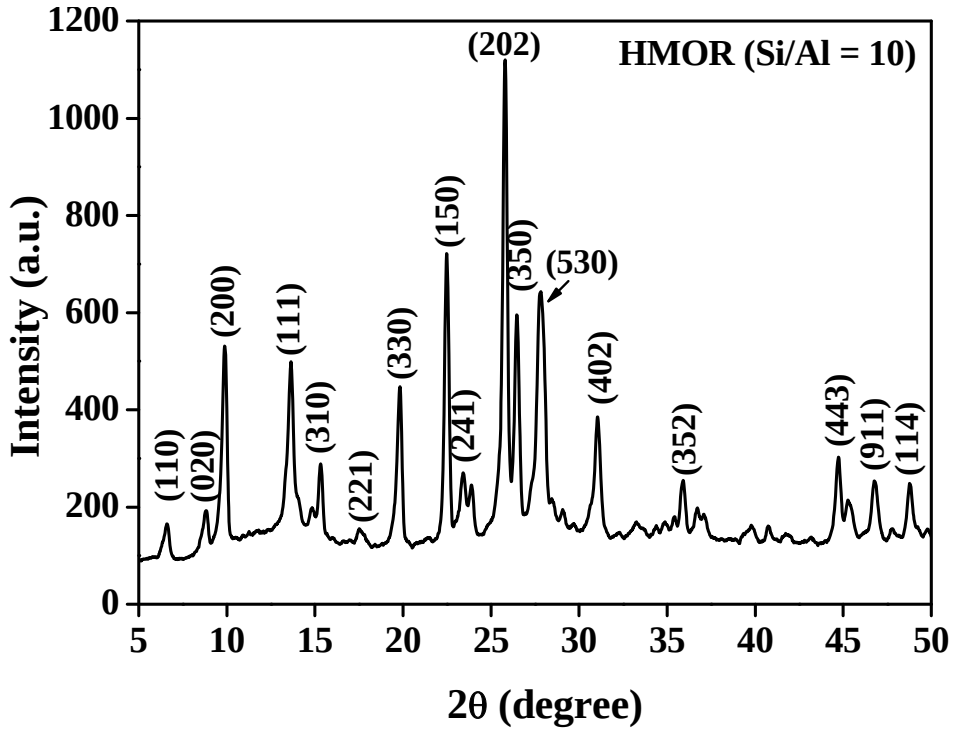

Fig. 3.9. XRD pattern of HMOR.

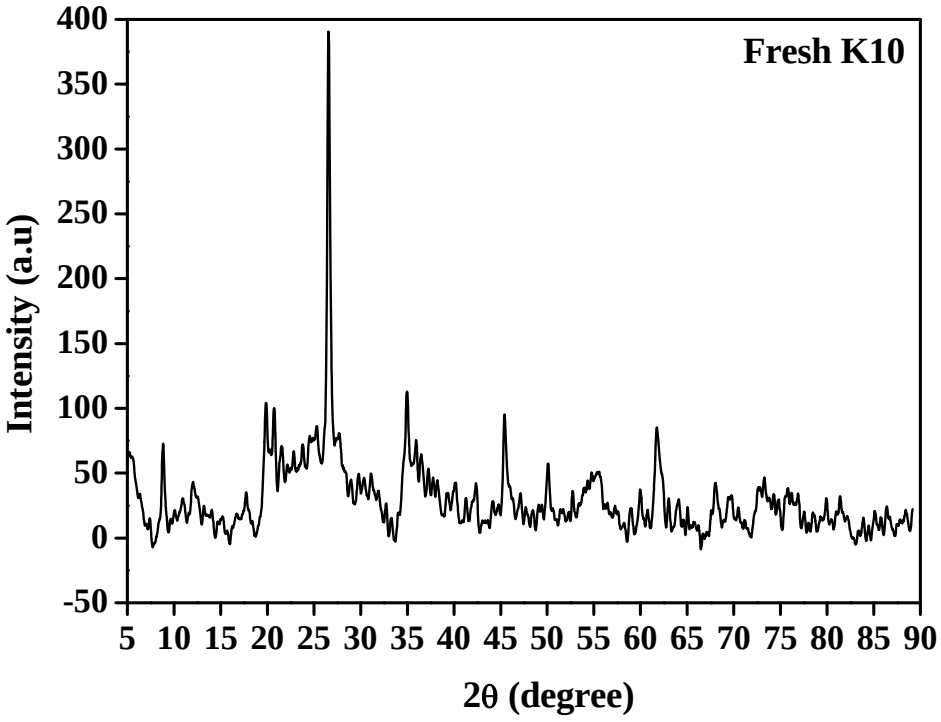

Fig. 3.10. XRD pattern of K10 clay.

Table 3.1. Chemical composition, structural and textural properties of solid acid catalysts

Catalyst	Si/Al molar ratio		Crystallite size (nm, XRD)	Particle size (μm, SEM)	Pore mouth dimension (Å)[a]	N_2-physisorption						
	As specified by the supplier	From ICP-OES				BET surface area (m^2/g)			Pore volume (mL/g)		Pore size (Å)	
						Total	External	Micropore	Total	Micropore	Average	HK
HY	2.6	3.4	53.7	0.6 – 0.8	7.4 x 7.4	767	53	714	0.37	0.29	19.2	6.2
HUSY	15	14.2	50.4	0.6 – 1	7.4 x 7.4	873	92	780	0.45	0.32	20.5	6.1
HUSY	40	42.6	48.9	0.6 – 0.8	7.4 x 7.4	909	87	821	0.47	0.35	20.4	6.1
Hβ	19	20.2	37.6	0.6 – 0.8	6.6 x 7.7	761	53	708	0.34	0.28	18.0	6.1
HMOR	10	11.3	56.8	0.6 – 1.2	6.7 x 7.0	528	17	511	0.22	0.20	16.6	6.1
HZSM-5	11.5	10.6	37.6	0.6 – 1.2	5.1 x 5.5	405	38	367	0.22	0.15	21.6	6.0
K10	-	-	50.2	2 – 3	-	246	228	18	0.30	0.002	48.1	6.1
Cs-HPA	-	-	26.3	0.1 – 0.2	-	-	-	-	-	-	-	-

[a]From the International Zeolite Association site (http://www.iza.com)

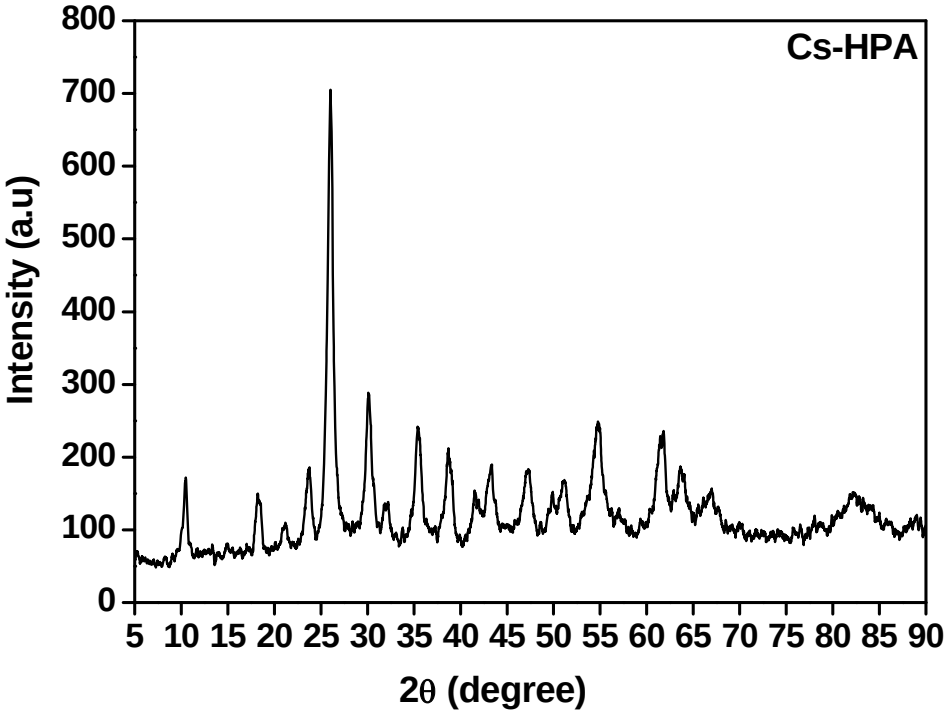

Fig. 3.11. XRD pattern of Cs-exchanged heteropoly acid.

3.4.1.2. N_2 Sorption Study

Table 3.1 lists the textural properties of different solid acid catalysts determined from N_2-physisorption studies. Adsorption-desorption isotherms of a few representative samples are shown in Fig. 3.12.

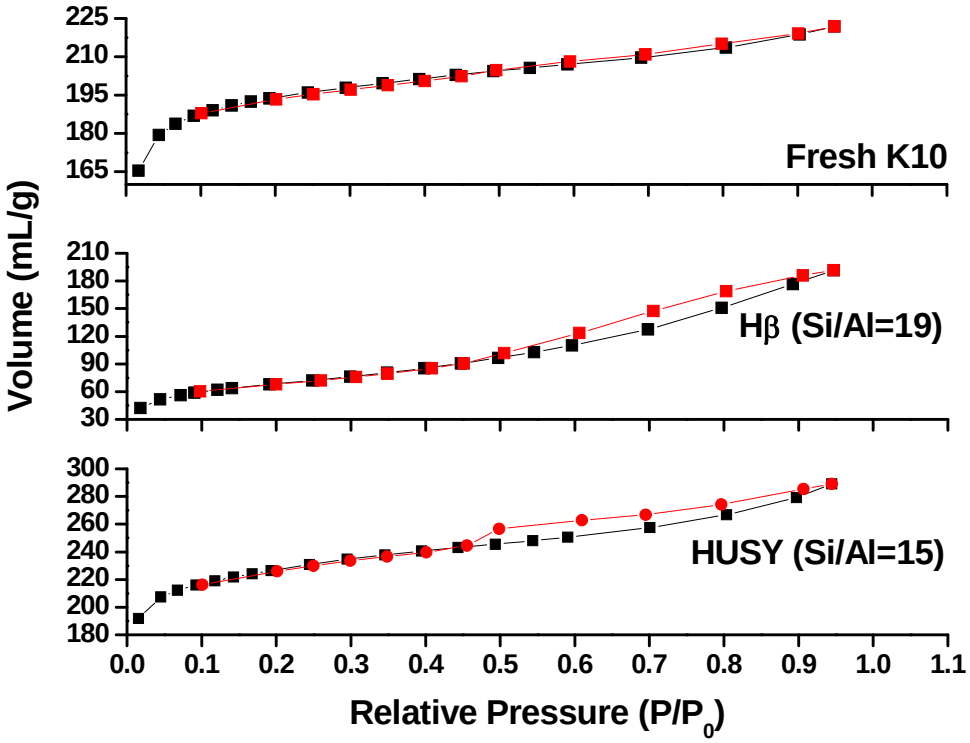

Fig. 3.12. N_2 sorption isotherms of solid acid catalysts.

Based on the data reported in Table 3.1 the following conclusions can be made:

(1) Among the Y-type zeolites, the specific surface area (SA) increased with increasing Si/Al molar ratio: HUSY (Si/Al = 40; SA = 909 m^2/g) > HUSY (Si/Al = 15; SA = 873 m^2/g) > HY (Si/Al = 2.6; SA = 767 m^2/g). This agrees well with the change in the crystallite size of these materials estimated from the XRD measurements. The SA of HY matches well with that reported by the zeolite supplier.

(2) Also an increase in the pore volume (PV) from 0.37 to 0.47 mL/g was observed for the Y zeolites with increasing Si/Al ratio.

(3) The adsorption-desorption isotherms depicted some hysteresis in dealuminated HUSY samples in the P/P_0 region of 0.5 to 1.0 which is not the case in HY (Si/Al = 2.6). This indicates that a few mesoporous cavities must have been created during the dealumination process.

(4) The surface area and pore volume of different zeolites of the present investigation decreased in the order: HUSY > HY ≥ Hβ > HMOR > HZSM-5. Hence, the structure and morphology of the zeolite plays a crucial role on its textural properties.

The Si/Al contents of various solid acid catalysts estimated from ICP-OES analysis are listed in Table 3.1. These values compare well with those quoted by the zeolite supplier.

3.4.1.3. Temperature-Programmed Desorption of Ammonia

The TPD-NH_3 profiles of all the solid acid catalysts of the present study consist of two overlapping peaks in the temperature range of 150-600°C. These were deconvoluted into a low temperature peak with maximum at 150-300°C and a high temperature peak with maximum at 350-500°C (zeolites) and 450-600°C (heteroply acid) (Fig. 3.13). These two NH_3 desorption peaks were assigned to weak and strong acid sites, respectively. The amounts of ammonia desorbed from these two types of acid sites are listed in Table 3.2. In zeolites, the acidity relates to the amount of Al present in the catalyst sample. As expected, the total acidity of Y-zeolites increased with increasing Al content. The relative ratio of strong to weak acid sites is higher in the case of dealuminated zeolites Y samples. HUSY (Si/Al = 15) has the highest number of strong acid sites than HY (Si/Al = 2.6). In the case of HY (Si/Al = 2.6),

aluminium is present both in the framework and extraframe work locations. While the former leads to strong acid sites, the latter leads to weak (Lewis-type) acid sites. In dealuminated samples, Al is present mainly in the framework locations leading to mainly the strong acidity. Among various solid acids, the total acidity decreased in the order: HY (Si/Al = 2.6) > HMOR (Si/Al = 10) > HZSM-5 (Si/Al = 11.5) > Hβ (Si/Al = 19) > HUSY (Si/Al = 15) > K10 > Nb_2O_5 > HUSY (Si/Al = 40) > Cs-HPA (Table 2.4). In spite of having higher aluminium content, HUSY (Si/Al = 15) has lower amount of total acidity than Hβ (Si/Al = 19). While the reason for this is not obvious at this point of time, perhaps the structure type too has a role on the acidity of the materials. The relative ratio of strong to weak acid sites in different solids decreased in the order: HUSY (Si/Al = 15) > K10 > HUSY (Si/Al = 40) > Hβ (Si/Al = 19)> HZSM-5 (Si/Al = 11.5) > HMOR (Si/Al = 10) > HY (Si/Al = 2.6) (Table 3.2). The zeolites Hβ, HMOR and HZSM-5 have the highest number of strong acid sites but their percentage is lower for HUSY (Si/Al = 15) (Table 3.2). All these differences in acidity are expected to influence the hydrolysis activity of these catalysts in the conversion of biomass into sugars and other products.

Table 3.2. Acidity of the catalysts

Catalyst	Total acidity mmol/g	Acidity distribution (mmol/g)		[Strong]/ [weak] acid sites
		Strong acid sites	Weak acid sites	
HY (Si/Al = 2.6)	1.50	0.20	1.30	0.15
HUSY (Si/Al = 15)	0.55	0.49	0.06	8.16
HUSY (Si/Al = 40)	0.20	0.15	0.05	3.00
Hβ (Si/Al = 19)	0.91	0.66	0.25	2.66
HMOR (Si/Al = 10)	1.15	0.65	0.50	1.30
HZSM-5 (Si/Al = 11.5)	0.98	0.61	0.37	1.67
K10	0.42	0.33	0.09	3.66
Cs-HPA	0.18	0.18	0	-
$Nb_2O_5 \cdot H_2O$	0.30	-	0.30	-

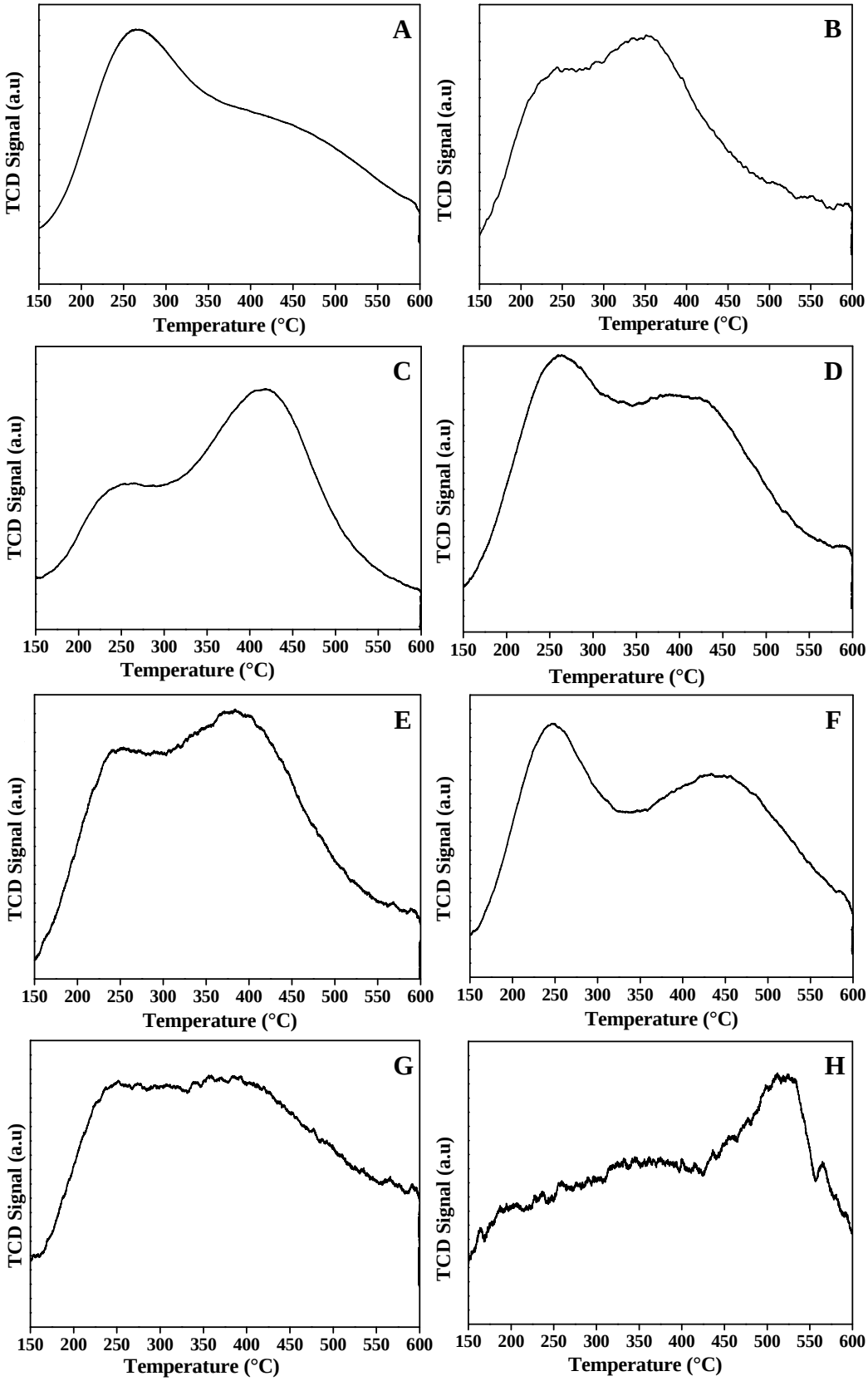

Fig. 3.13. TPD-NH_3 profiles of (A) HY (Si/Al = 2.6), (B) HUSY (Si/Al = 15), (C) HUSY (Si/Al = 40), (D) Hβ (Si/Al = 19), (E) HMOR (Si/Al = 10), (F) HZSM-5 (Si/Al = 10), (G) K10 and (H) Cs-HPA.

3.4.1.4. Scanning Electron Microscopy

Representative SEM photographs of HUSY (Si/Al = 15), K10, Hβ (Si/Al = 19) and Cs-HPA are presented in Fig. 3.14. The particle sizes estimated from SEM are listed in Table 3.1. The Y-type zeolites have a cuboidal / hexagonal morphology with particle sizes in the range 0.6 x 1 μm. Zeolite Hβ particles have a near spherical morphology with particle diameter in the range 0.6 - 0.8 μm. HMOR and HZSM-5 particle are of 0.6 - 1.2 μm dimension. K10 has no definite morphology but the particle size is larger than the zeolite catalysts. Cs-HPA particles have dimension of 0.1 - 0.2 μm.

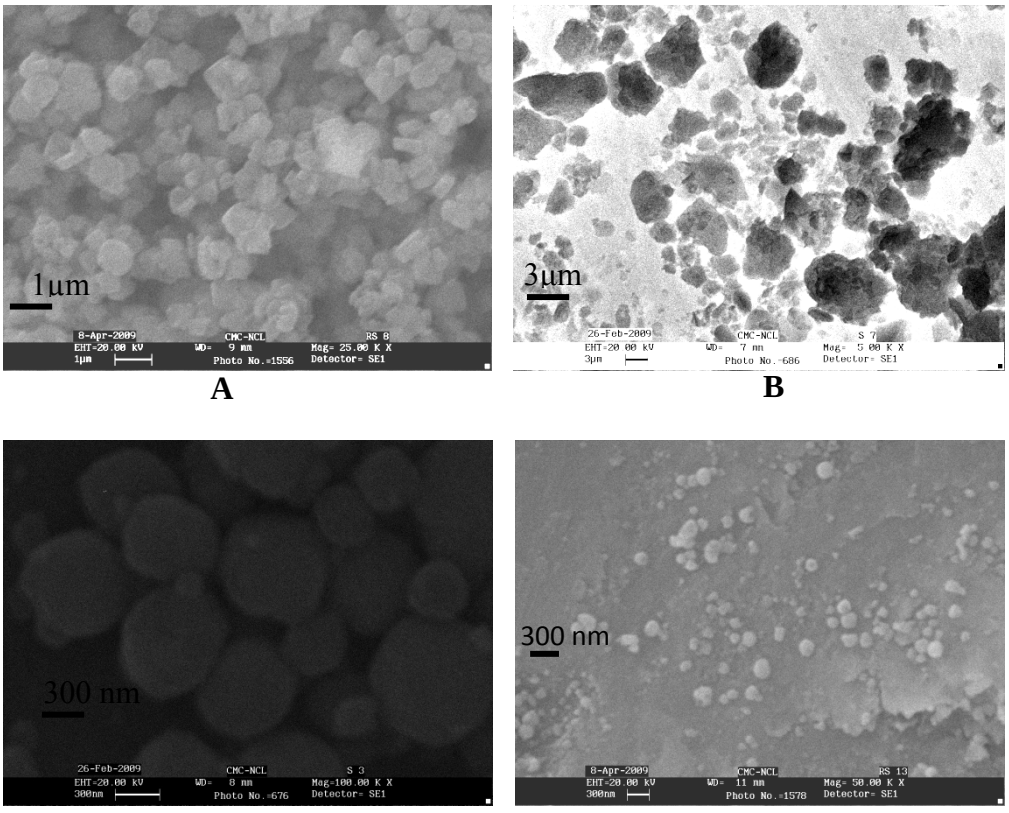

Fig. 3.14. SEM photographs of **(**A) HUSY (Si/Al = 15), (B) K10, (C) Hβ (Si/Al = 19) and (D) Cs-HPA.

3.4.1.5. Structures of Solid Acid Catalysts

The HY zeolite is formed by large supercages (~ 13 Å diameters) accessed through 12-membered silicate rings with 7.4 x 7.4 Å diameter, much smaller sodalite cages accessed through 6-membered silicate rings, and hexagonal prisms connecting the sodalite cages. The sodalite cage (or β-cage) consisting of 24 T atoms (six 4-rings, four 6-rings, three 6-2 units or four 1-4-1 units) is shown in Fig. 3.15. The two-dimensional periodic building unit (PerBU) is obtained when β-cages are linked

through double 6-rings (D6Rs) into the hexagonal HY layer [27]. Zeolite HY crystallizes in a cubic unit cell.

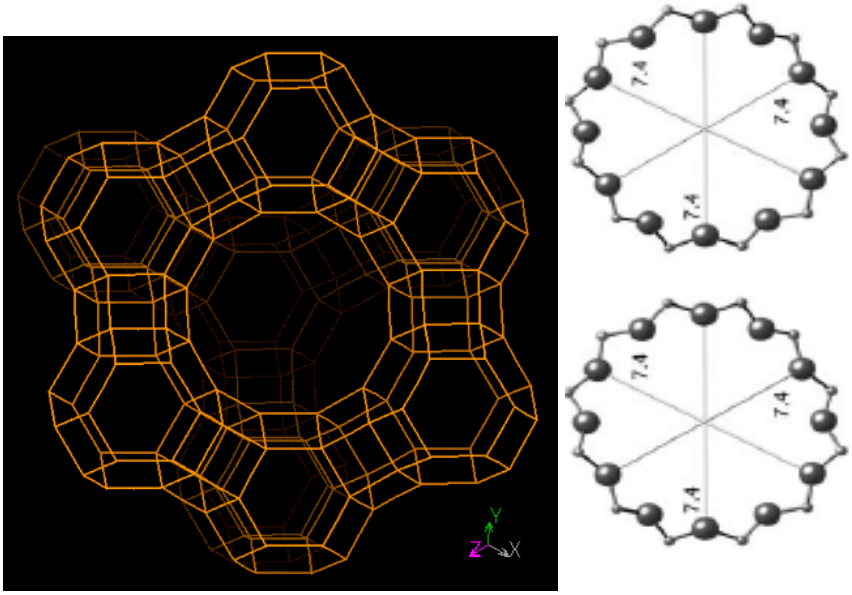

Fig. 3.15. Structure of HY zeolites.

The framework of BEA zeolites gives rise to two different channel types, both formed by 12-membered rings but with definitely different diameters, one (5.5 x 5.5 Å) in the medium pore range and the other (7.6 x 6.4 Å) in the large pore range. Hβ is a disordered, three-dimensional structure. The PerBU is composed of T16 units (four fused 6-rings or eight fused 5-rings). This zeolite belongs to the class of tetragonal symmetry (Fig. 3.16) [27].

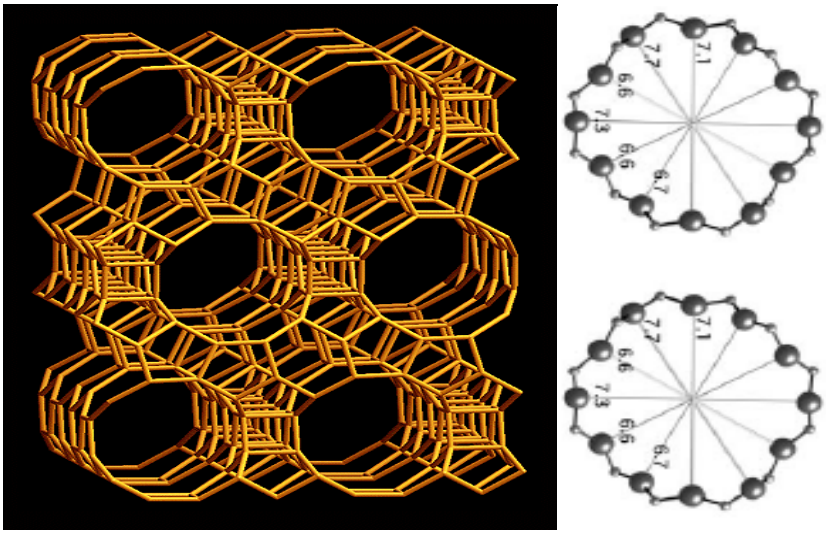

Fig. 3.16. Structure of Hβ zeolites.

MOR has a one-dimensional, 12-membered silicon-oxygen ring with a pore of 7.0 x 6.5 Å in diameter. Finite building units of 12 T atoms are composed of two 5-1

units. Additionally, 8-ring "side pockets" exist in the (010) direction, the opening of which is 3.4 x 4.8 Å. The side pockets connect the main channels to a distorted 8-ring "compressed" channel also running parallel to the (001) direction, but having an elliptical small opening, 5.7 x 2.6 Å wide. The orthorhombic mordenite structure is characterized by nearly straight channels running along the (001) crystallographic direction (Fig. 3.17) [27].

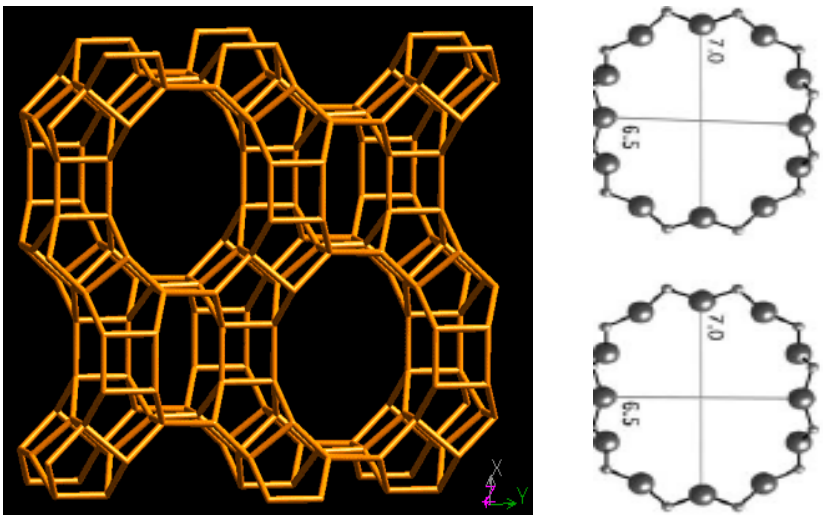

Fig. 3.17. Structure of HMOR zeolite.

ZSM-5 is a medium pore zeolite (Fig. 3.18). Its framework [27] shows a two-dimensional pore system consisting of two intersecting sets of tubular channels both formed by 10-membered silicate rings.

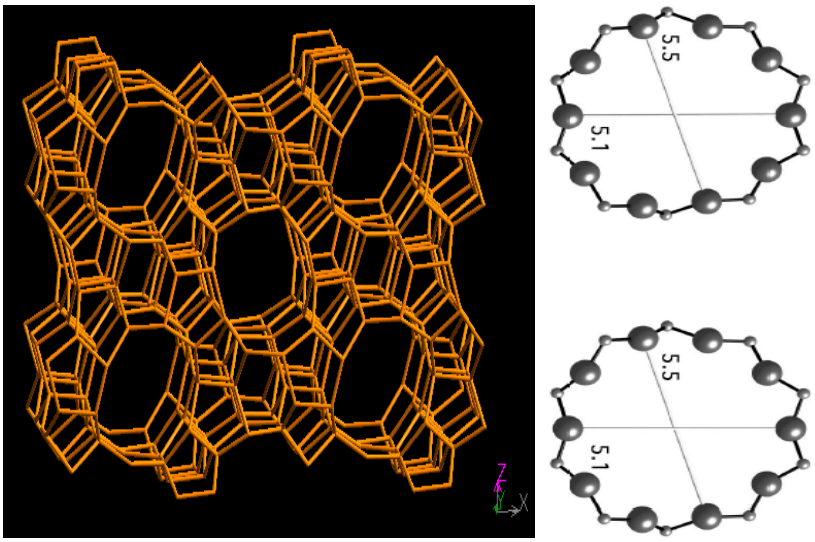

Fig. 3.18. Structure of HZSM-5 zeolite.

One channel type is straight and has a nearly circular opening (5.3 x 5.6 Å) along (010), whereas the other one is sinusoidal and has an elliptical opening (5.1 x

5.5 Å) along (100). ZSM-5 can be built using units of 12 T atoms. T12-units consist of two 5-1 units. ZSM-5 material has orthorhombic crystal symmetry.

Montmorillonite clay is a hydrated 2:1 layered dioctahedral aluminosilicate of the smectite group of clays (Fig. 3.19). It is composed of two tetrahedral (predominantly silicate) sheets which are bonded to either side of an octahedral (predominantly aluminate) sheet. Isomorphous substitution of Mg^{2+} for the octahedral aluminium, and of Al^{3+} for the tetrahedral silicon, results in charge deficit. This layer charge is balanced by hydrated exchangeable cations (e.g. Na^{+} or Ca^{2+}) which occupy the surfaces between clay layers, termed the interlayer [28, 29].

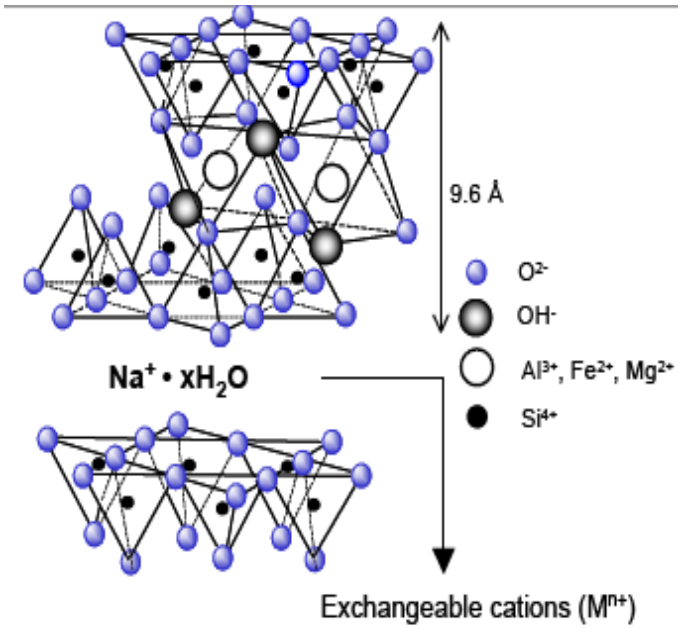

Fig. 3.19. Structure of montmorillonite (K10).

Heteropoly acid consists of large polyanions that are linked together. This polyanionic Keggin structure specially the α-type has T_d symmetry and consists of a centrally located XO_4 tetrahedron (X = central atom) surrounded by twelve edge and corner sharing MO_6 octahedra (M = addenda atom). The octahedral are arranged in four M_3O_{13} groups. Each group is formed by three octahedra sharing edges and having a common oxygen atom which is also shared with the central tetrahedron XO_4 (Fig. 3.20) [30].

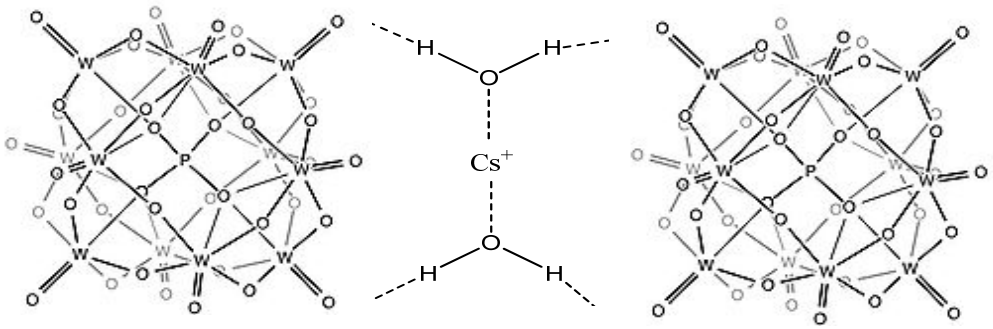

Fig. 3.20. Structure of Cs-HPA.

3.4.2. Catalytic Activity

Fig. 3.21 shows the catalytic performance of several solid acid catalysts in the hydrolysis of isolated, softwood-derived hemicellulose. The reactions were conducted at 130°C for 48 h. The products of the reaction were classified into three groups: (1) water-soluble oligomeric sugars (dimers to pentamers), (2) monomeric sugars (xylose and arabinose) and (3) furfural (Scheme 3.2). HUSY (Si/Al = 15), HMOR (Si/Al = 10) and Hβ (Si/Al = 19) exhibited higher catalytic performance than the rest of the catalysts. HZSM-5 (Si/Al = 11.5) showed the lowest activity. Controlled experiments at the same reaction conditions revealed that the hydrolysis reaction of hemicellulose occurs even without a catalyst, but oligomers were the main products; xylose + arabinose formed with a yield of about 5% only. Acid catalysts enhanced the enhanced the formation of monomeric sugars, which in the presence of Hβ (Si/Al = 19) formed with a yield of 46%. Further conversion of xylose + arabinose to furfural is higher over K10 and Nb_2O_5 than with the rest of the catalysts.

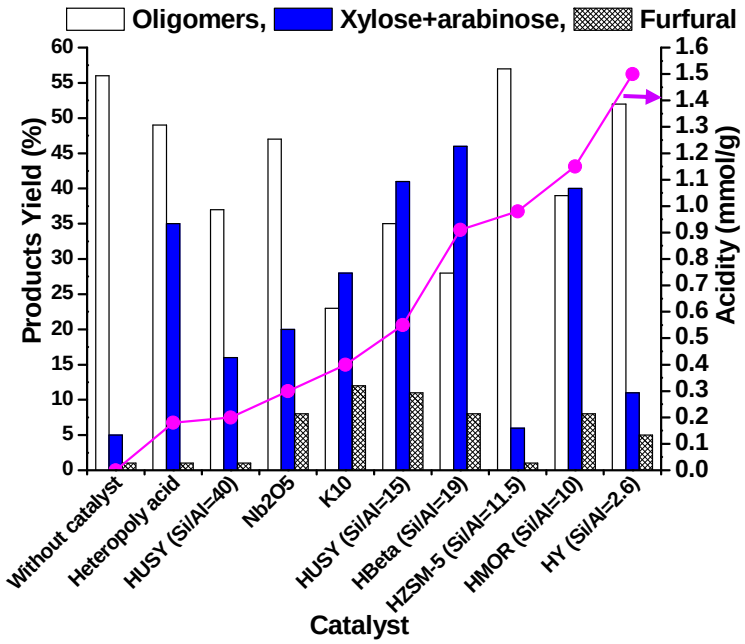

Fig. 3.21. Hydrolysis of softwood hemicellulose over different solid acid catalysts. *Reaction conditions:* softwood hemicellulose (0.6 g), catalyst (0.3 g), water (60 g), N_2 pressure (50 bar @ RT), reaction temperature (130°C) and reaction time (48 h).

3.4.2.1. Influence of Reaction Parameters

3.4.2.1.1. Effect of Time

Fig. 3.22 shows the hydrolysis activity of HUSY (Si/Al = 15) as a function of reaction time. This figure is typical of several consecutive reactions involved in the hydrolysis of hemicellulose. Hemicellulose is converted into several long-chain oligomers, which are further converted sequentially to penta-, tetra-, tri- and dimers. These dimers are hydrolyzed and give the monomeric sugars. Sugars upon dehydration yield furfural. The oligomeric products (dimers to pentamers) are water soluble and detectable by HPLC technique. At the end of 6 h, pentamer was the main product. As the reaction progressed, the xylose + arabinose content increased and at the end of 48 h, it was the highest selective product. Yield of furfural (a dehydration product of sugars) was also increased with time.

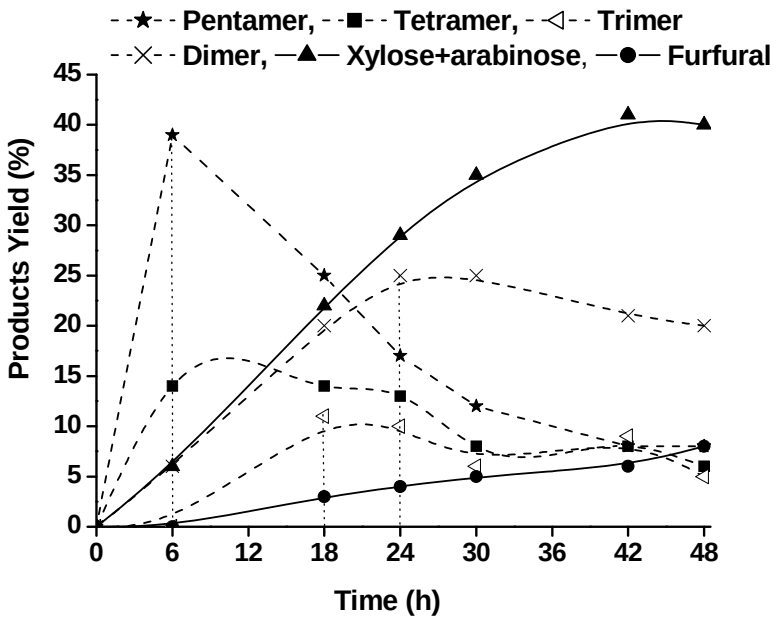

Fig. 3.22. Effect of reaction time on softwood hemicellulose conversion over HUSY (Si/Al=15). *Reaction conditions:* Softwood hemicellulose (0.6 g), HUSY (0.3 g), water (60 g), N_2 pressure (50 bar at 25°C) and reaction temperature (130°C).

3.4.2.1.2. Effect of Reaction Temperature

Temperature has a major effect on rate of hemicellulose conversion (Fig. 3.23). At 170°C, a xylose + arabinose yield of 41% and furfural yield of 11% were obtained in just 3 h over HUSY (Si/Al = 15) catalyst. However, 48 h was needed to get these yields of the products at 130°C. Hence, higher the temperature higher was the catalytic activity and rate of hemicellulose conversion. At a temperature higher than 130°C, the conversion of monomeric sugars to furfural was insignificant.

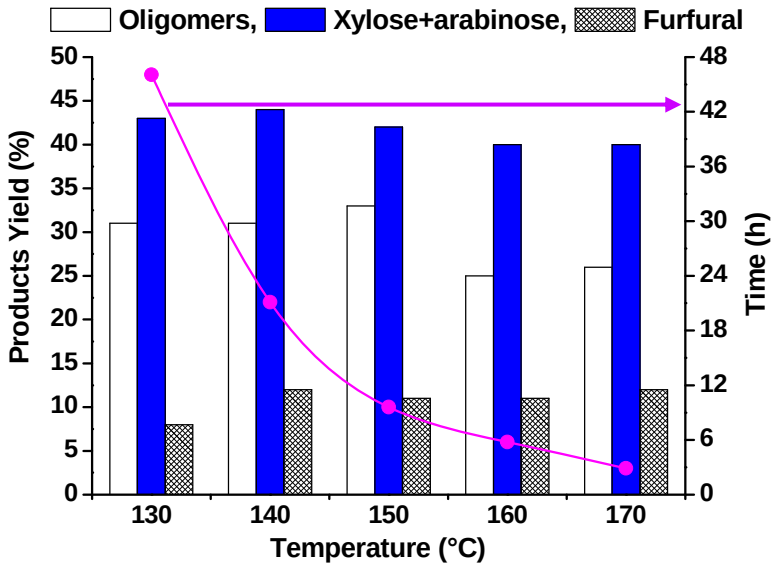

Fig. 3.23. Effect of temperature on the rate of hemicellulose conversion. *Reaction conditions:* Softwood hemicellulose (0.6 g), HUSY (Si/Al = 15) (0.3 g), water (60 g), N_2 pressure (50 bar @ RT).

3.4.2.1.3. Effect of Pressure

The effect of pressure on the conversion of softwood hemicellulose (0.6 g) over HMOR (Si/Al = 10; 0.3 g) was studied at 130°C (reaction time = 24 h). 60 g of water was taken in this reaction. Upon increasing the pressure (from 1 to 5 bar), the xylose + arabinose yield increased from 20 to 34%. Any further increase in pressure did not lead to significant increase in the product yield. Hence, at least 5 bar pressure is essential to get a maximum yield of the sugars. Pressure keeps the reactants (water and oligomers) in liquid phase and enhances their contact with the active sites on the catalyst surface.

3.4.2.1.4. Effect of Stirring Speed

Hydrolysis of hemicellulose was conducted at two stirring speeds (500 and 1000 rpm) over HUSY (Si/Al = 15). As seen from Fig. 3.24, the stirring speed has an impact on the product (xylose + arabinose) yield, at least in the initial stages. The product yield was higher when the reaction was performed at a stirring speed of 1000 rpm. However, at 48 h, the yield was the same irrespective of the stirring speed. Stirring speed affects the miscibility of reactants and enhances the contact of reactants with catalyst particles.

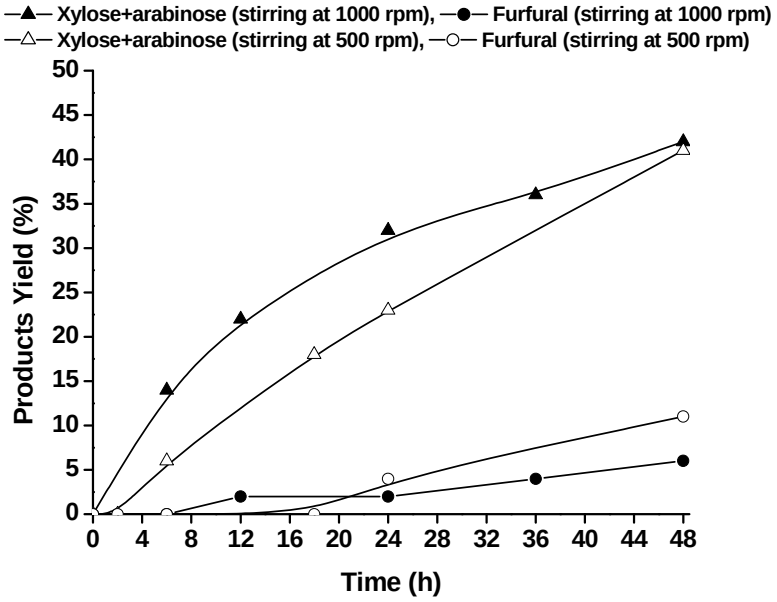

Fig. 3.24. Effect of stirring speed in the conversion of hemicellulose. *Reaction conditions:* Softwood hemicellulose (0.6 g), HUSY (Si/Al = 15, 0.3 g), water (60 g), N_2 pressure (50 bar @ RT), temperature (130°C), reaction time (48 h).

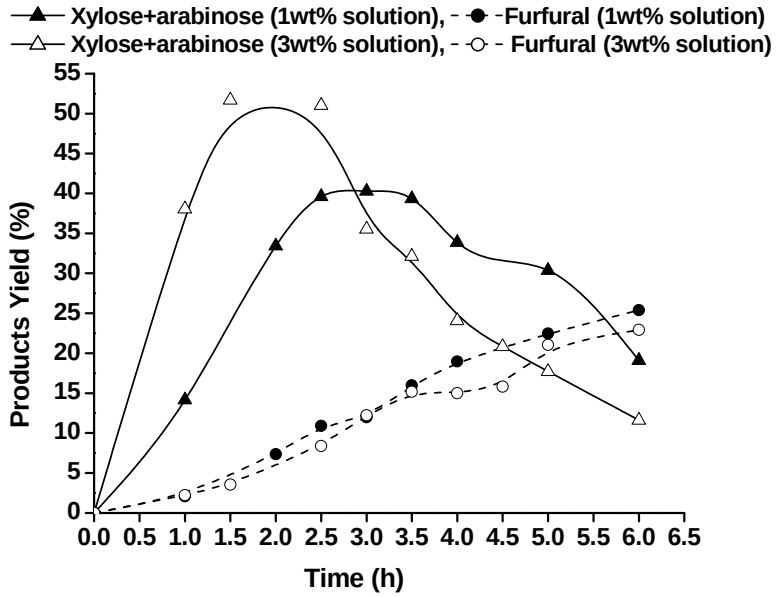

Fig. 3.25. Effect of hemicellulose concentration on its conversion. *Reaction conditions:* Softwood hemicellulose (0.6 or 1.8 g), water (60 g), HUSY (Si/Al = 15, 0.3 or 0.9 g), temperature (170°C), reaction time (6 h).

3.4.2.1.5. Effect of Hemicellulose Concentration

Fig. 3.25 shows the product yield verses time plots for the reactions conducted with 1 and 3 wt% hemicellulose concentrations. At higher concentrations (3 wt%), the time required for getting maximum sugar yield was shorter. With 1 wt%

hemicellulose concentration in water, a xylose + arabinose yield of 41% was obtained in 3 h. However, with 3 wt% hemicellulose in water, a product yield of 51% was obtained in 1.5 h itself. It may be noted that although in this experiment, the substrate to catalyst ratio was maintained the same, the catalyst concentration with respect to total reaction volume was changed.

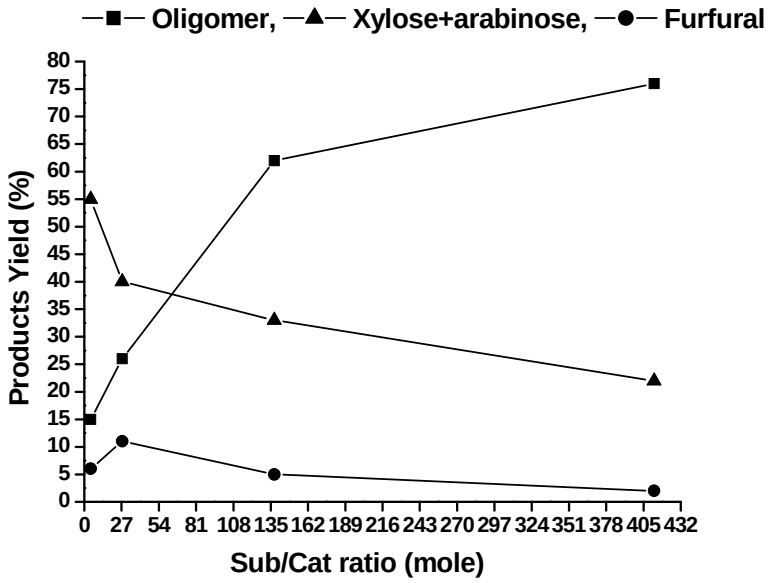

Fig. 3.26. Effect of hemicellulose/catalyst ratio on the product yield. *Reaction conditions:* Softwood hemicellulose (0.6 g), HUSY (Si/Al = 15, 1.8 - 0.003 g), water (60 g), temperature (170°C), reaction time (3 h).

3.4.2.1.6. Effect of Substrate/Catalyst Ratio

The mole ratio of hemicellulose to catalyst (Sub/Cat) was varied between 4.5 and 415 by keeping all other parameters (temperature, pressure, solvent, stirring speed and substrate) the same and the results are presented in Fig. 3.26. The mole ratio was calculated based on weight of hemicellulose taken and the molar concentration of the acid sites (from TPD analysis) present in the catalyst HUSY (Si/Al = 15). A xylose + arabinose yield of 41% was observed at sub/cat mole ratio of 25. Yield of 55% of these sugars was obtained at sub/cat molar ratio of 4.5. In other words, higher the catalyst amount higher was the product yield.

3.4.2.2. Catalytic Activity: Softwood Vs. Hardwood Hemicellulose

Catalytic conversion of softwood as well as hardwood hemicelluloses were conducted at 130°C and 50 bar of nitrogen pressure (at RT) over HMOR (Si/Al = 10) catalyst. The softwood-derived hemicellulose (oat spelt; ≥70% xylan, ≤ 10%

arabinose, ≤ 15% glucose) is more heterogeneous in nature and has a lower degree of polymerization (70-130). On the contrary, the hardwood-derived hemicellulose (birch wood; >90% xylan) possesses symmetric rigid structure with a higher degree of polymerization (100-200). From the Fig. 3.27, it is evident that the nature of substrate has an effect on the progress of the reaction. While the softwood-hemicellulose resulted in 41% xylose + arabinose in 48 h, only 33% yield of these sugars was obtained with hardwood hemicellulose. Furfural formation is not depended on the source of hemicellulose. The higher reactivity of softwood hemicellulose is due to its low degree of polymerization and more heterogeneous characteristics as compared to the hardwood hemicellulose.

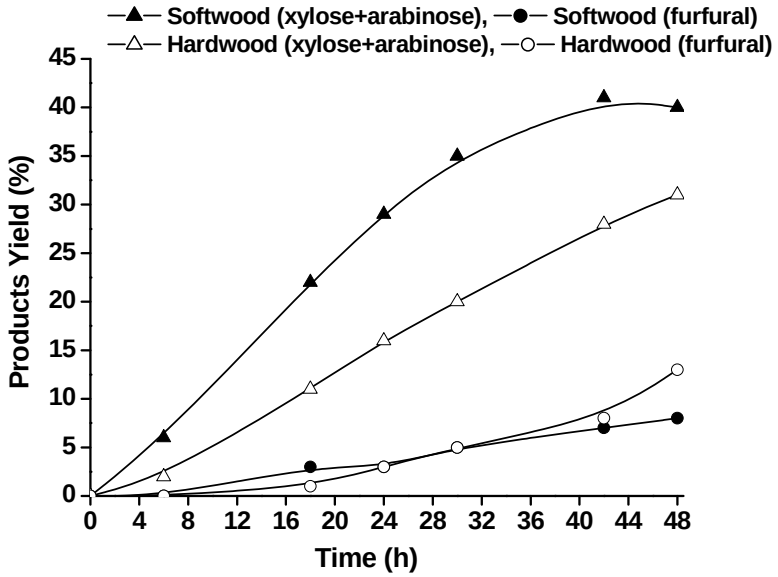

Fig. 3.27. Effect of the nature of hemicellulose on its conversion. *Reaction conditions:* Substrate (0.6 g), HMOR (Si/Al = 10; 0.3 g), water (60 g), N_2 pressure (50 bar @ RT), temperature (130°C) and reaction time (48 h).

Turnover frequency (moles of product formed per mol of acid sites per min) was determined at different temperatures and plotted in Fig. 3.28. It may be noted that TOF increased linearly with temperature. From the slope of the plot, activation energy (E_a) for the hydrolysis reaction was determined (slope = $-E_a/R$) and it was found to be 21.3 kcal/mol.

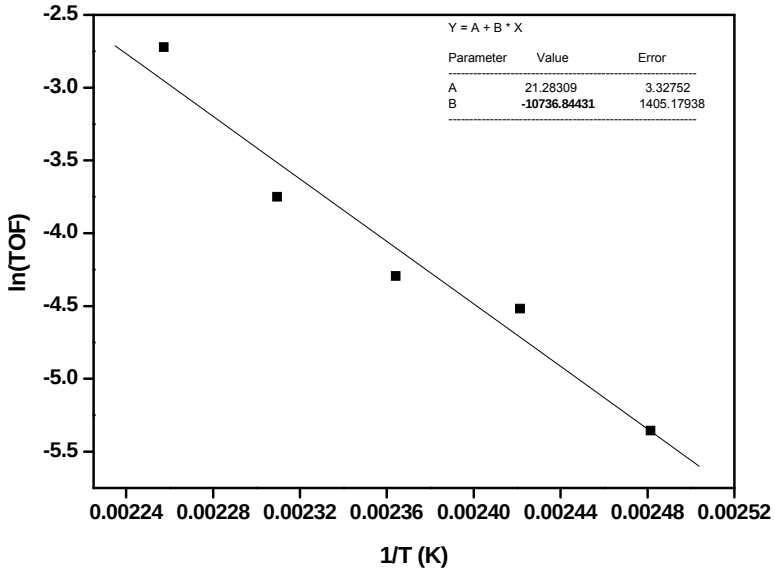

Fig. 3.28. Plot showing the variation of ln(TOF) as a function of temperature. *Reaction conditions:* Softwood hemicellulose (0.6 g), HUSY (Si/Al = 15; 0.3 g), water (60 g), N_2 pressure (50 bar @ RT), temperature (130-170°C), reaction time (1 h).

3.4.2.3. Catalyst Recyclability and Leaching Studies

The hydrolysis reactions of softwood-derived hemicellulose were conducted at 170°C with 50 bar of pressure over HUSY (Si/Al = 15) catalyst for 3 h. After completion of the reaction, the black coloured catalyst was separated out by filtration, washed with hot water to remove adsorbed oligomers and then dried under high-vacuum (10^{-3} bar) at 150°C for 6 h. This spent catalyst was reused in next reaction. But a loss in catalytic activity was found. In another experiment, the spent catalyst washed above was subjected to calcination at 550°C for 12 h. It was then used in the recycle study. The catalyst is recyclable in at least five recycling experiments (Fig. 3.29). The product yield decreased marginally from ~ 55% to 44% during the 7^{th} recycles. The decrease in activity was due to the progressive deactivation of Brönsted acid sites of the catalyst by partial exchange with sodium and potassium ions present in the substrate, which was confirmed by the ICP-OES analysis. Al content in the solid catalyst remained unchanged during the course of the recycles. Detailed characterization study of the spent catalyst will be described in Chapter 4 (section 4.4.).

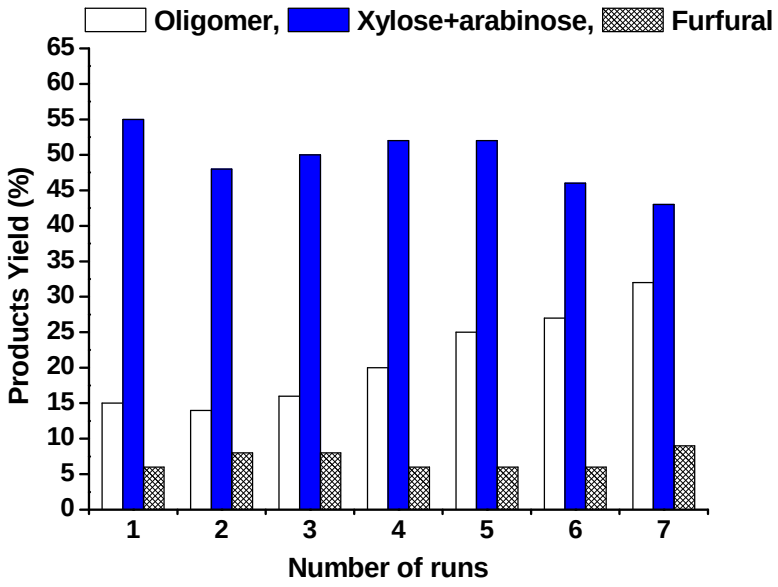

Fig. 3.29. Catalyst recycles studies. *Reaction conditions:* Softwood hemicellulose (0.6 g), HUSY (Si/Al = 15; 1.8 g), water (60 g), N_2 pressure (50 bar @ RT), temperature (170°C), reaction time (2 h).

In order to make sure that there is no leaching of the active sites (acids or aluminium) into the liquid portion, the reaction was carried out for 12 h at 130°C under nitrogen atmosphere using a freshly activated HUSY (Si/Al=15) catalyst. The reaction was stopped and catalyst was separated out by filtration and then, the filtrate was stirred for another 36 h under the same reaction conditions without any catalyst. It was found that in absence of the catalyst, there was no further increase in the product yield, which indicates that leaching of acid sites into the reaction mixture had not occurred. This observation confirms that the reaction was catalyzed heterogeneously on the surface of the solid catalyst.

3.4.3. Structure-Function Correlations

With a view to understand better the factors influencing the catalytic activity of solid acid catalysts, the product (xylose + arabinose + oligomers) yield was plotted as a function of several parameters in Figs. 3.30 and 3.31. As seen from Fig. 3.30, the product yield increased with the concentration of acid sites (determined from NH_3-TPD studies; Table 3.2) in the catalysts. Further, the catalytic activity was found to increase linearly with an increase in the concentration of strong acid sites. But, in spite of having higher concentration of acid sites (Table 3.2), HMOR (Si/Al = 10), HY (Si/Al = 2.6) and HZSM-5 (Si/Al = 11.5) deviated from the above relationship

indicating that factors other than acidity (surface area and pore size, for example) also contribute to the overall activity of the catalysts.

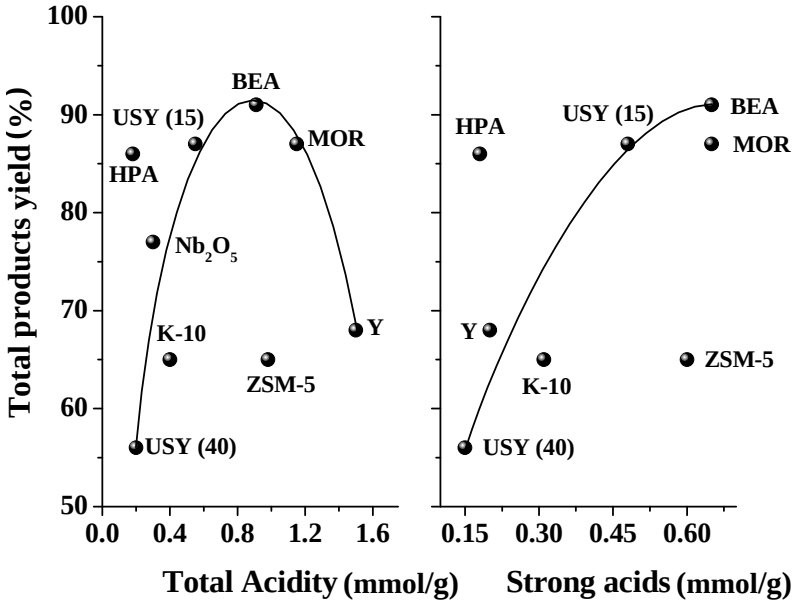

Fig. 3.30. Variation of product yield over different solid catalysts as a function of their acidity.

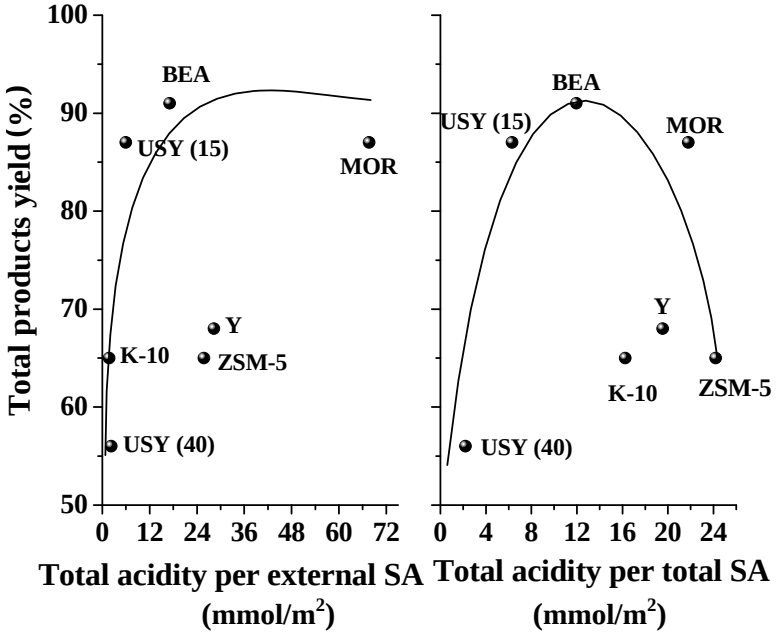

Fig. 3.31. Variation of product yield with acidity per unit surface area (SA) of the catalysts.

Fig. 3.31 depicts the variation of product (xylose + arabinose + oligomers) yield as a function of acid sites per unit external and total surface area. Even in this figure, HMOR (Si/Al = 10), HY (Si/Al = 2.6) and HZSM-5 (Si/Al = 11.5) deviated

from the linearity. Hβ (Si/Al = 19) having a total acidity of 0.9 mmol/g and surface area of 761 m^2/g showed highest catalytic activity (product yield = 90%). However, unlike HUSY (Si/Al = 15), the catalyst Hβ is not stable at our reaction conditions and looses its activity. All these relationships indicate that acidity is an important parameter, but the textural properties of the catalysts (surface area and pore dimension) also contribute to a greater extent to the catalytic activity of solid acid catalysts in the hydrolysis reaction of hemicellulose.

Hemicellulose is a water insoluble bio-polymer. Initially, water soluble oligomeric compounds are formed by thermal decomposition or by catalytic reaction on the external acid sites of the zeolite catalyst. In general, the average size of the oligomer (tetramer, for example) is 5.9 × 19.1 Å (from Chem. Draw software). These oligomers can be included in the cavities of zeolite (Fig. 3.32) and now, the reaction occurs to a larger part within the pores of a large pore zeolite. Therefore, the catalytic activity is influenced by both acidity and pore dimensions of the catalyst.

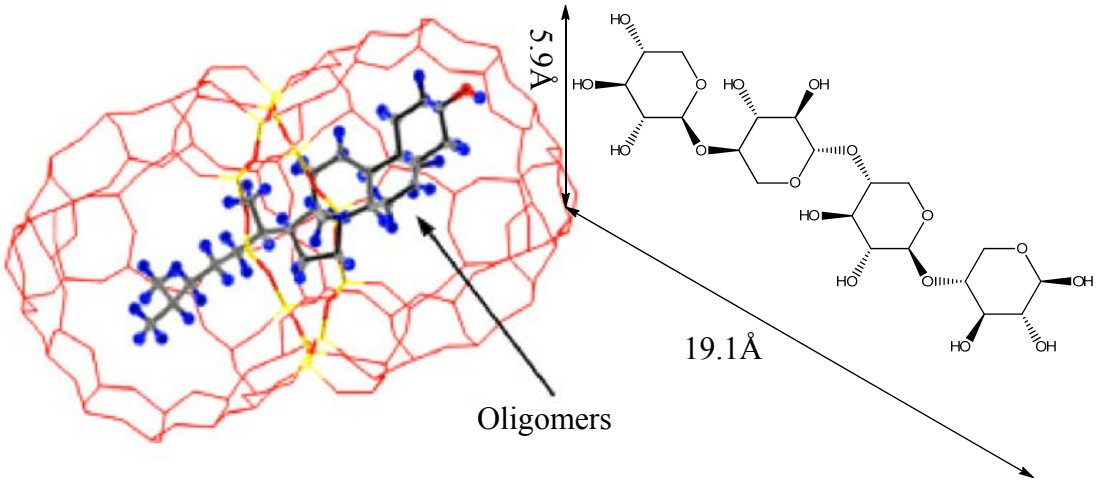

Fig. 3.32. Zeolite-encapsulated tetramers.

The three FAU samples [HY (Si/Al = 2.6), HUSY (Si/Al = 15) and HUSY (Si/Al = 40)] used in this study cover a wide range of acidity (0.2-1.5 mmol/g). In general, the pore openings of FAU group catalysts provide sufficient space to allow the formation of relatively bulky transition state intermediates (oligomers) involved in the production of xylose and arabinose. In addition, the HY (FAU group material) from which HUSY was derived possesses an inherently low Si/Al ratio, thus providing a great number of acid sites for use in catalytic applications. The sample with a Si/Al ratio of 15, performed well in catalyzing the hemicellulose reaction. The

yield towards xylose and arabinose over this catalyst was high (about 41 wt%). The formation of furfural was 11% while oligomer formation was 36%. The dealuminated sample, HUSY (Si/Al = 40), contained very low acidity (0.2 mmol/g) as compared to HUSY (Si/Al = 15; 0.55 mmol/g) and thereby showed lower activity (xylose +arabinose yield = 16%). Though, HY (Si/Al = 2.6) has high acidity (1.5 mmol/g), hemicellulose conversion towards xylose + arabinose was only 11%. From the TPD-NH_3 experiment it was found that the HY catalyst contains less number of strong acid sites as compared to HUSY (Si/Al = 15). This is one of the reasons to for its lower catalytic activity. Moreover, HY is more hydrophilic than HUSY. Hence, adsorption of oligomers on its surface would be lower as compared to that on HUSY (Si/Al = 15). The Hβ (Si/Al = 19) catalyst having acid sites concentration of 0.91 mmol/g and pore diameter of 6.6 x 7.7 Å gave 46% yield of xylose + arabinose. Similarly, HMOR (Si/Al = 10) having acid sites concentration of 1.15 mmol/g and pore diameter of 6.7 x 7.0 Å gave 40% yield of xylose + arabinose. In spite of having higher acid density (0.98 mmol/g), HZSM-5 (Si/Al = 11.5) showed very low activity. This is because of its low surface area and small pore size (5.4 x 5.6 Å for straight and 5.1 x 5.5 Å for sinusodial channels) [31]. Because of the small pore openings, the acid sites present inside the pores will not be accessible to the oligomeric molecules or the channels are not sufficiently large to accommodate the transition state intermediate required for monomer production. Hence, HZSM-5 was found to be less active.

Cs-HPA having an acid density of 0.18 mmol/g gave a product yield of 35%. This catalyst is partially soluble in water and hence, the activity observed has contributions also from the homogeneous reaction. It may be noted that this catalyst has almost lost its activity (product yield = 5%) in the first recycle experiment itself. Sulphated zirconia belongs to the category of super acids. Therefore, the reaction ends with 15% furfural and unwanted product like humines. γ-Al_2O_3 is only weakly active (xylose + arabinose yield = 14%) as it contains less number of strong acidity sites.

Pore size limitation is not the issue with mesoporous materials (Al-SBA-15 (Si/Al = 50) and Al-MCM-41(Si/Al = 50). Even then they are less active (12% and 9% yield of xylose + arabinose, respectively). This is because of their greater hydrophilic nature that doesn't allow the oligomers to get adsorbed and activated on their surface. Among all the solid acids evaluated, it is clear that the catalysts having acidity of 0.5-1.2 mmol/g and pore diameter ~7 Å are the most active catalysts and showed ~40% xylose + arabinose yield. It may be said that other zeolites having

acidity and pore dimension falling in the above range and possessing hydrophobic surface may be equally active.

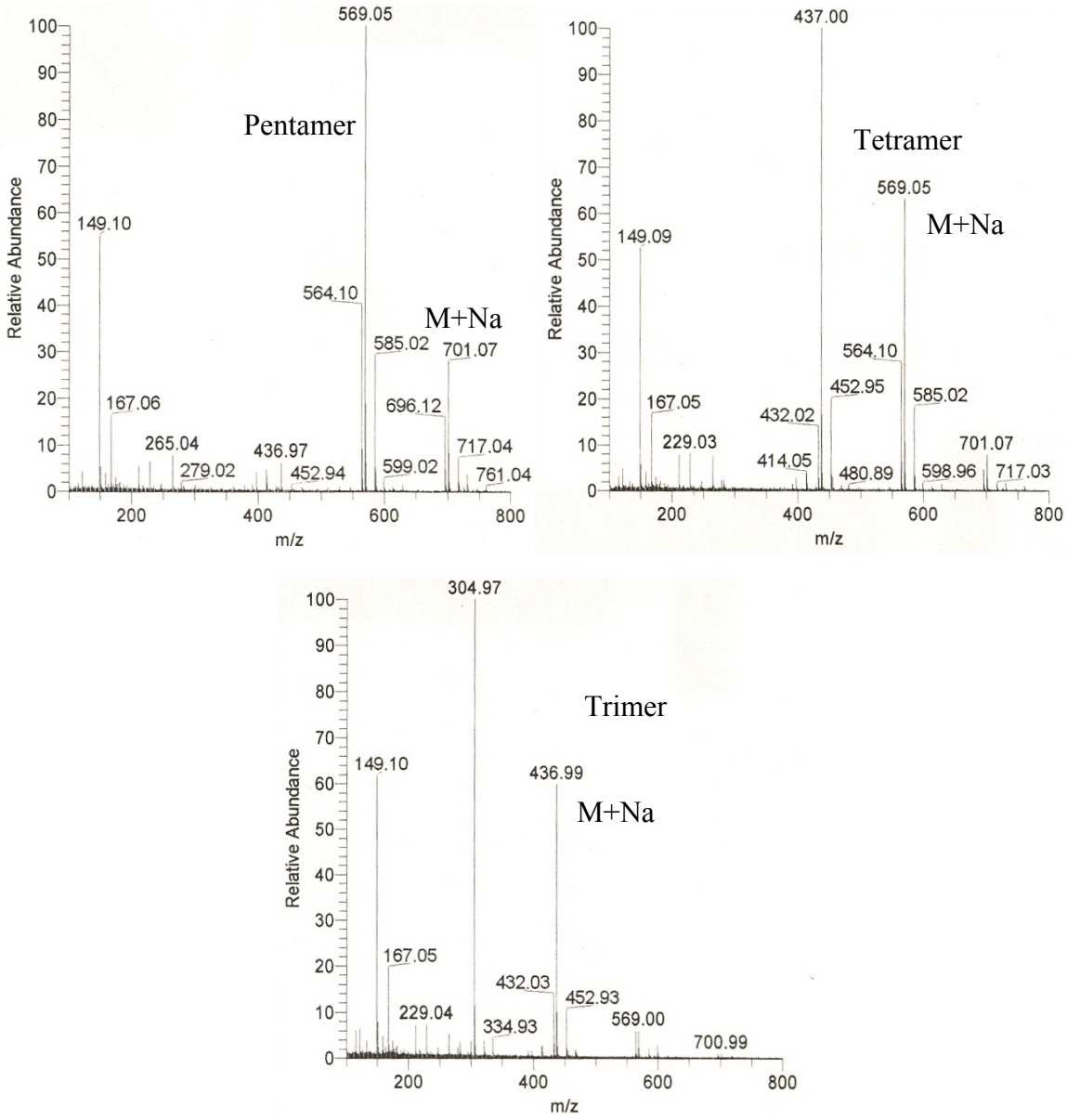

Fig. 3.33. LC-MS analysis of oligomers formed in the hydrolysis of softwood hemicellulose.

3.5. Proposed Reaction Mechanism

From the experimental data and literature reports [32] a tentative reaction scheme for the conversion of hemicellulose into chemicals is proposed in Scheme 3.3.

Hemicellulose (solid xylan) → water-soluble oligomers (pentamer to dimer) → water-soluble xylose and arabinose → decomposition products (furfural or humines)

Scheme 3.3. Reaction scheme for the conversion of hemicellulose to chemicals.

The conversion of solid xylan in presence of water involves a series of reactions including hydrolysis and dehydration. Firstly, the hemicellulose is hydrolyzed and converted into water soluble xylo-oligosaccharides (pentamer, tetramer, trimer and dimer). These oligosaccharides are further hydrolyzed over the solid acid catalyst to yield xylose and arabinose monomers [33]. The xylose is dehydrated over the same acid sites to form furfural and furan resins (humins). The possibility of decomposition of xylose and furfural to other products cannot be completely ruled out [34]. However, at our reaction conditions, such decompositions are less significant. The formation and identification of oligomers (penta-, tetra-, tri and dimers) was confirmed by LC-MS (Fig. 3.33; peaks at m/z of 701, 569 and 437 correspond to pentamer ($C_{25}H_{41}O_{21}Na$), tetramer ($C_{20}H_{33}O_{17}Na$) and trimer ($C_{15}H_{25}O_{13}Na$), respectively.

The possible mechanism of solid acid-catalyzed hydrolysis of hemicellulose is presented in Fig. 3.34. Acid hydrolysis proceeds in three steps. The first step involves the protonation of the glycosidic oxygen linking in the two sugar units by the proton from the acid, forming a conjugate acid. This results in the cleavage of the C-O bond to form xylose and one cyclic xylose carbocation. Then finally lone pair of water molecule attacks at the carbocation to form xylose [10].

Furfural formation from xylose involves several steps. Under acidic media, protonation of the xylose ring takes place at C_2 the position, which then forms a carbocation with the loss of one water molecule. Then again, protonation takes place at the OH group of C_3 position, along with this, ring opening takes place. This intermediate loses one water molecule and creates a carbocation at C_3 position. This process continues with the formation of carbocation at C_4 position. This carbocation, then, finally, rearranges to form furfural molecule. Hence, the overall process of formation of furfural involves the loss of three water molecules as shown in Fig. 3.34.

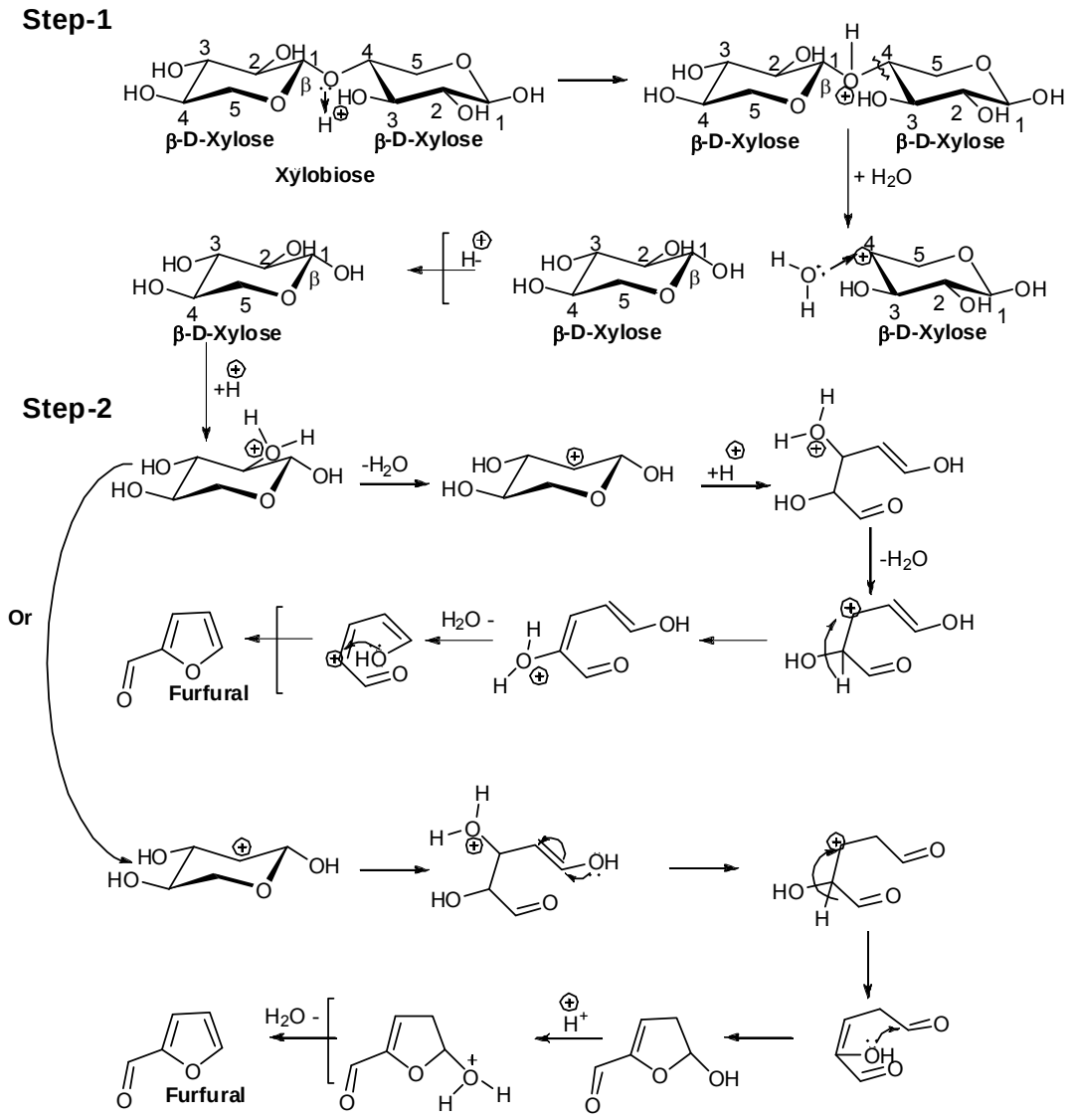

Fig. 3.34. Proposed reaction mechanism of hemicellulose conversion.

3.6. Conclusions

In this study, for the first time, a one-pot process for the conversion of solid hemicellulose (without any pretreatment) into xylose, arabinose and furfural using solid acid catalysts (zeolites, clays and metal oxides) in aqueous media is presented. Among several solid acid catalysts investigated, Hβ (Si/Al = 19) was found to be the best catalyst. HUSY (Si/A = 15) also showed very high activity. The stability of HUSY was found to be the better than Hβ. No leaching of active sites into the liquid medium was detected. A maximum 41% yield of xylose + arabinose was obtained at optimized reaction conditions. Structure-function correlations revealed that in addition to acidity, surface area and pore size of the catalysts influence the catalytic

activity and product yield. To the best of knowledge, this is the first study using zeolite catalysts on the conversion of hemicellulose into value-added chemicals.

3.7. References

[1] L. P. Minke, A. Noordermeer, *Green Chem.* **2006**, 8, 861.

[2] T. Werby, G. Peterson, *in Top Value-Added Chemicals from Biomass*, US Department of Energy, http://www.eere.energy.gov

[3] W. E. Mabee, J. N. Saddler, *Bioresour. Technol.* **2010**, 101, 4806.

[4] A. J. Ragauskas, C. K. Williams, B. H. Davision, G. Britovsek, J. Cairnert, C. A. Eckert, *Science* **2006**, 311, 484.

[5] Y. Yu, X. Lou, H. Wu, *Energy & Fuels* **2008**, *22,* 46.

[6] Y. Sun, J. Cheng, *Bioresour. Technol.* **2002**, *83*, 1.

[7] O. Bobleter, *Prog. Poly. Sci*. **1994**, 19, 797.

[8] E. Sjöström, *Wood Chemistry Fundamentals and Applications*, 2nd ed., Academic Press, San Diego **1993**.

[9] K. Shimizu*, Chemistry of Hemicelluloses In Wood and Cellulosic Chemistry*, 2nd ed., Marcel Dekker Inc., New York **2001**.

[10] D. Fengel, G. Wegener, *Wood Chemistry Ultrastructure Reactions,* Walter de Gruyter, Berlin **1989**.

[11] L. P. Ramos, *Quim. Nova* **2003**, 26, 863.

[12] D. Fengel, G. Wegener, *Polyosen und Libnin-polysaccharid-Komplexe: In Polysaccharide*, Springer, Berlin **1985**.

[13] D. Fengel, G.Wegener, *Wood*, Springer, Berlin **1989**.

[14] D. Gullu, *Energy Source* **2003**, 25, 753.

[15] A. P. Dunlop, *Ind. Eng. Chem*. **1948**, 40, 204.

[16] R. J. Ulbricht, J. Sharon, J. Thomas, *Appl. Toxicol.* **1984**, 4, 843.

[17] A. Herrera, S. J. Tellez-Luis, J. J. Gonzalez-Cabriales, J. A. Ramirez, M. Vazquez, *J. Food Eng.* **2004**, 63,103.

[18] S. Miller, R. Hester, *Chem. Eng. Comm.* **2007**, 194, 85.

[19] K. Karimi, S. Kheradmandinia, *Biomass Bioenergy* **2006**, *30*, 247.

[20] B. C. Saha, *J. Ind. Microbiol. Biotechnol.* **2003**, 30, 279.

[21] D. Shallom, Y. Shoham, *Current Opinion in Microbiol.* **2003**, 6, 219.

[22] M. Fitzpatrick, P. Champagne, M. F. Cunningham, R. A. Whitney, *Bioresor. Technol.* **2010**, 101, 8915.

[23] S. B. Kimm, Y. Y. Lee, *Hydrolysis of Hemicellulose by Solid Super Acid*, *Biotechnol. Bioeng.* Symp. **1986**, 15, 81.

[24] K. Chao, D. Shy, S. Sheu, C. Lin, *Micro. Mater.* **1994**, 2, 91.

[25] C. Milone, M. Dhanagopal, S. Santangelo, M. Lanza, S. Galvagno, G. Messina, *Ind. Eng. Chem. Res.* **2010**, 49*,* 3242.

[26] J. Philip, A. Wallis, P. Will, A. F. Patti, J. L. Scott, E. Teoha, *Green Chem*. **2007**, 9, 980.

[27] C. Baerlocher, W. M. Meier, D. H. Olson, *Atlas of Zeolites Framework Type*, www.iza-online.org/database

[28] L. M. Barclay, D. W. Thompson, *Nature* **1969**, 222, 263.

[29] B. Velde, *Introduction to Clay Minerals: Chemistry, Origins, Uses and Environmental Significance*, Chapman & Hall, London **1992**.

[30] B. Gruttner G. Jander, *Handbook of Preparative Inorganic Chemistry*, Vol.2, 2nd ed., Academic Press, New York **1976**.

[31] S. G. Hegde, R. Kumar, R. N. Bhat, P. Ratnasamy, Zeolites 1989, 9, 231.

[32] G. Marton, J. Dencs, L. Szokonya, *Principles of Biomass In Handbook of Heat and Mass Transfer*, Gulf Publishing, Houston **1989**.

[33] Y. Kamiyama, Y. Sakai, *Carbohydr. Res*. **1979**, 73, 151.

[34] A. Dunlop, F. Peters, *The Furans*, Rheinhold, New York **1953**.

CHAPTER-4

SELECTIVE CONVERSION OF HEMICELLULOSE IN BAGASSE TO CHEMICALS

4.1. Introduction

In recent years, there has been a worldwide interest in the utilization of lignocellulosic (biomass) materials like agricultural residues to synthesize value-added chemicals. Application of such agro-residues (especially bagasse) in chemical production provides alternative substrates and reduces the air pollution. Otherwise these residues cause disposal problem. Freshly harvested sugarcane is shredded, mixed with water and crushed between heavy rollers to extract the juice that contains 10-15% sucrose. After extraction of juice from sugarcane, the fibrous residue left out is called bagasse (Fig. 4.1). Approximately, 1743 MMT (million metric tonne) of sugarcane is produced globally every year, which results in about 488 MMT of bagasse [1]. Typically, one ton of sugarcane can produce, ~0.125 ton of dry bagasse or ~0.280 ton of wet bagasse (~49% of water), ~0.1 ton of sucrose, ~0.035 ton of molasses and 0.585 ton of water [2]. The bagasse contains ~49% of water, ~49% of fibres and ~2% of water soluble solids [3]. These constituents vary according to its maturity, methods of harvesting, condition of the soil, the climate and efficiency of the milling plant.

Fig. 4.1. Bagasse from sugarcane.

Next to Brazil, India is the second largest producer of sugarcane. In India, about 4 million hectares of land is used for sugarcane farming which can produce ~348 MMT of sugarcane per year [4]. From this sugarcane, ~96 MMT of bagasse is produced, out of that ~10 MMT is used in industries for generating energy and 86 MMT of bagasse is lying surplus per year [5]. The market price of bagasse in India is

about Rs. 1500/ton. Besides Brazil and India, Australia, South Africa, Cuba, China and tropical and subtropical countries are also the major contributors for sugarcane bagasse production. Bagasse is used in cattle fodder, roofing and making compost. Now part of the bagasse is burnt in boilers which move the turbines for power generation and the remaining can be stockpiled [3]. Although bagasse is regarded as a waste material, if it is to be further utilized outside mill it must bear the costs of handling and storage, which must be added. Bagasse has the potential ability to displace fossil feedstock for chemicals and fuels production.

Dry bagasse fibre consists of ~43% of cellulose (a polymer of glucose), ~30% of hemicellulose (polymer usually composed of pentoses - xylose, arabinose, etc. and hexoses - galactose, glucose mannose, etc.), ~20% of lignin (phenolic compounds) and ~7% of extractives and ash [6]. They are all inter-chained to each other. Their composition varies from plant to plant, source to source and region to region etc. The ellulose in dry bagasse is also bound with gums, tannins, fats and colouring materials. Its degree of polymerization is in the range of 2000-30000 [7, 8].]. Lignin in bagasse has a complex structure formed by polymerization of phenolic compounds which combined with hemicellulose covers the cellulose matrix to protect it from the enzymatic and chemical degradation [9, 10]. Hemicellulose is the second most abundant fraction in bagasse. The composition and degree of polymerization varies according to the source. Cellulose and hemicellulose in bagasse can be hydrolyzed using mineral acids and enzymes [11].

Generation of power by direct combustion of sugarcane bagasse in boilers has an efficiency of about 26% because it contains large number oxygen atom. Burning of dry bagasse in direct way has low efficiency and leads to major health hazards due to fly ash residue generated. Recently, the overall efficiency of the process is being improved by proper utilization of heat and effective waste heat recovery [4, 12].

There are mainly two basic processes to convert bagasse into chemicals i.e. dilute or concentrated mineral acid process and enzymatic process. Lot of research has been devoted on the homogeneous acid catalyzed hydrolysis process [13-16]. During hydrolysis, xylose, arabinose and other constituent sugars are produced. Depending on reaction conditions, the sugars may be further dehydrated to form furfural and furan resins. Furfural has many industrial uses. It is used as a selective solvent for the refining of lubricating oils, an intermediate in the production of nylon-6,6 and resins used for moulding powders. Furfural on hydrogenation yields furfuryl

alcohol which can produce inexpensive, heat-stable and corrosion-resistant resins. Furfuryl alcohol is also used in the manufactal of pharmaceuticals, fungicides and insecticides and as a solvent.

Enzymatic hydrolysis of hemicellulose in bagasse is of great interest. Several enzymes are involved in the hydrolysis hemicellulose in bagasse. They include Endo-xylanase, Exo-xylanase, β-xylosidase and several accessory enzymes, such as α-L-rabinofuranosidase, α-glucuronidase, acetylxylan esterase, ferulic acid esterase and *p*-coumaric acid esterase. The endo-xylanase attacks the main chains of xylans, and β-xylosidase hydrolyzes xylooligosaccharides to xylose. The α-arabinofuranosidase and α-glucuronidase remove the arabinose and 4-O-methyl-D-glucuronic acid substituents, respectively, from the xylan backbone [17, 18]. Bio-ethanol from lignocellulosic materials such as bagasse has been studied in the past few decades with great interest [19]. Studies taking into account the yield of fermentation process and the integration of unit operations are still needed in order to make hydrolysis a competitive technology [20, 21].

The homogeneous acid-catalyzed reaction has a lot of drawbacks such as difficulty in separation of products and catalysts (acids). It generates a lot of neutralization waste and requires a special (acid resistant) reactor. Although the enzymatic hydrolysis process is specific and produces selective product, the process is quite slow and difficult to separate enzyme from the broth. Use of enzymes for hydrolysis of bagasse is uneconomical since, the production of enzymes is presently quite expensive and hence, this process is uneconomical.

The conversion of isolated hemicellulose into constituent sugars and furfural has been reported in Chapter 3 (section 3.4.). This chapter, probes the selective conversion of hemicellulose in bagasse into chemicals over solid catalysts. As mentioned above cellulose is a highly crystalline glucose polymer and requires more harsh conditions to hydrolyze. At those severe conditions, the sugars in hemicellulose get decomposed into undesired chemicals. Hence, in order to get more value out of bagasse, it is recommended that a two-step process is followed where in the first-step hemicellulose in bagasse is hydrolyzed first at moderate conditions and the sugars formed are recovered. In the second step, cellulose is hydrolyzed at higher temperatures. This method would enable higher yield of the value-added sugar products.

4.2. Materials and Methods

4.2.1. Chemicals and Composition of Bagasse

All chemicals and clays (K10) used in this study were purchased from Aldrich. Zeolites [HUSY (Si/Al = 15), Hβ (Si/Al = 19), HMOR (Si/Al = 10)] were procured from Zeolyst International, USA. These chemicals and materials were used as received without any further purification. Deionised water was used to prepare the standard solutions as well as in the reactions. The zeolites were calcined at 550°C for 12 h in the presence of air. Clay was activated at 80°C for 6 h under high-vacuum (10^{-3} bar). The activated catalysts were stored in a desiccator over silica gel. Bagasse used in this study was procured from a sugar industry in Latur district, Maharashtra, India. After receiving, the bagasse was washed with cold water followed by hot water (~70°C) to remove water-soluble matter. Then the bagasse was dried at 70°C in an oven for 24 h. It was crushed into small pieces and sieved (150 BSS) into particles of size less than 0.1 mm. The chemical composition of bagasse is given in Table 4.1.

Table 4.1. Chemical composition of Indian dry bagasse

Compound	Wt%
Hemicellulose	30 ± 2
Cellulose	42 ± 2
Lignin	18 ± 2
Others (metals, wax, ash etc.)	≤ 10

4.2.2. Reaction Procedure and Analytical Methods

All the reactions were carried out in a batch reactor as discussed in Chapter 3 (section 3.3.3.). In a typical reaction, known quantities of catalyst (zeolite or clay), bagasse and deionised water were all taken in a 100 mL Parr reactor at a time. The reactor was purged with nitrogen gas three times to remove oxygen from the autoclave. Then, it was pressurized with nitrogen (at RT) to 50 bar. The autoclave was heated to a desired temperature and the reaction was conducted for a desired period of time. At the end of the reaction, the reactor was allowed to cool in air to RT. The liquid portion was separated by filtration. The solid residue containing both the catalyst and unconverted bagasse was washed thoroughly with hot water (70°C, 100

mL) and dried under vacuum (10^{-3} bar) at 80°C for 6 h. The weight of the residue was noted to account for the conversion of hemicellulose in bagasse. The influence of reaction parameters (substrate concentration, amount of catalyst, temperature, pressure, reaction time, etc.) on product yield was investigated. In some experiments, the liquid samples were withdrawn during the reaction at intermittent times, filtered and analyzed for their composition. The samples were analyzed as described in Chapter 3 (section 3.3.4.) using a Shimadzu HPLC system. In all the reactions, 0.6 g of bagasse was taken. As per the composition listed in Table 4.1, this contains 0.18 g of hemicellulose. Details of the product yield calculations were described in Chapter 3 (section 3.3.4.).

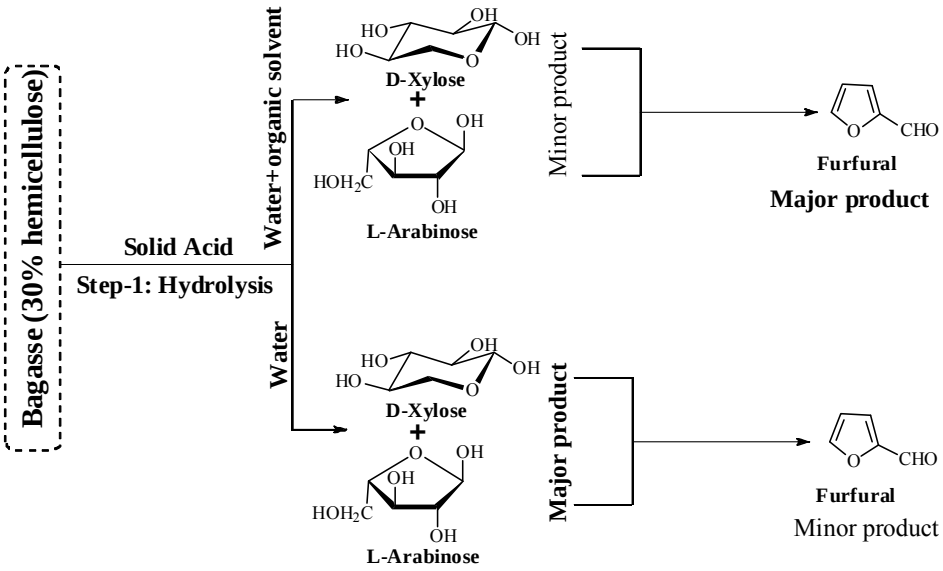

Scheme 4.1. Conversion of hemicellulose in bagasse into chemicals.

4.3. Results and Discussion

Bagasse contains 30% of hemicellulose which can be hydrolyzed in the presence of a solid acid catalyst into arabinose, xylose and glucose. These sugars can be transformed into furfural and 5-hydroxymethyl furfural (HMF) via the dehydration process (Scheme 4.1). The reactions were conducted 170°C for 1 h in the presence of three different types of zeolites [HUSY (Si/Al = 15), Hβ (Si/Al = 19) and HMOR (Si/Al = 10)] or K10 clay catalysts. It is already known that under these experimental conditions cellulose in bagasse cannot be hydrolyzed due to its robust structure [22, 23]. Controlled experiments revealed that when the reaction was conducted in the absence of any catalyst the product contained mainly the oligomers (pentamer-dimer). Only 7% of xylose + arabinose formed in this case (Fig. 4.2) [24]. In the presence of solid acid catalysts, the water-soluble oligomers got converted in high amount to the

monomeric sugars. The relative activity (product yield) over different solid acid catalysts of the present study decreased in the order: Hβ (63%) > HMOR (61%) > HUSY (55%) > clay (31%) (Fig. 4.2). These results are in agreement with those for isolated hemicellulose reported in Chapter 3 (section 3.4.2.).

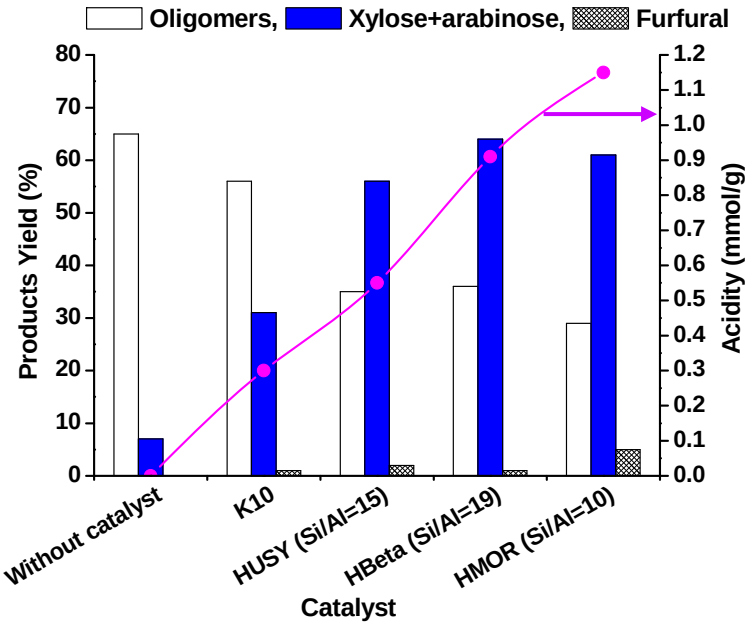

Fig. 4.2. Conversion of bagasse into chemicals over solid acid catalysts. *Reaction conditions:* Bagasse (0.6 g), catalyst (0.3 g), water (60 g), N_2 pressure (50 bar @ RT), temperature (170°C), reaction time (1 h).

4.3.1. Influence of Reaction Parameters

4.3.1.1. Effect of Reaction Time

Fig. 4.3 shows the progress of the reaction as a function of time in the presence of HUSY catalyst. The amount of oligomers in the product increased with increasing in the reaction time, reached a maximum (38%) at 0.5 h and then onwards decreased. Xylose + arabinose formation has also shown a similar trend but the maximum (56%) occurred at about 1.5 h. The amount of furfural formation increased with increasing in the reaction time. This behaviour is typical of three consecutive reactions: (i) conversion of hemicellulose (in bagasse) to oligomers, (ii) conversion of oligomers into xylose + arabinose monomeric sugars, and (iii) conversion of monomeric sugars to furfural.

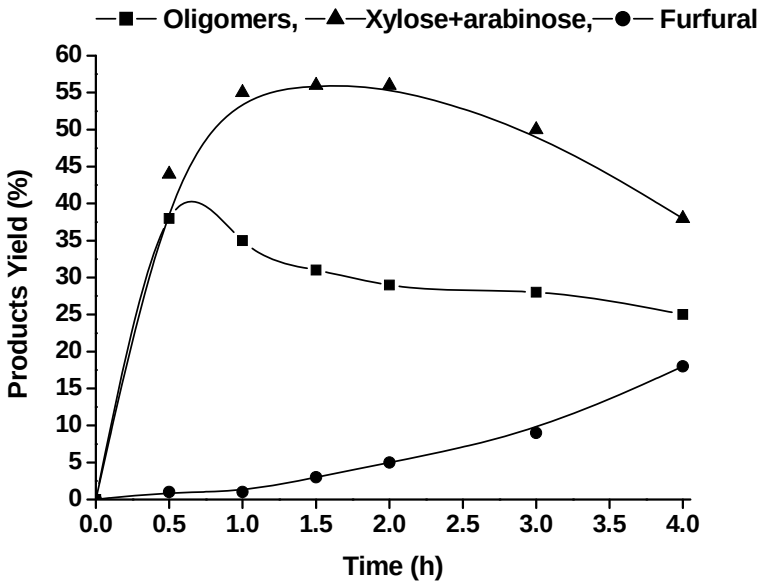

Fig. 4.3. Effect of time on bagasse conversion. *Reaction conditions:* Bagasse (0.6 g), HUSY (Si/Al = 15; 0.3 g), water (60 g), pressure (50 bar @ RT) and temp. (170°C).

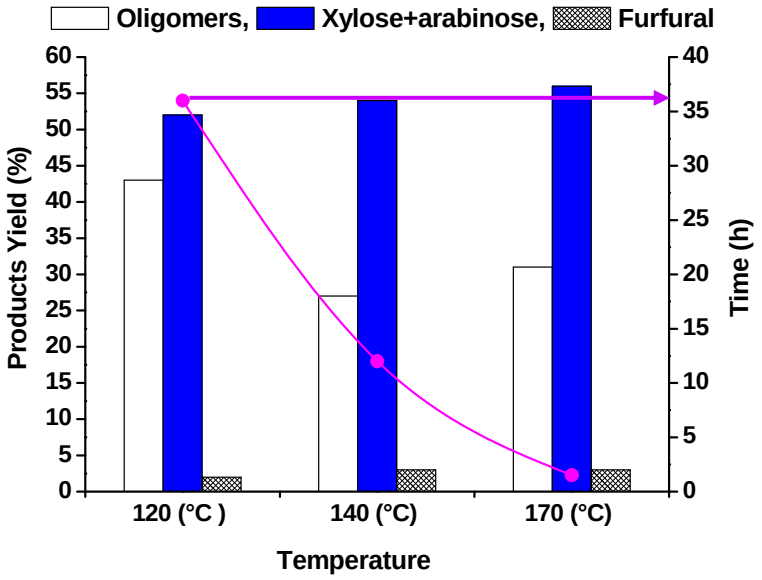

Fig. 4.4. Effect of the reaction temperature on bagasse conversion. *Reaction conditions:* Bagasse (0.6 g), catalyst (0.3 g), water (60 g) and pressure (50 bar).

4.3.1.2. Effect of Temperature

Temperature has a marked effect on the product yield. The influence of temperature on the product yield over HUSY (Si/Al = 15) is presented in Fig. 4.4. When temperature was raised from 120 to 170°C, the time required to get maximum yield of xylose + arabinose (55%) decreased from 36 to 1 h. At higher temperatures, if the reaction is prolonged for longer reaction times, the yield of xylose + arabinose decreased as these sugars partially got converted to furfural.

4.3.1.3. Effect of Pressure

The influence of pressure on bagasse conversion was studied by varying the pressure from 1 to 50 bar at a reaction temperature of 170°C using a HUSY (Si/Al = 15) catalyst. There was an increase in the product yield (from 32% to 50%) when the pressure was increased from 1 to 5 bar (reaction time = 1 h). No notable increase in product yield was observed above 5 bar. A pressure of 5 bar is, therefore, good enough to keep water in the liquid phase at 170°C and to give high product yield.

4.3.1.4. Effect of Substrate Concentration

While the substrate to catalyst ratio was kept the same, the ratio of water to bagasse was changed from 100:1 to 100:5 (i.e., 1 to 5 wt% of bagasse with respect to water). The reaction was conducted at 170°C over HUSY (Si/Al = 15) and product yield was monitored as a function of time (Fig. 4.5). More amounts of xylose + arabinose had formed when the concentration of the substrate was higher. The amount of furfural formed is nearly the same irrespective of the concentration. In concentrated solutions, the contact of substrate (bagasse) with the catalyst active sites is more possible and thereby leading to formation of higher amount of monomeric sugar products.

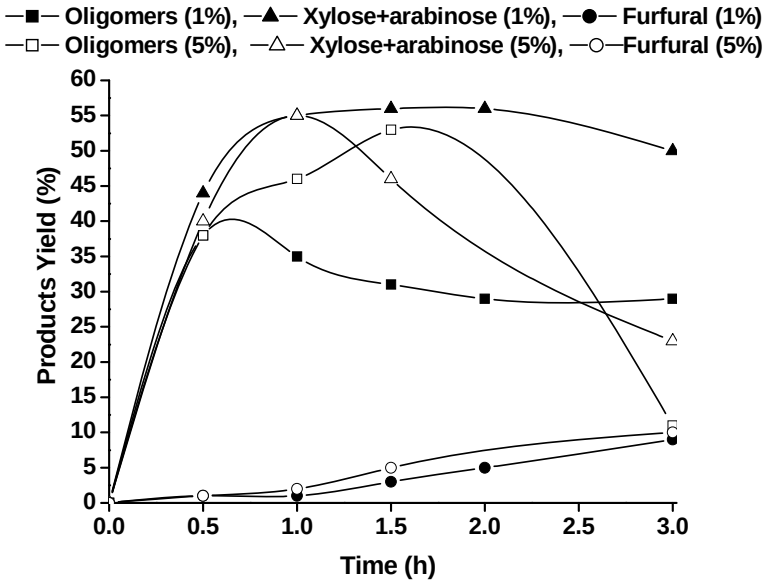

Fig. 4.5. Effect of substrate concentration on bagasse conversion. *Reaction conditions:* Bagasse (0.6-3 g), catalyst (0.3-1.5 g), water (60 g), N_2 pressure (50 bar @ RT), temperature (170°C), reaction time (0.5-3 h).

4.3.1.5. Effect of Substrate/Catalyst Ratio

The reaction of bagasse with water was carried out at 170°C over HUSY catalyst taking substrate/catalyst weight ratio of 2, 10 and 30. As seen from Fig. 4.6, product yield increased with increasing amount of catalyst. Only 7% of xylose + arabinose was obtained when the substrate/catalyst ratio was 30. This yield increased to 55% when the ratio of substrate/catalyst was 2. By increasing the catalyst amount, higher yield of products was obtained relatively in a shorter period of time. With increasing amount of the catalyst, the number of acid sites increased and thereby more and more molecules of bagasse-hemicellulose got hydrolyzed yielding higher amount of monomeric sugars.

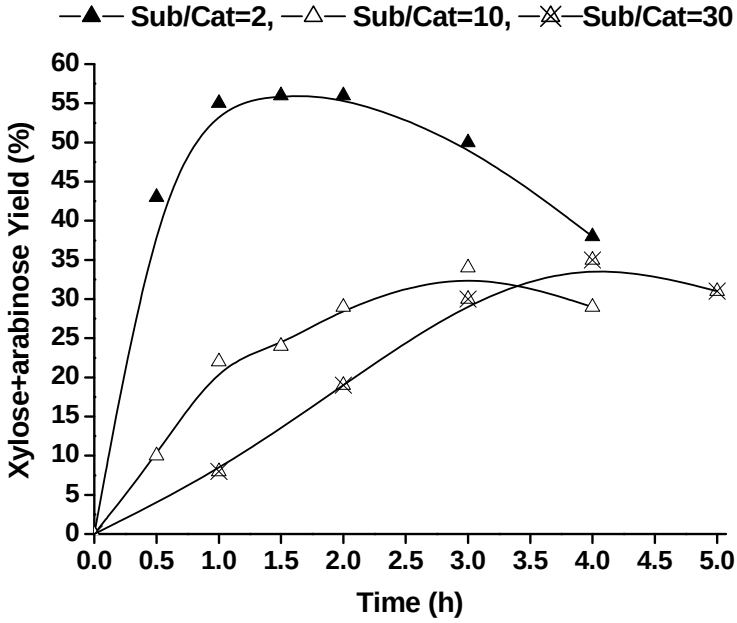

Fig. 4.6. Effect of substrate/catalyst ratio on products yield from bagasse. *Reaction conditions:* Bagasse (0.6 g), catalyst (0.3 g), water (60 g), N_2 pressure (50 bar @ RT), temperature (170°C) and reaction time (0.5-6 h).

4.3.1.6. Effect of Solvent

The influence of organic solvent on bagasse conversion was studied over HUSY (Si/Al = 15) catalyst at 170°C for 6 h. The results are presented in Fig. 4.7. The solvents used are toluene, methyl isobutyl ketone (MIBK), *p*-xylene and cyclohexanol. In these experiments, the liquid sample was taken after completion of reaction. The two layers (aqueous and organic) were separated. Each layer was filtered through 0.22 μm syringe filter. The water layer was analyzed by HPLC as described in Chapter 3 (section 3.3.4.). The organic layer was analyzed using a Varian CP-3800 GC gas chromatograph equipped with a flame ionization detector and HP-5

column (length = 50 m and I.D. = 0.25 mm). About 28% of furfural formation was observed in the absence of any solvent. When toluene (30 g) was added, an enhancement in furfural formation to 58% was observed. Similar enhancements in furfural formation were observed also when 30 g of MIBK (55%) or *p*-xylene (56%) was added. However, with cyclohexanol as solvent, the yield of furfural decreased to 23%. Furfural is soluble in water and to a greater extent in organic solvents mentioned above. In the absence of a solvent, furfural is in direct contact with the catalyst. However, when organic solvents are present, as soon as furfural is formed it goes into the organic phase than into the aqueous phase (Fig. 4.8). In other words, it doesn't come in contact with the solid catalyst unlike that happens when water alone is present in the reaction medium. Furfural gets further reacted at acid sites to form furan resins and humins. Formation of these unwanted products gets suppressed by using the above organic solvents. With cyclohexanol as solvent the yield of furfural was lower than that with water alone. This is because, the –OH group of the solvent (cyclohexanol) and –CHO group of furfural can react at the reaction conditions and form acetal-like compounds which could not be detected on our chromatographic system. A decrease in the yield of oligomers and xylose + arabinose was observed in the presence of organic solvents.

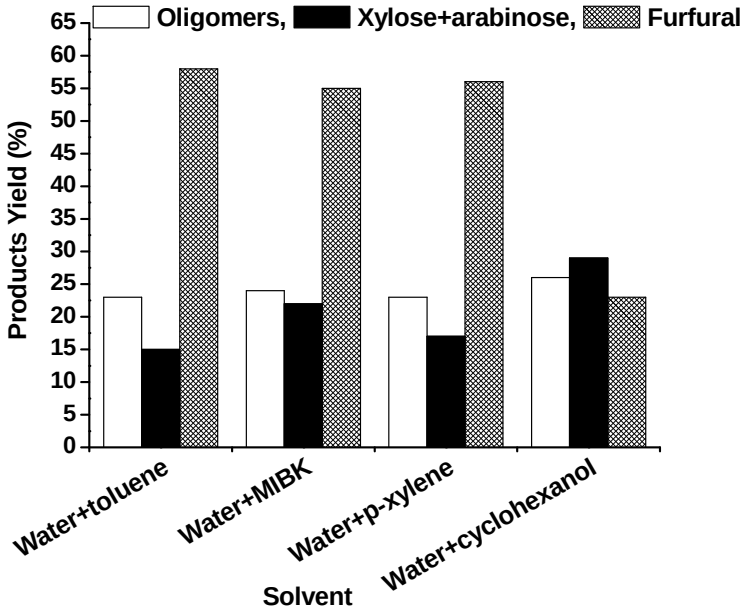

Fig. 4.7. Effect of solvent on bagasse conversion over HUSY (Si/Al = 15). *Reaction conditions:* Bagasse (0.6 g), catalyst (0.3 g), water (30 g), solvent (30 g), N_2 pressure (50 bar @ RT), temperature (170°C) and reaction time (6 h).

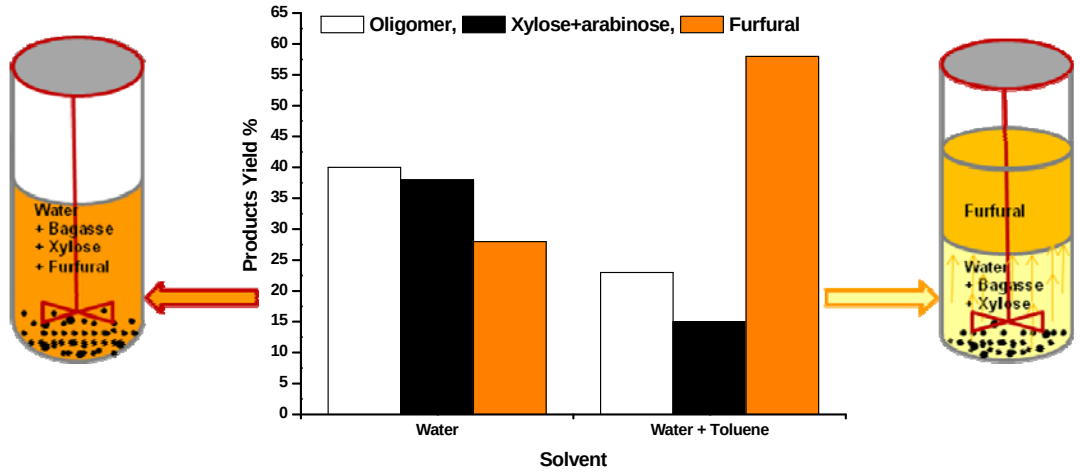

Fig. 4.8. Effect of solvent on bagasse conversion over HUSY (Si/Al = 15). *Reaction conditions:* Bagasse (0.6 g), catalyst (0.3 g), water (30 g), toluene (30 g), N_2 pressure (50 bar@ RT), temperature (170°C) and reaction time (6 h).

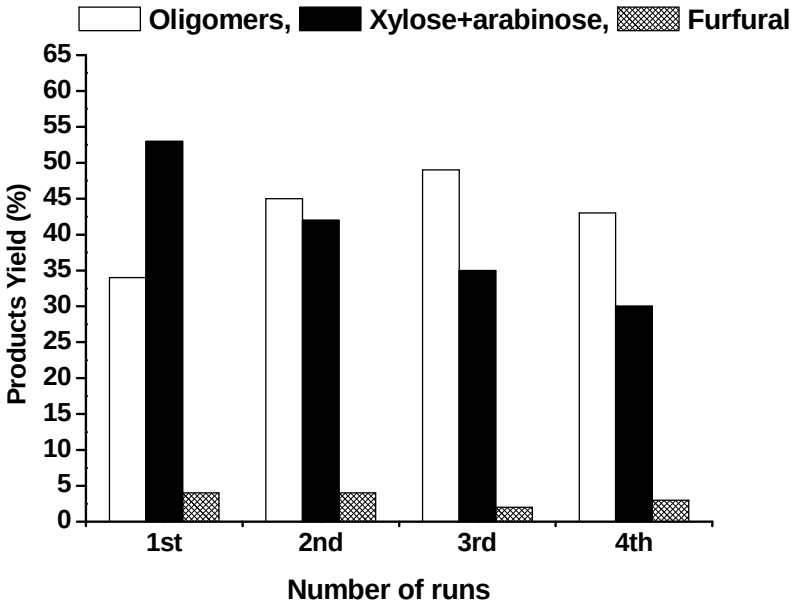

Fig. 4.9. Catalyst recycling studies. *Reaction conditions:* Bagasse (0.6 g), HUSY (Si/Al = 15; 0.3 g), water (60 g), N_2 pressure (50 bar @ RT), temperature (170°C) and reaction time (2 h).

4.3.2. Recycle Study

The reaction of bagasse was conducted at 170°C for 2 h over HUSY (Si/Al = 15). The catalyst was separated from the reaction mixture by filtration, washed thoroughly with water (100 mL) and dried under high-vacuum (10^{-3} bar) at 150°C for 6 h. Brown coloured material obtained was calcined at 550°C for 12 h. It was then used in the recycling experiment. A total of three similar such recycling experiments were done. As seen from Fig. 4.9, the catalyst gradually looses its activity in the

recycling experiments. The xylose + arabinose yield decreased from 53 to 30% at the end of 4th run.

With a view of understand whether any leaching of acid sites during the reaction had occurred, catalytic runs were conducted for 15 min, reaction was stopped, catalyst was removed and the run was continued without any catalyst. No increase in product yield was noted indicating that there was no leaching of active acidic sites into the liquid phase.

To probe further the causes for deactivation of HUSY in the conversion of bagasse to chemicals, the spent catalysts were characterized by several physicochemical techniques and compared with of the fresh catalyst. The following section describes these studies.

4.4. Characterization of Spent Catalysts

4.4.1. X-Ray Powder Diffraction

Fig. 4.10 shows the XRD patterns of fresh and spent catalysts. While the overall X-ray pattern remained the same even after reuse, some decrease in intensity of XRD peaks was observed. This could possibly due to partial collapse of structure of the materials.

4.4.2. N_2 Sorption Study

All the fresh and spent catalysts of zeolites showed typical type-I N_2 sorption isotherms (Fig. 4.11). The textural properties of the fresh and spent catalysts are listed in Table 4.2. BET surface area and pore volume of the spent catalysts were found to be lower than those of the fresh catalyst. However, pore diameter of the catalyst was nearly the same even after use. This decrease in surface area and pore volume was found higher in the case of Hβ than in HUSY and HMOR. K10 also showed a significant decrease in surface area and pore volume. As this decrease cannot be related to blocking of pores due to accumulated organic matter (as revealed by C & H microanalysis), partial collapse of the structure in the case of some crystallites could be the possible reason.

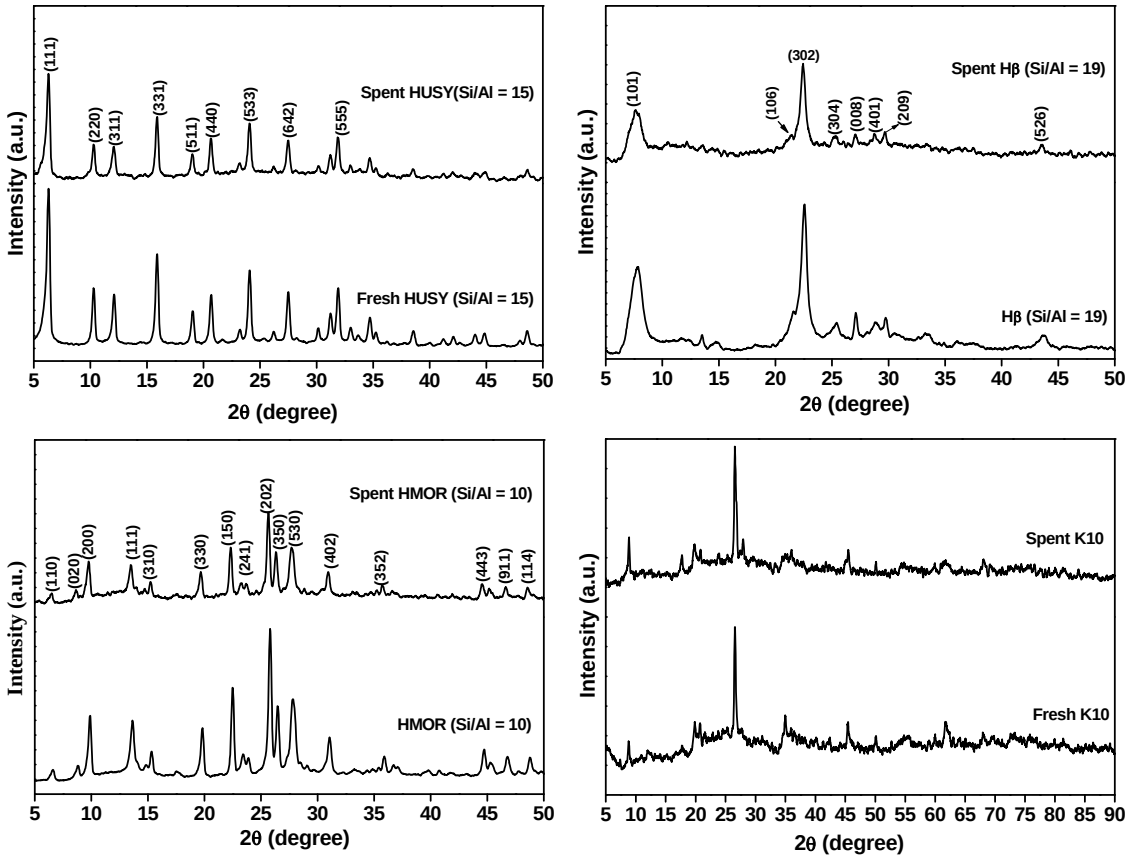

Fig. 4.10. X-Ray diffractographs of fresh and spent solid acid catalysts.

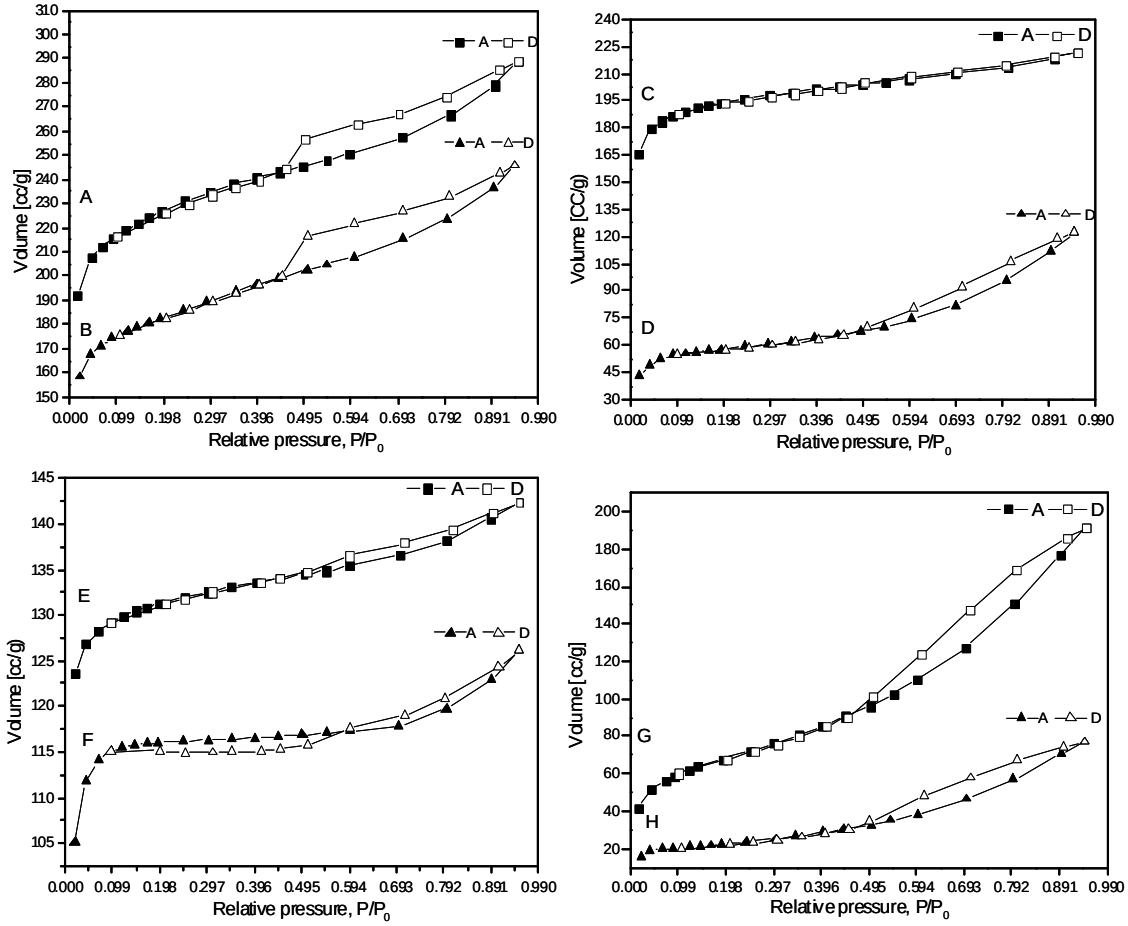

Fig. 4.11. N_2 sorption isotherms: (A) fresh HUSY (Si/Al = 15), (B) spent HUSY (Si/Al = 15), (C) fresh Hβ (Si/Al = 19), (D) spent Hβ (Si/Al = 19), (E) fresh HMOR (Si/Al = 10), (F) spent HMOR (Si/Al = 10), (G) fresh K10, and (H) spent K10.

Table 4.2. N_2 sorption data of fresh and spent solid acid catalysts

Catalysts	BET Surface area (m^2/g)			Pore volume (mL/g)		Pore diamater (Å)[a]
	Total	External	Micropore	Total	Micropore	
HUSY (Si/Al = 15) – fresh	873	92	780	0.45	0.32	6.1
HUSY (Si/Al = 15) – spent	704	101	603	0.38	0.25	6.2
Hβ (Si/Al = 19) – fresh	761	53	708	0.34	0.28	6.1
Hβ (Si/Al = 19) – spent	225	84	140	0.19	0.05	6.2
HMOR (Si/Al = 10) –fresh	528	17	511	0.22	0.2	6.1
HMOR (Si/Al = 10) – spent	478	7	471	0.19	0.18	6.1
K10 – fresh	246	228	18	0.30	0.002	6.1
K10 – spent	84	84	0	0.12	0.000	6.0

[a]Determined by HK (Horvath-Kawazoe) method.

4.4.3. Nuclear Magnetic Resonance Spectroscopy

Magic-angle spinning NMR is a powerful tool for structural elucidation of solid samples. The position of the NMR signal is sensitive to the nature and chemical environment of a magnetic nucleus [25]. MAS NMR of ^{29}Si can differentiate Si nuclei in different structural environments (i.e, Si coordinated to four Si atoms and Si coordinated to one, two or three Al atoms and the rest being Si in its tetrahedral structure). MAS NMR of Al distinguishes the Al in tetrahedral framework location from that of hexa/pentacoordinated aluminum located in the extra framework sites [26-29].

4.4.3.1. ^{29}Si MAS NMR

Fig. 4.12 presents the ^{29}Si MAS NMR spectra of fresh and spent HUSY (Si/Al=15) samples. HUSY showed signals at -83.45, -90.37, -95.35, -101.3 and -107.73 with a shoulder at -112.25 ppm corresponding to Q^0 (4Al), Q^1 (3Al), Q^2 (2Al), Q^3 (1Al) and Q^4 (0Al) species, respectively [30-33]. The spent catalyst (Fig. 12B) showed broad a signal at -104.2 ppm which can be as assigned to Q^3 species. Simultaneously, in the spent catalyst, the intensity of the signal at -107.7 ppm increased significantly as compared to the fresh catalyst. This implies that in spent catalyst more of Q^4 species are formed than the fresh catalyst. The origin of this Q^4 species (in the spent catalyst) can be described on the basis of conversion of Q^3 species into Q^4 species. It can be postulated that after removal of framework Al higher degree of condensation to form $Si(OSi)_4$ species may occur. Due to the strong overlap of the signals of different Si(nAl) sites in the spectra of zeolite made a quantitative evaluation complicated.

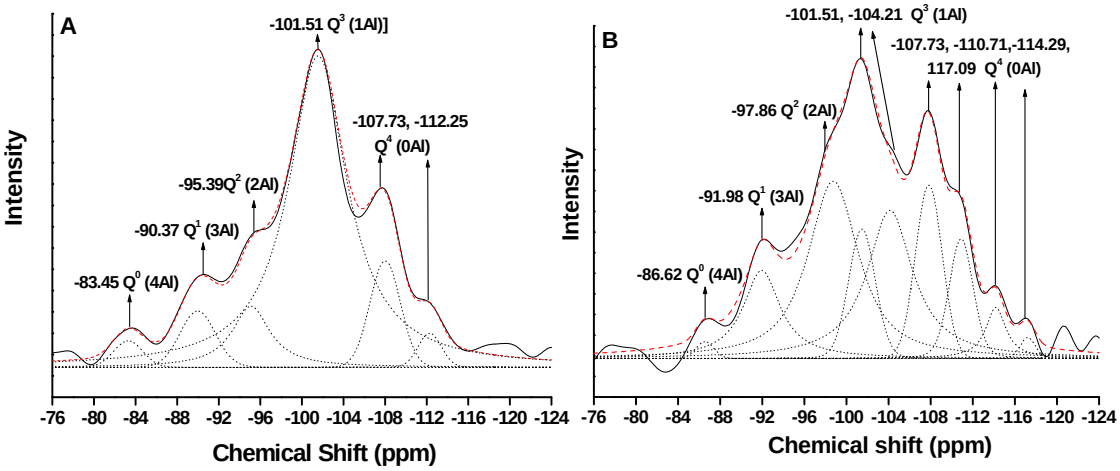

Fig. 4.12. ^{29}Si MAS NMR spectra of (A) fresh and (B) spent HUSY (Si/Al = 15) zeolite.

Fig. 4.13 shows the ^{29}Si MAS NMR spectra of fresh and spent Hβ (Si/Al = 19) samples. Fresh Hβ (Si/Al = 19) showed signals corresponding to Q^3 at -102.35 to -108.5 ppm, Q^4 at -111 to -115.88 ppm, Q^2 at –96.45 ppm and Q^1 at –91.54 ppm [34-37]. The spectra of the spent catalysts were highly complex. Several new signals have appeared. Significant changes in the intensities of the peaks compared to their fresh samples (Fig. 4.13A) were observed. All these features reveal that there is a partial collapse of the zeolite structure upon use.

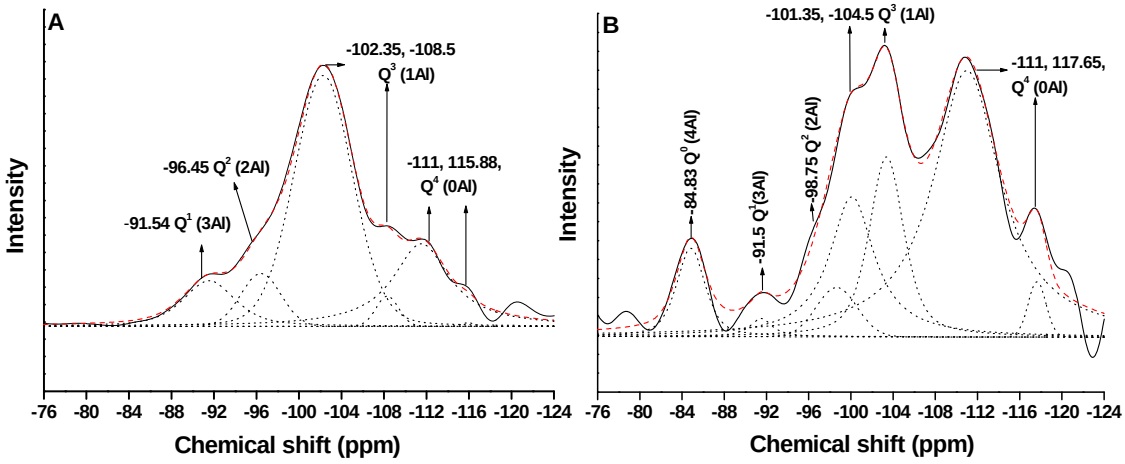

Fig. 4.13. ^{29}Si MAS NMR spectra of (A) fresh and (B) spent Hβ (Si/Al = 19) zeolite.

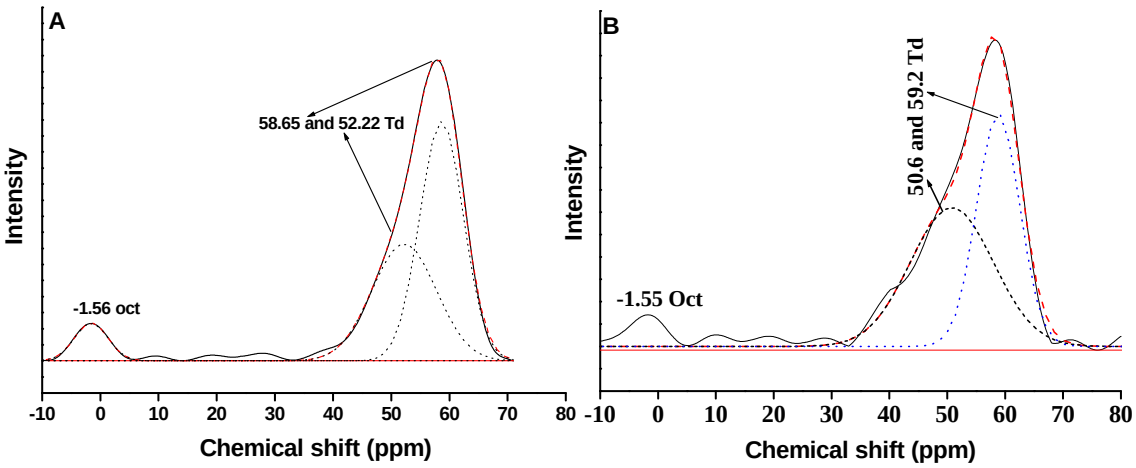

Fig. 4.14. ^{27}Al MAS NMR spectra of (A) fresh and (B) spent HUSY (Si/Al = 15) zeolite.

4.4.3.2. ^{27}Al MAS NMR

^{27}Al MAS NMR spectra of fresh and spent HUSY (Si/Al = 15) sample are presented in Fig. 4.14. The peak at 58.65 ppm is assigned to Al in tetrahedral environment ($Al(OSi)_4$). The other peak at -1.56 ppm is assigned to Al in octahedral

environment (AlO_6) [38]. The T_d and O_h signals arise from the Al in framework and extra-framework locations, respectively [39, 31]. The ^{27}Al NMR data of fresh and spent catalyst is in agreement with the data obtained from ^{29}Si NMR studies. The intensity of the signal (~58 ppm for tetrahedral Al (Al^{IV}) decreased in the spent catalyst compared with fresh catalyst. This indicates that the Al^{IV} (tetrahedral) species were converted into new species. It is known from the literature that a few of the Al species such as Si(OH)Al [40] and oligomeric Al are NMR invisible [41] and it can be considered that these species might have formed in spent catalysts. It may be noted that upon hydrothermal treatment the Al leaches out and it forms extra framework aluminium species (EFAL). The oxoaluminum cations, such as AlO^+, $Al(OH)_2^+$, and $AlOH^{2+}$, and some neutral species such as AlOOH and $Al(OH)_3$ are proposed to be the EFAL species though the detailed structures are not certain. Adsorbed water molecules break the Al-O bonds due to the thermal treatment, releasing $Al(OH)_3$ species out of the framework and leading to the formation of a silanol nest where the silanol groups are in close proximity with each other [42,43].

The ^{27}Al MAS NMR spectra of a spent Hβ (Si/Al = 19) (Fig. 4.15) look completely different from that of the fresh sample spectrum. The signal corresponding to tetrahedral Al sites showed a broad shoulder towards lower ppm range indicating that different types of Al sites (possibly pentracoordinated Al) are formed during the reactions. In other words, the solid state NMR studies reveal that there are structural and geometrical changes in the case of spent catalysts.

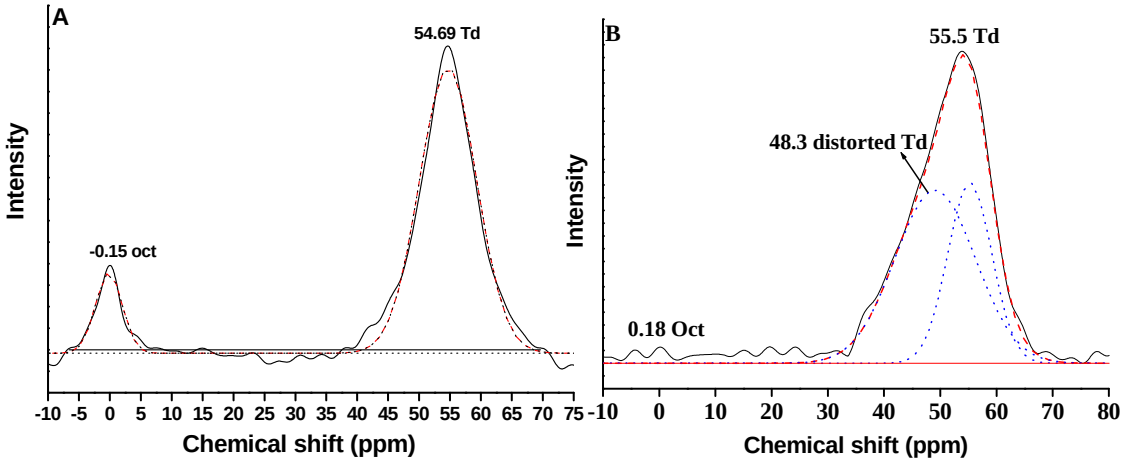

Fig. 4.15. ^{27}Al MAS NMR spectra of (A) fresh and (B) spent Hβ (Si/Al = 19) zeolite.

4.4.4. Chemical Composition

The spent uncalcined catalysts contained higher amounts of C and H content in their composition (Table 4.3). This is because of the accumulation of organic matter in the pores and external surface of zeolite and clay material. However, upon calcination, the organic matter got decomposed and the samples had the same content of C and H elements as in their fresh samples. In other words, blocking of pores is perhaps not the cause for the decrease in activity of the spent catalysts. The catalyst samples were also analyzed by ICP-OES technique. As seen from Table 4.4, the Si/Al ratio did not change upon reuse. However, an increase in the alkali content (Na + K) was observed in the case of spent calcined catalysts. It is known that plants require several nutrients (K, Na, Ca, Mg, Fe, etc.) for their growth and survival. During the separation process of hemicellulose from cellulose and lignin by the Kraft process, alkaline solutions are used. These alkali ions get trapped in the hemicellulose. Hence, biomass is the source for the Na and K in spent zeolites. A part of H^+ ions, perhaps, got replaced with these alkali ions. Hence, reduction in acidity of the spent catalyst is the possible cause for the lower activity of the spent catalysts. This is further substantiated by the TPD-NH_3 studies (Table 4.4).

Table 4.3. Element analyses of zeolite samples

Element	HUSY (Si/Al = 15)			Hβ (Si/Al = 19)		
	Fresh	Spent	Spent calcined	Fresh	Spent	Spent calcined
C (%)	0.3	6.1	0	0.3	6.2	0.4
H (%)	0.5	1.9	2.1	1.3	1.4	0.6

4.4.5. Temperature-Programmed Desorption of Ammonia

The acidities of fresh and spent catalysts were determined using NH_3 as a probe molecule. Experimental procedure adopted in these studies was discussed in Chapter 2 (section 2.4.1.3). Fig. 4.16 shows the TPD-NH_3 profiles of fresh and spent HUSY (Si/Al = 15) catalysts. Total acidities of different catalysts before and after use are listed in Table 4.6. A significant decrease in total acidity of the catalysts was observed after their use. This decrease in the case of HUSY (Si/Al = 15) after the 4^{th} run was from 0.55 to 0.21 mmol/g. Hemicellulose and bagasse are the source for the supply of these alkali ions, which replaced partially the acidic protons of the zeolite.

Table 4.4. ICP-OES analysis and TPD-NH_3 data of fresh and spent catalysts

Catalyst	ICP-OES analysis		Acidity (mmol/g; TPD-NH_3)
	Si/Al	Na+K (mmol/g)	
HUSY (Si/Al = 15) - fresh	14.2	0.02	0.55
HUSY (Si/Al = 15) - spent	15.4	0.28	0.21
Hβ (Si/Al = 19) - fresh	20.2	0	0.91
Hβ (Si/Al = 19) - spent	20.8	0.37	0.74
HMOR (Si/Al = 10) - fresh	11.3	0	1.15
HMOR (Si/Al = 10) - spent	12.2	0.49	0.81
K10 - fresh	-	-	0.42
K10 - spent	-	-	0.3

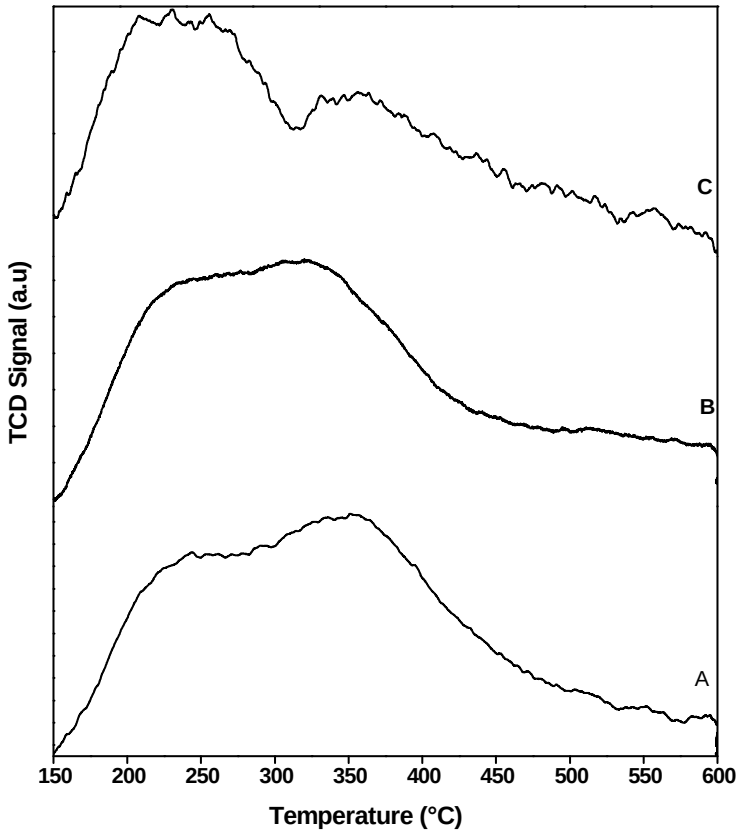

Fig. 4.16. TPD-NH_3 profiles of reused HUSY (Si/Al = 15): (A) 1st run, (B) 2nd run, (C) 4th run.

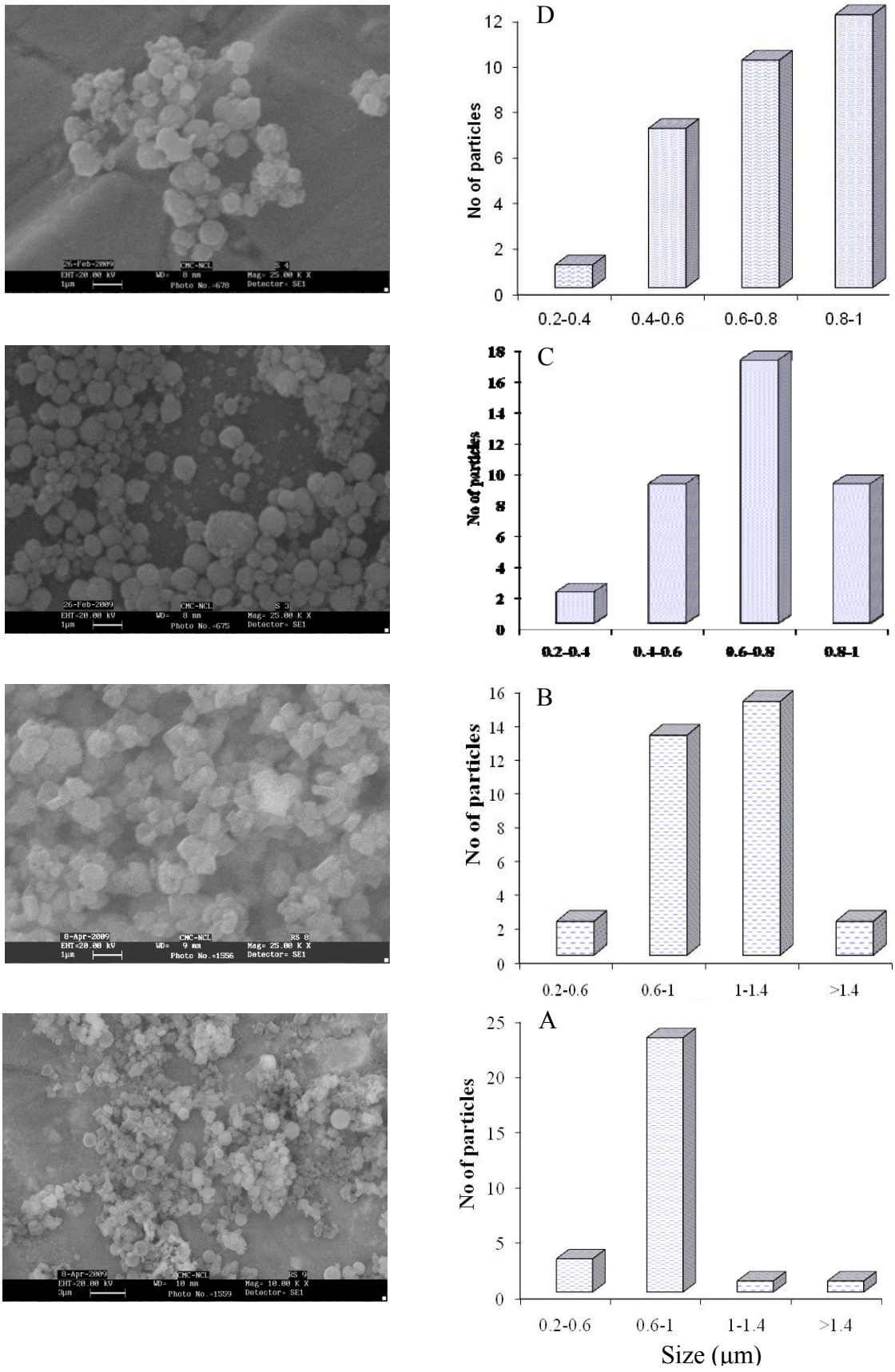

Fig. 4.17. SEM photographs and particle size distribution of fresh and spent catalysts: (A) fresh HUSY (Si/Al = 15), (B) spent HUSY (Si/Al = 15), (C) fresh Hβ (Si/Al = 19) and (D) spent Hβ (Si/Al = 19).

4.4.6. Scanning Electron Microscopy

The morphologic characteristics of fresh and spent HUSY and Hβ catalysts were examined by scanning electron microscopy (SEM; Fig. 4.17). In general, both HUSY and Hβ are spherical in shape. An increase in the particle from ~0.6 to 1 μm for HUSY and from ~0.8 to 1.0 μm for Hβ was observed in the case of spent catalysts. A decrease in surface area of the spent catalyst (N_2 adsorption-desorption studies) can, therefore, be attributed to an increase in their particle size.

All these characterization studies of fresh and spent catalysts, thus, reveal that deactivation of zeolite catalyst in bagasse conversion is because of the following reasons: (1) loss in acidity as a consequence of exchange of acidic protons by alkali ions present in bagasse, (2) decrease in surface area due agglomeration of particles during reaction, and (3) structural and geometrical changes.

4.5. Conclusions

In this chapter, the catalytic conversion of hemicellulose in bagasse into sugars and furfural has been investigated. The studies were carried out in the presence of HUSY (Si/Al = 15), Hβ (Si/Al = 19) and HMOR (Si/Al = 10) catalysts. These three were found as the best catalysts in Chapter 3 (section 3.4.2.) in the conversion of isolated hemicellulose. The highest yield of xylose + arabinose observed in this study was ~55% based on the hemicellulose present in bagasse. It was about 15% based on dried bagasse. This value is very low when compared to that obtained in the case of isolated hemicellulose. This could be due to relatively low content of C_5-sugars in bagasse. Xylose + arabinose got converted via dehydration to furfural. The latter is a high value chemical. In this study it was found that by adding an organic solvent like toluene, MIBK or *p*-xylene to the reaction medium the formation of furfural could be increased significantly.

In general, all the solid catalysts used in this study got deactivated in recycling experiments. Detailed characterization studies of fresh and spent catalysts revealed that the deactivation is due to loss of acidity, decrease in surface area and structural and geometrical changes of the catalysts. Alkali ions present in bagasse are responsible for the loss in acidity of the catalysts. To the best of knowledge, this is the first study reporting the application of solid catalysts in the conversion of bagasse into useful chemicals.

4.6. References

[1] Food and Agriculture Organization of United Nations: Economic and Social Department: The Statistical Division, www.en.wikipedia.org/wiki/sugarcane #cite-note-FAOSTAT-0

[2] M. Perez, A. Chaala, C. Roy, *J. Anal. Appl. Pyrolysis* **2002**, 65, 111.

[3] J. M. Paturau, *By-products of the Cane-Sugar Industry*, Elsevier Publishing Company, Amsterdam-London-New York **1969**.

[4] P. Dasa, A. Ganesha, P. Wangikar, *Biomass Bioenergy* **2004**, 27, 445.

[5] TIFAC Report **2009**.

[6] M. G. Adsul, A. J. Varmab, D. V. Gokhale, *Green Chem*. **2007**, 9, 58.

[7] S. I. Aronovsky, *Pulp and Paper Manufacture,* Elsevier Publishing Company, Vol.3, Amsterdam-London-New York **1951**.

[8] F. A. Rodrigues, R. Cuirardello, *Chem. Eng. Technol.* **2008**, 31, 883.

[9] Y. Sun, J. Cheng, *Bioresour. Technol.* **2002**, 83, 1.

[10] C. Ververis, K. Georghiou, D. Danielidis, D. G. Hatzinikolaou, P. Santas, R. Santas, V. Corleti, *Bioresour. Technol.* **2007**, 98, 296.

[11] V. Betancur, N. Pereira, *Electr. J. Biotechnol.* **2010**, 13, 1.

[12] A. R. Drummond, I. W. Drummond, *Ind. Eng. Chem. Res.* **1996**, 35, 1263**.**

[13] G. Marton, J. Dencs, L. Szokonya, *Principles of Biomass Refining: In Handbook of Heat and Mass Transfer,* Gulf Publishing, Houston **1989**.

[14] K. Youssef, M. Ghareib, M. Nour El Dein, *Acta. Microbiologica. Polonica* **1991**, 40, 187.

[15] R. Torget, P. Werdene, M. Himmel, K. Grohman, *Appl. Biochem. Biotechnol.* **1990**, 24, 115.

[16] M. El-Taaboulsi, M. Nassar, E. A. E. Rehim*, J. Chem. Technol. Biotechnol.* **1983**, 33A, 387.

[17] B. C. Saha, R. J. Bothast, *Enzymology of Xylan Degradation in Biopolymers Utilizing Natures Advanced Materials*, ACS, Washington **1999**.

[18] B. C. Saha, *Ind. Microbiol. Biotechnol.* **2003**, 30, 279.

[19] M. Balat, H. Balat, V. Öz, *Progress in Bioethanol Process* **2008**, 34, 551.

[20] J. Zaldivar, J. Nielsen, L. Olsson, *App. Microbiol. Biotechnol*. **2001**, 56, 17.

[21] C. A. Cardona, Ó. J. Sánchez, *Bioresour. Technol.* **2007**, 98, 2415.

[22] A. Onda, T. Ochi, K. Yanagisawa, *Green Chem.* **2008**, 10, 1033.

[23] A. Fukuoka, P. L. Dhepe, *Angew. Chem. Int. Ed.* **2006**, 45, 5161.

[24] S. E. Jacobsen, C. E. Wyman, *Ind. Eng. Chem. Res.* **2002**, 41, 1454.

[25] E. Lippama, M. Magi, A. Samoson, M. Tarmak, G. Engelhardt, *J. Am.Chem. Soc*. **1981**, *103*, 4992.

[26] J. Klinowski, J. M. Thomas, C. A. Fyfe, J. S. Hartman, *J. Phys. Chem.* **1981**, 85, 2590.

[27] N. Dewaele, P. Bodart, Z. Gabelica, J. B. Nagy, *Acta. Chem. Acad. Sci. Hung*. **1985**, 119, 233.

[28] P. Bodart, N. Dewaele, Z. Gabelica, J. B. Nagy, E. G. Derouane, *J. Chim. Phys. Phys. Chim. Biol.* **1986**, 83, 777.

[29] S. Hayashi, K. Suzuki, S. Shin, K. Hayamizu, O.Yamamoto, *Chem. Phys. Lett.* **1984**, 110, 54.

[30] T. I. Koranyi, J. B. Nagy, *J. Phys. Chem. C* **2007**, 111, 2520.

[31] I. Hannus, Z. Konya, J. B. Nagy, P. Lentz, I. Kiricsi, *Appl. Catal. B: Environ.* **1998**, 17, 157.

[32] I. E. Maxwell, W. A. van Erp, G. R. Hays, *J. Chem. Soc., Chem. Comm.* **1982**, 523.

[33] B. Xu, S. Borddiga, R. Prins, J. A. van Bokhoven, *Appl. Catal. A: General* **2007**, 333, 245.

[34] R. Hajjar, Y. Millot, P. P. Man, M. Che, S. Dzwigaj, *J. Phys. Chem. C* **2008**, 112, 20167.

[35] W. Zhang, P. G. Smirniotis, M. Gangoda, R. N. Bose, *J. Phys. Chem. B* **2000**, 104, 4122.

[36] J. P. Pariente, J. Sanz, V. Fornes, A. Corma, *J. Catal.* **1990**, 124, 217.

[37] J. Sanz, V. Fornes, A. Corma, *J. Chem. Soc, Faraday Trans.* **1988**, 84, 3113.

[38] K. Pitchumani, M. Warrier, V. Ramamurthy, *J. Am. Chem. Soc.* **1996**, 118, 4527.

[39] M. J. Remy, D. Stanica, G. Poncelet, E. J. P. Grobet, J. A. Martens, P. A. Jacobs, *J. Phys. Chem*. **1996**, 100, 12440.

[40] H. Ernst, D. Freude, I. Wolf, *Chem. Phy. Lett.* **1993**, 212, 588.

[41] P. J. Grobet, H. Geerts, M. Tielen, J. A. Martens, P. A. Jacobs, *Studies in Surface Science and Catalysis* **1989**, 46, 721.

[42] S. Li, A. Zheng, Y. Su, H. Zhang, L. Chen, J. Yang, C. Ye, F. Deng, *J. Am. Chem. Soc.* **2007**, 129, 11161.

[43] J. Klinowski, *chem. Rev.* **1991,** 91, 1459.

CHAPTER-5
AERIAL OXIDATION OF FURAN CHEMICALS USING SUPPORTED METAL CATALYSTS

5.1. Introduction

Acid-catalyzed dehydration of sugars results in value-added furan compounds [1-3]. The furanic products [5-hydroxymethyl furfural (HMF), 2,5-diformylfuran (DFF), 2,5-furandicarboxylic acid (FDCA), 2,5-bis(hydroxymethyl) furan (BHF) and 2,5-dimethylfuran (DMF)] are used as starting materials in the synthesis of new products and as replacement for the oil-derived chemicals. As a dehydration product of hexoses, HMF has been considered as an important and renewable platform chemical [4-7]. Its derivatives including 2,5-furfuryldiamine, 2,5-furfuryldiisocyanate and 5-hydroxymethyl furfurylidenester are particularly suitable as starting materials in the preparation of polymers such as polyesters, polyamides and polyurethane [8-9]. The obtained furan-based polymer exhibits unique properties. The polyurethane derived from furan compounds shows very high resistance to thermal treatment. The kevlar-like polyamide produced from furan diamines and diacids exhibits liquid crystal behaviour. The photoreactive polyesters have been used in the printing ink formulations. Further, the furan-based polyconjugated polymers possess good electrical conductivity [10]. Hence, research on the synthesis of bio-furan compounds is of considerable current interest. Dehydration of pentoses (xylose and arabinose, for example) yields furfural while dehydration of hexoses (glucose and fructose, for example) results in HMF (Fig. 5.1). Annually, 200,000 tons of furfural is industrially produced. HMF is being prepared on a pilot plant scale only [11].

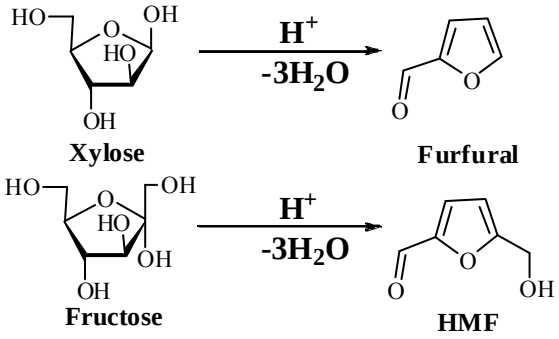

Fig. 5.1. Synthesis of furfural and HMF from xylose and fructose, respectively.

Furoic acid and FDCA are synthesized from furfural and HMF through oxidation processes (Scheme 5.1). The catalytic oxidation of these chemicals is carried out in the presence of supported metal catalysts in basic aqueous medium.

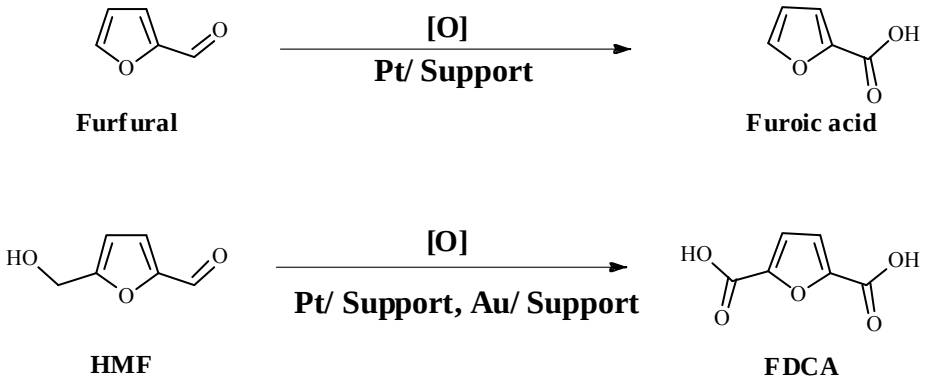

Scheme 5.1. Oxidation of furfural and HMF.

Conventionally, oxidations are carried out using stoichiometric reagents. These methods are not eco-friendly and generate significant amount of waste products, disposal of which is an issue. The use of molecular oxygen or air instead of stoichiometric oxidation reagents makes the process sustainable [12]. One of the major issues is the selectivity in aerial oxidation reaction. Development of solid, selective oxidation catalysts is a challenging task in the area of oxidation reactions.

Supported noble metals are widely used as catalysts in oxidation reactions. Supported Au and Pt have shown highly efficient catalytic activity for aqueous phase oxidation of alcohols and aldehydes [13-15]. Hence, these metals are considered as catalysts in the present study for the oxidation of furfural and HMF.

The support plays a crucial role in catalytic systems. It increases the surface area of the supported noble metal. It reduces the crystallite size and enhances the dispersion of metals. It can prevent sintering of metal species. It can also improve the thermal and chemical stability of the catalytic material and enhance the lifetime of the catalyst. Sometimes support also takes part in the reaction and acts as a co-catalyst [16].

In this study, Pt and Au are deposited on different supports having varying properties (γ-Al_2O_3, activated carbon (AC), ZrO_2, TiO_2 and CeO_2). While CeO_2 is a highly reducible oxide, TiO_2 and ZrO_2 are weakly reducible. γ-Al_2O_3 and AC are non-reducible oxides. These variations in the redox behaviour of the supports are expected to influence the catalytic properties of supported Pt and Au in the oxidation of furfural and HMF. Scheme 5.2 presents the possible oxidation products of HMF.

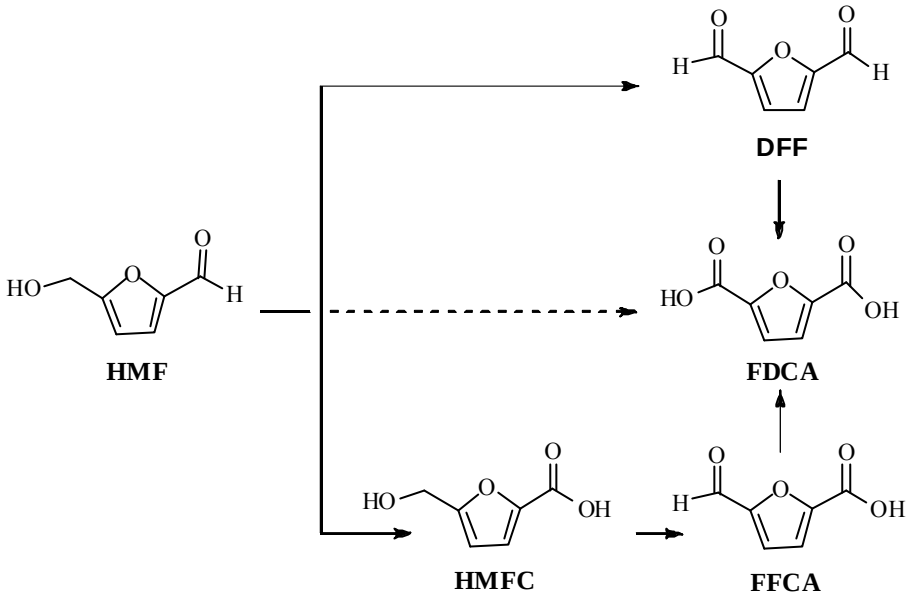

Scheme 5.2. Oxidation products of HMF.

Depending on the reaction conditions, pH of the solution and catalysts, various partial oxidation products such as 5-hydroxymethyl furfural carboxylic acid (HMFC), formyl furan carboxylic acid (FFCA) and diformyl furan (DFF) are formed (Scheme 5.2) [17]. In the ongoing chapter, we designate HMFC and FFCA as intermediate products. Selective FDCA formation from HMF using supported metal catalysts, in one-pot, is of particular interest. This study therefore targets the oxidation of furfural and HMF in the aqueous medium in the presence of supported nano Pt and Au catalysts. Reaction conditions are optimized to get higher yield of the corresponding carboxylic acid. Structure-activity correlations are discussed.

5.2. Experimental

5.2.1. Materials and Methods

All chemicals used in this chapter are of analytical grade and used as received. HMF, furoic acid and d_6-DMSO were purchased from Sigma-Aldrich. Sodium hydroxide, potassium permanganate, ethyl acetate, acetic acid, dichloro methane and methanol (>98% purity) were purchased from Loba Chemicals, India. Deionized water was used to prepare various solutions.

A standard sample of FDCA was prepared as follows. 0.13 g of HMF was dissolved in 5 g of water taken in a round-bottom flask placed in an ice-bath. 0.96 g of NaOH was dissolved in 5 g of water and added to the above solution while stirring. Then, 0.37 g of solid $KMnO_4$ was added. The round-bottom flask was removed from

the ice- bath and the solution was allowed to stir for another 1 h at ~30°C. The reaction mixture was filtered and acidified with 6 N HCl solution (pH ~ 2). The acidified solution was extracted with ethyl acetate where FDCA was soluble. Ethyl acetate solvent was dried with sodium sulphate and solvent was evaporated by rota-vapour. A brown colour solid, FDCA, thus obtained, was used as a standard sample [18]. The purity of this compound was confirmed by thin layer chromatography (TLC), ^{1}H and ^{13}C NMR spectra, mass spectra and elemental analysis (C, H & N). The solvent medium for TLC was a mixture of dichloromethane, methanol and acetic acid in a volume ratio of 6 : 2 : 0.5.

Several supported metals (Pt/γ-Al_2O_3, Au/γ-Al_2O_3, Pt/AC, Pt/ZrO_2, Pt/TiO_2, and Pt/CeO_2) were used as catalysts in this study. Their preparation has been reported in Chapter 2 (section 2.2.4).

5.2.2. Reaction and Analytical Procedures

All the reactions were carried out in a 300 mL Teflon-lined Parr batch reactor. A known quantity of substrate (furfural or HMF), water, catalyst and base (Na_2CO_3 or NaOH) were taken in the reactor. Oxygen was purged three times and then, the reactor was pressurized with oxygen to a desired value. The reactor was heated and the reaction was conducted for a specified period of time. In between, the samples were withdrawn, centrifuged, filtered and analyzed by a Shimadzu HPLC unit equipped with a HC-75 H^+ column (length = 305 mm and I.D. = 7.8 mm) and refractive index detector (Model No. RID-6A). An aqueous solution of H_3PO_4 (0.1 wt%) was used as the mobile phase (flow rate = 0.6 mL/min). Column temperature was maintained at ~30°C. The concentration of each compound in the reaction mixture (FDCA, HMF and furoic acid) was estimated from the calibration curves generated using standards of the above compounds. Conversion and product yield calculation were according to the known procedures.

The purity of isolated FDCA was confirmed by the LC-MS technique. The sample was dissolved in methanol and analyzed by LC-MSMS-TOF (API QStar Pulsar, Applied Bio-system, UK) instrument. The sample was run at a flow rate of 10 μL/min and detected by a multichannel plate (MCP) detector.

5.3. Results and Discussion

5.3.1. Catalyst Characterization

5.3.1.1. X-Ray Powder Diffraction

Fig. 5.2 depicts the powder XRD of Pt (3.5 wt%) and Au (2 wt%) supported on γ-Al_2O_3, activated carbon (AC), ZrO_2, CeO_2, and TiO_2. The peaks corresponding to the metal crystallites are indexed. The intensity of the metal peaks is very low in the case of CeO_2 than in the case of γ-Al_2O_3 and AC supports. Pt showed diffraction peaks at 2θ = 39.70°, 46.18°, 67.00° and 81.3° which are assigned to (111), (200), (220) and (311) planes, respectively of the face-centered cubic (fcc) lattice [19]. Au showed reflections at 2θ values at 38.14°, 44.42°, 64.98° and 77.70° due to (111), (200), (220) and (311) planes, respectively [20]. Crystallite size (CS) of these metals on different supports was estimated using the Scherrer equation and it was found to vary in the order: Pt (3.5 wt%/CeO_2 (CS = 29.4 nm) > Pt (3.5 wt%)/TiO_2 (CS = 27.6 nm) > Pt (3.5 wt%)/ZrO_2 (CS = 19.7 nm) > Pt (3.5 wt%)/AC (CS = 14 nm) > Pt (3.5 wt%)/γ-Al_2O_3 (CS = 13 nm). Gold supported on γ-Al_2O_3 has a crystallite size of 13 nm.

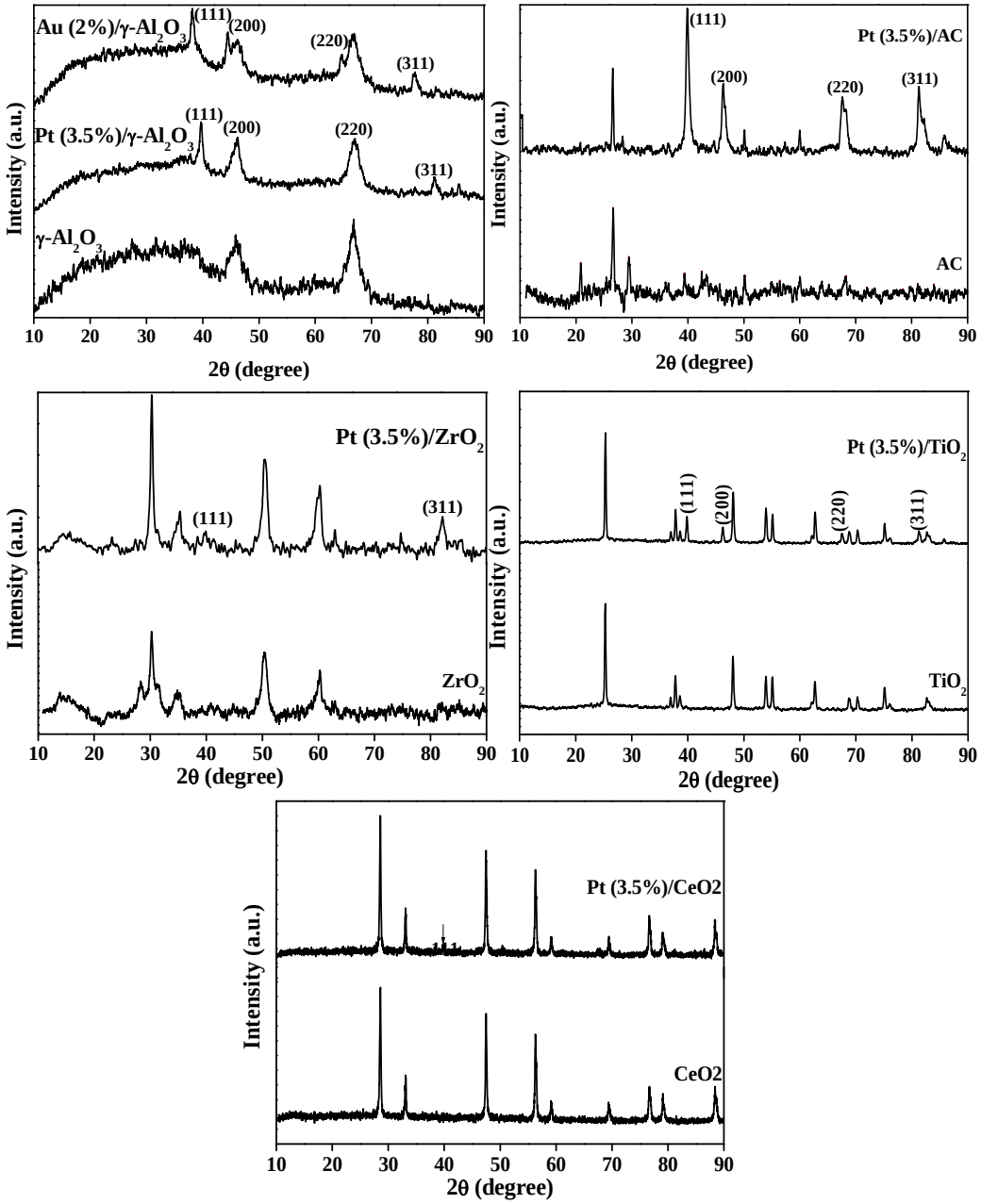

Fig. 5.2. XRD patterns of supported metal catalysts in their reduced form.

5.3.1.2. N_2 Sorption

The specific surface area, pore volume and pore diameter values of the supports estimated from N_2 adsorption-desorption isotherms are listed in Table 5.1. The pore size was determined by the HK (Horvath-Kawazoe) method. The surface area of different supports decreased in the order: AC > γ-Al_2O_3 > ZrO_2 > TiO_2 > CeO_2. The crystallite size of metal determined from XRD results agrees well with the variation in the surface area of different supports.

Table 5.1. Textural properties of different supports determined from N_2 - physisorption studies

Support	Surface area (m^2/g)	Pore volume (mL/g)	Pore size (Å)
γ-Al_2O_3	225	0.09	11.62
AC	552	0.21	11.62
ZrO_2	87	0.02	12.48
TiO_2	37	0.14	11.42
CeO_2	23	0.008	11.38

5.3.1.3. Inductively Coupled Plasma-Optical Emission Spectroscopy

The metal content was estimated by ICP-OES. The amount of Pt and Au in these catalysts was determined to be 3.7 and 2.0 wt%, respectively.

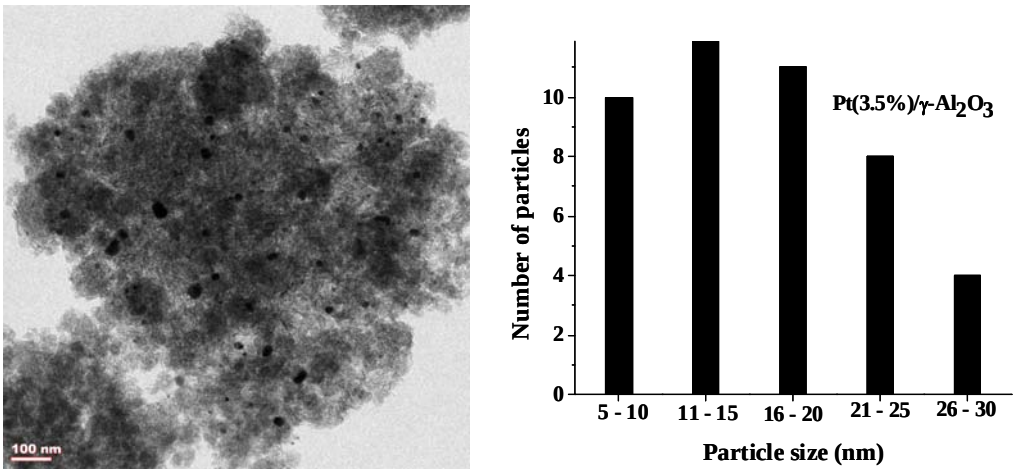

Fig. 5.3. TEM image of Pt (3.5 wt%)/γ-Al_2O_3 and metal particle size distribution.

5.3.1.4. Transmission Electron Microscopy

Figs. 5.3 - 5.5 show the transmission micrographs and metal particle size distribution of Pt (3.5 wt%)/γ-Al_2O_3, Pt (3.5 wt%)/AC and Au (2 wt%)/γ-Al_2O_3 catalysts, respectively. The black dots in the micrographs correspond to the metal particles. The average metal particle size in the above three catalysts estimated by the statistical method was 15.7, 12.5 and 10.3 nm, respectively. This variation is in accordance with the surface area of the supports.

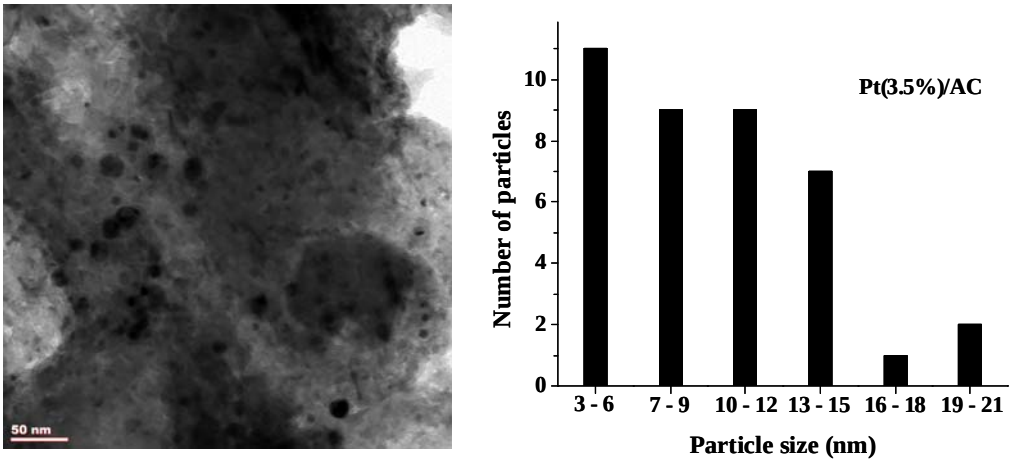

Fig. 5.4. TEM image of Pt (3.5% wt%)/AC and metal particle size distribution.

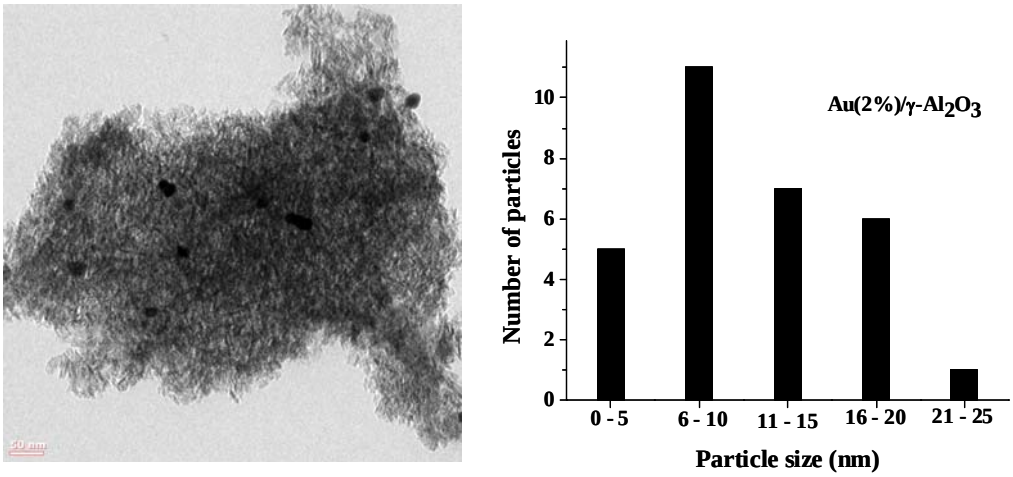

Fig. 5.5. TEM image of Au (2% wt%)/γ-Al_2O_3 and metal particle size distribution.

5.3.2. Catalytic Activity

5.3.2.1. Oxidation of HMF

5.3.2.1.1. Effect of Base

The pH of the reaction medium (base addition) had a major effect on HMF conversion and product selectivity. The reactions were conducted at 100°C and oxygen pressure of 10 bar; Pt(3.5 wt%)/γ-Al_2O_3 was used as the catalyst. In the absence of a base, HMF conversion of about 49% was observed. However, upon adding 1 equivalent of Na_2CO_3, the conversion of HMF increased to 90%. When NaOH instead of Na_2CO_3 was added, the conversion of HMF was nearly 95%. An increase in the amount of Na_2CO_3 by four fold had increased the HMF conversion only to a lesser extent (from 90 to 95%). As seen from Fig. 5.6, the yield of FDCA and intermediates together did not account for the total HMF converted indicating

formation of undesired products which could not be detected by our analytical techniques (HPLC and GC). Formation of such undesired products is higher in the absence of base than with 1 equivalent of Na_2CO_3. The product yield (FDCA + intermediates) was higher with 1 equivalent of Na_2CO_3 (56%) than with NaOH (42%). Increasing the concentration of Na_2CO_3 had a negative effect on the product yield (48%). The pH of the reaction medium was 11.5 in the presence of 1 equivalent of Na_2CO_3 and it was 13 with NaOH. Hence, too high a pH is detrimental on the product yield. The acid products are insoluble in water. Base converts them into water soluble sodium salts and thereby avoids their deposition on the actives sites of the catalyst. Having understood that the addition of 1 equivalent of Na_2CO_3 is good enough to get higher product yield, subsequent reactions were carried out with this base concentration in the reaction medium.

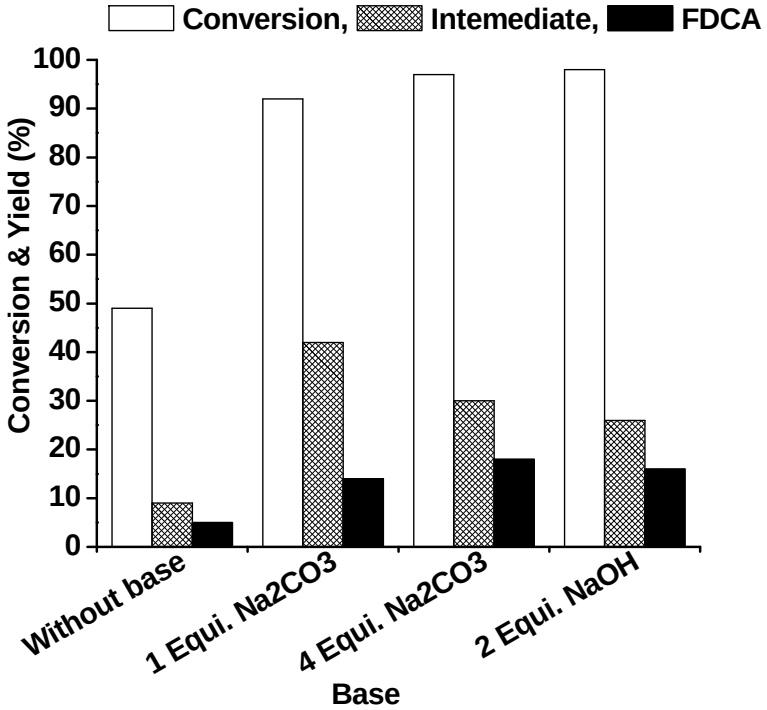

Fig. 5.6. Effect of base on the oxidation of HMF. *Reaction conditions*: HMF (0.1 g), water (60 g), Pt (3.5 wt%)/γ-Al_2O_3 (0.1 g), O_2 pressure (10 bar @ RT), temperature (100°C) and reaction time (24 h).

5.3.2.1.2. Effect of Oxidant

The reaction of HMF over Pt(3.5 wt%)/γ-Al_2O_3 was carried out in the presence of nitrogen, pure oxygen and air (Fig. 5.7). Rest of the reaction conditions were maintained the same. About 50% of HMF got converted at the end of 48 h even in the presence of nitrogen. Yield of FDCA + intermediates was only 5%. The balance

was undesired products which could not be identified. However, in the presence of oxygen, the conversion of HMF increased to more than 90%. The total oxidation products yield was nearly 84 wt%, the balance being undesired products. Use of air instead of pure oxygen did not alter the conversion or oxidation products yield significantly. Hence, air can be used instead of pure oxygen in the oxidation of HMF.

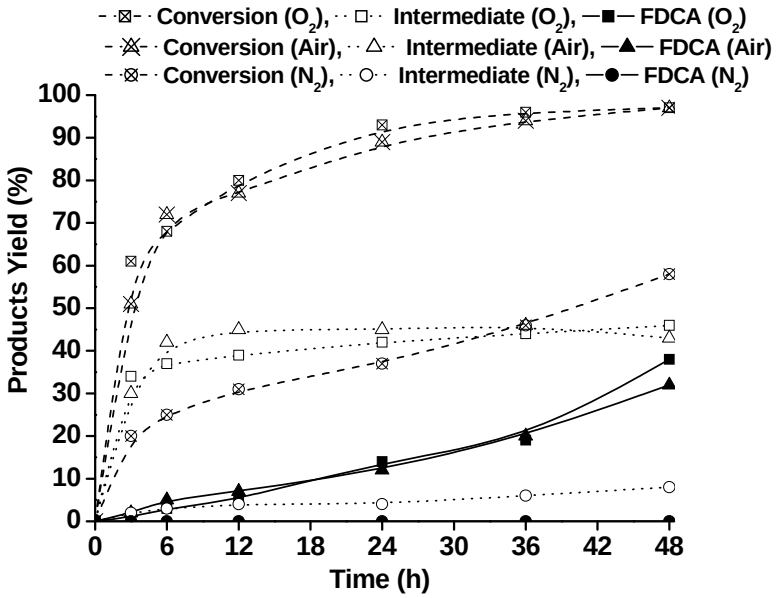

Fig. 5.7. Oxidation of HMF. *Reaction conditions:* HMF (0.1 g), water (60 g), Pt (3.5 wt%)/γ-Al_2O_3 (0.1 g), Na_2CO_3 (0.0841 g; 1 equivalent of HMF), pressure (10 bar @ RT) and temperature (100°C).

5.3.2.1.3. Effect of Temperature

Fig. 5.8 demonstrates the influence of temperature on the oxidation of HMF over Pt(3.5 wt%)/γ-Al_2O_3. As the temperature increased from 100 to 140°C, FDCA formation increased from 37 to 52%. The conversion of HMF could reach 100% irrespective of temperature but longer reaction times were required at lower temperatures.

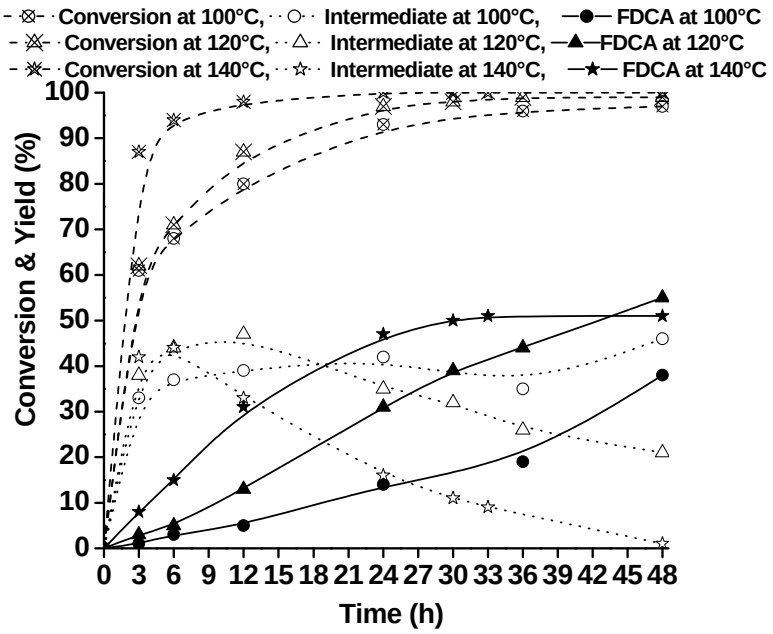

Fig. 5.8. Influence of reaction temperature on HMF oxidation. *Reaction conditions*: HMF (0.1 g), water (60 g), Pt (3.5 wt%)/γ-Al_2O_3 (0.1 g), O_2 pressure (10 bar @ RT) and Na_2CO_3 (0.0841 g; 1 equivalent with respect to HMF).

Table 5.2. Oxidation of HMF over Pt(3.5 wt%)/Al_2O_3: effect of O_2 pressure[a]

O_2 Pressure (bar @ 25°C)	Time (h)	HMF conversion (wt%)	Products yield (wt%)	
			Intermediates	FDCA
10	24	100	16	47
	30	100	11	50
	48	100	9	52
5	24	100	10	53
	30	100	6	56
1	24	100	7	61
	36	100	1	67
	48	100	0	69

[a]*Reaction conditions:* HMF (0.1 g), water (60 g), catalyst (0.1 g), temperature (140°C), Na_2CO_3 (0.0841 g; 1 equivalent of HMF) and reaction time (48 h).

5.3.2.1.4. Effect of Oxygen Pressure

The pressure of oxygen has a marked effect on the yield of FDCA. Oxygen pressure was varied from 1 to 10 bar. HMF conversion was nearly 100% irrespective of oxygen pressure. However, as seen from Table 5.2, FDCA formation was higher (69% at the end of 48 h) when the pressure was 1 bar than when it was 5 bar (56%) or 10 bar (52%). Higher pressure of oxygen leads to adverse effect on the FDCA yield. An optimum pressure of 1 bar is sufficient to oxidize the intermediates especially the primary alcohol substituent of the furan derivatives.

Table 5.3. Oxidation of HMF over Pt (3.5 wt%)/Al_2O_3: effect of step-wise increase in reaction temperature[a]

Temperature (°C)	Time (h)	HMF conversion (wt%)	Products yield (wt%)	
			Intermediates	FDCA
one-stage reaction				
140	24	100	7	61
140	36	100	1	67
140	48	100	0	69
Two-stage reaction				
75	18	84	62	10
140	24 (Total 42 h)	100	4	88

[a]*Reaction conditions:* HMF (0.1 g), water (60 g), catalyst (0.1 g), pressure (O_2: 1 bar@ RT) and Na_2CO_3 (0.0841 g; 1 equivalent of HMF).

5.3.2.1.5. Effect of Step-wise Increase in Temperature

In all the above experiments, a good amount of undesired products formation was detected. Mass balance was not satisfactory. Hence, the reaction was conducted in two-stages. In the first-stage, reaction was carried out at 75°C for 18 h and then the temperature was raised to 140°C and the reaction was conducted for another 24 h. By this way, a significant increase in the products yield and mass balance (92% and

above) was achieved. Table 5.3 presents the experimental results obtained from the reactions conducted in one stage and in two stages. When the reaction was carried out at 140°C (one stage), only 69% of FDCA yield was obtained. At this temperature, mass balance was only 69%. The yield of FDCA increased to 88% and mass balance to 92% when the reaction was conducted in two stages. At higher temperatures, HMF decomposes to undesired products. When the reaction was carried out at lower temperature this decomposition of HMF to undesired products could be arrested to a minimum extent and thereby, the yield of FDCA could be increased. All the subsequent reaction optimization experiments were conducted in two-stages as described in this section.

Table 5.4. Effect of HMF concentration on its oxidation

Temperature (°C)	HMF conc. (wt%)	Time (h)	Conversion (wt%)	Products yield (wt%)	
				Intermediate	FDCA
75 (Stage I)	0.16	18	84	62	10
140 (Stage II)		24 (Total 42 h)	100	4	88
75 (Stage I)	0.5	3	86	60	23
140 (Stage II)		10 (Total 13 h)	100	7	93

Reaction conditions: Water (60 g), HMF/catalyst molar ratio = 50, Pt (3.5 wt%)/γ-Al_2O_3 (0.1 or 0.3 g), O_2 pressure (1 bar @ RT) and Na_2CO_3 (0.0841or 0.2523 g; 1 equivalent of HMF).

5.3.2.1.6. Effect of Substrate Concentration

While maintaining the substrate/catalyst molar ratio and substrate/Na_2CO_3 ratio the same, the concentration of the substrate (HMF) in water was changed from 0.16 to 0.5 wt%. Oxidation reactions with 1 bar of O_2 were conducted in a closed reactor in two temperature stages. In the first-stage, the reaction was conducted at 75°C and in the second-stage, it was conducted at 140°C. As seen from Table 5.4, complete conversion of HMF was observed irrespective of the concentration. However, the yield of FDCA was higher (by 5%) when the concentration of HMF

was 0.5 instead of 0.16 wt%. Most importantly, the reaction time to achieve this concentration decreased from 42 to 13 h when the concentration of the substrate was increased. At higher concentrations, contact of HMF with the catalyst was more probably than at the lower concentrations and thereby, an enhancement in catalytic activity was observed. About 93% of FDCA was produced selectively with 0.5 wt% of the substrate concentration in water.

5.3.2.1.7. Effect of Substrate/Catalyst Mole Ratio

While keeping the substrate (HMF) concentration in water and base/HMF molar ratio the same, the ratio of HMF/catalyst molar ratio was varied from 50 to 150. The reaction was conducted in two-stages (75°C for 12 h and then at 140°C for another 12 h). Pressure of oxygen was 1 bar. As seen from Table 5.5, a marginal decrease in the yield of FDCA from 96 to 88% was observed when the substrate to catalyst ratio was changed from 50 to 150. A major difference in FDCA conversion was observed.

Table 5.5. Effect of substrate/catalyst ratio on HMF oxidation over Pt(3.5 wt%)/γ-Al_2O_3 catalyst

Temperature (°C)	Sub/Cat ratio (mole)	Time (h)	HMF con. (%)	Product yield (%)	
				Intermediate	FDCA
75	50	12	95	51	45
140	50	12 (Total 24 h)	100	0	96
75	150	12	86	57	21
140	150	12 (Total 24 h)	100	1	88

Reaction conditions: HMF (0.3 g), water (60 g), catalyst (0.3 or 0.1 g), O_2 pressure (1 bar @ RT), two-stage reaction (75°C for 12 h and then at 140°C for another 12 h), Na_2CO_3 (0.2523 g; 1 equivalent of HMF) and total reaction time (24 h).

5.3.2.1.8. Effect of Support and Metal

The oxidation reactions were conducted in the presence of Pt (3.5% wt) and Au (2 wt%) supported on different reducible and non-reducible oxides. While keeping the conditions the same, reactions were conducted in two-stages (75°C for 12 h and 140°C 12 h). Na_2CO_3 (2 equivalents of HMF) was used as the base. Controlled

experiments revealed that the reaction progressed (52%) even in the absence a catalyst. But the yield of the oxidation product was only 4%. Perhaps, HMF gets thermally decomposed in the absence of a catalyst. Pt/γ-Al_2O_3, Pt/ZrO_2 and Pt/AC showed superior activity to the rest of the catalysts (Fig. 5.9). About 90% of FDCA formed selectivity at 100% HMF conversion. The yields of FDCA and intermediates were 40 and 39%, respectively at 99% conversion of HMF over Au/γ-Al_2O_3 catalyst. Platinum supported on TiO_2 and CeO_2 resulted in the FDCA yield of about 5% only. Pt supported on non-reducible oxides (γ-Al_2O_3 and ZrO_2) and AC resulted in more than 18 times higher yield of FDCA than that observed on reducible oxides (TiO_2 and CeO_2).

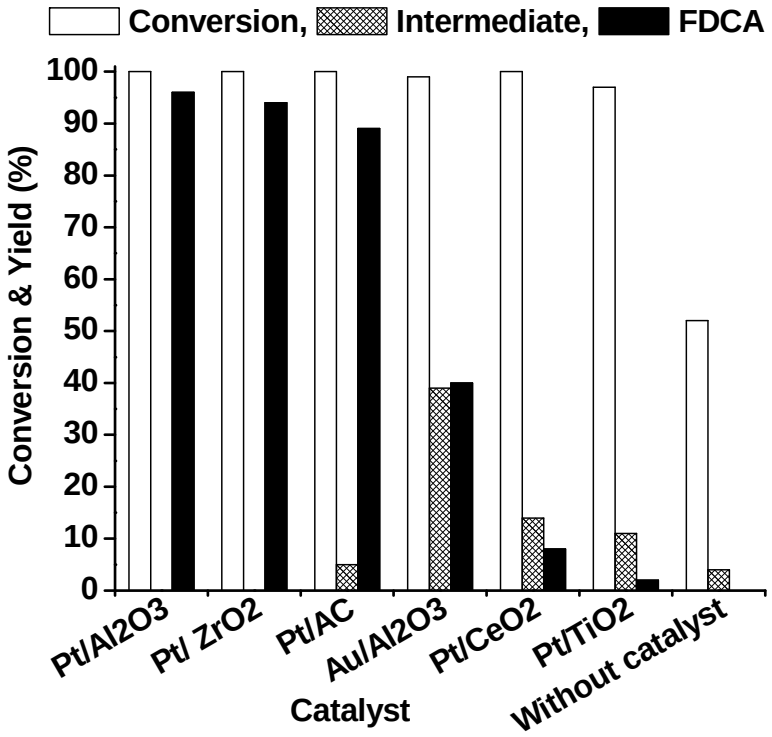

Fig. 5.9. Catalysts evaluation study on HMF oxidation. *Reaction conditions:* HMF (0.3 g), water (60 g), catalyst (0.3 g), pressure (O_2:1 bar@ RT), temperature (75-140°C), base (0.2523 g; 1 equivalent of HMF) and reaction time (24 h).

5.3.2.1.9. Recyclability Study

Fig. 5.10 depicts the recyclability of the catalyst. Recycling of the catalyst was attempted by separating the catalysts by filtration followed by drying at 80°C under high-vacuum (10^{-3} bar). The dried catalyst was used in the next run. The yield of the product FDCA decreased by 50%. In another approach, the dried catalyst was reduced for 2 h under a flow of hydrogen (30 mL/min) at 400°C. This catalyst was then used

in the second run. As seen from Fig. 5.10, the catalyst is nearly stable and recyclable. FDCA yield in the first run was 96% and that in the second run was 92%. HMF conversion was 100% in both the runs. From these results it can be concluded that there is no appreciable loss in catalytic activity and the catalyst could be reused.

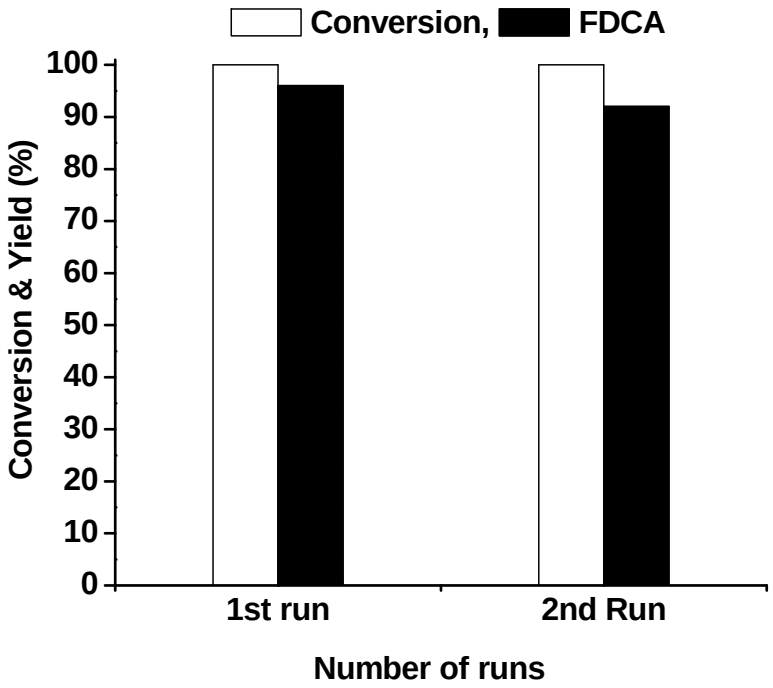

Fig. 5.10. Catalyst recyclability study in the oxidation of HMF. *Reaction conditions:* HMF (0.3 g), water (60 g), Pt (3.5 wt%)/γ-Al_2O_3 (0.3 g), O_2 pressure (1 bar @ RT), two-stage reaction (75°C for 12 h and then at 140°C for another 12 h) and Na_2CO_3 (0.2523 g; 1 equivalent of HMF).

In order to check the leaching of supported metal from the catalyst into the liquid portion, the reaction was carried out at 100°C for 24 h using a fresh Pt (3.5 wt%)/γ-Al_2O_3 catalyst. The reaction was stopped and the catalyst was separated by filtration. Then the reaction was continued without any catalyst. No significant increase in conversion and FDCA yield was observed indicating that the reaction occurs on the catalyst surface. No homogeneous reaction was taking place. The filtrate was analyzed by ICP-OES and it was found that 5 ppm of Pt leached into the solution. But this leached Pt did not catalyze the reaction.

Based on crystallite size and the amount of Pt loaded, the metal dispersion was estimated and correlated with the product yield (FDCA + intermediates). As seen from Fig. 5.11, FDCA yield increased with increasing metal dispersion up to a certain value and above that it decreased. Pt(3.5 wt%)/γ-Al_2O_3 has the right kind of metal

dispersion and metal particle size and hence, turned out to be the best catalyst among those investigated in this work.

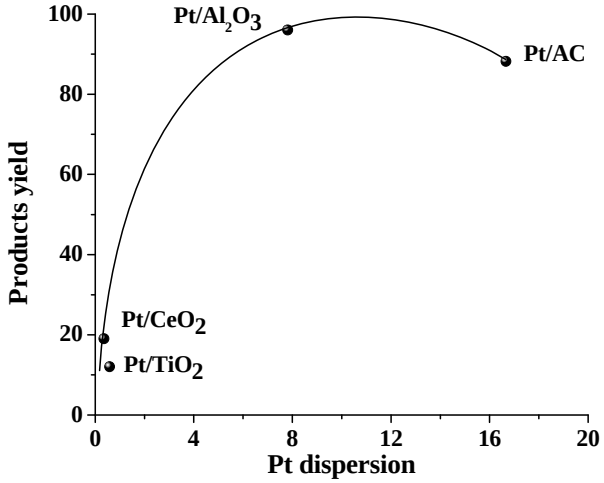

Fig. 5.11. Variation of product yield with metal dispersion.

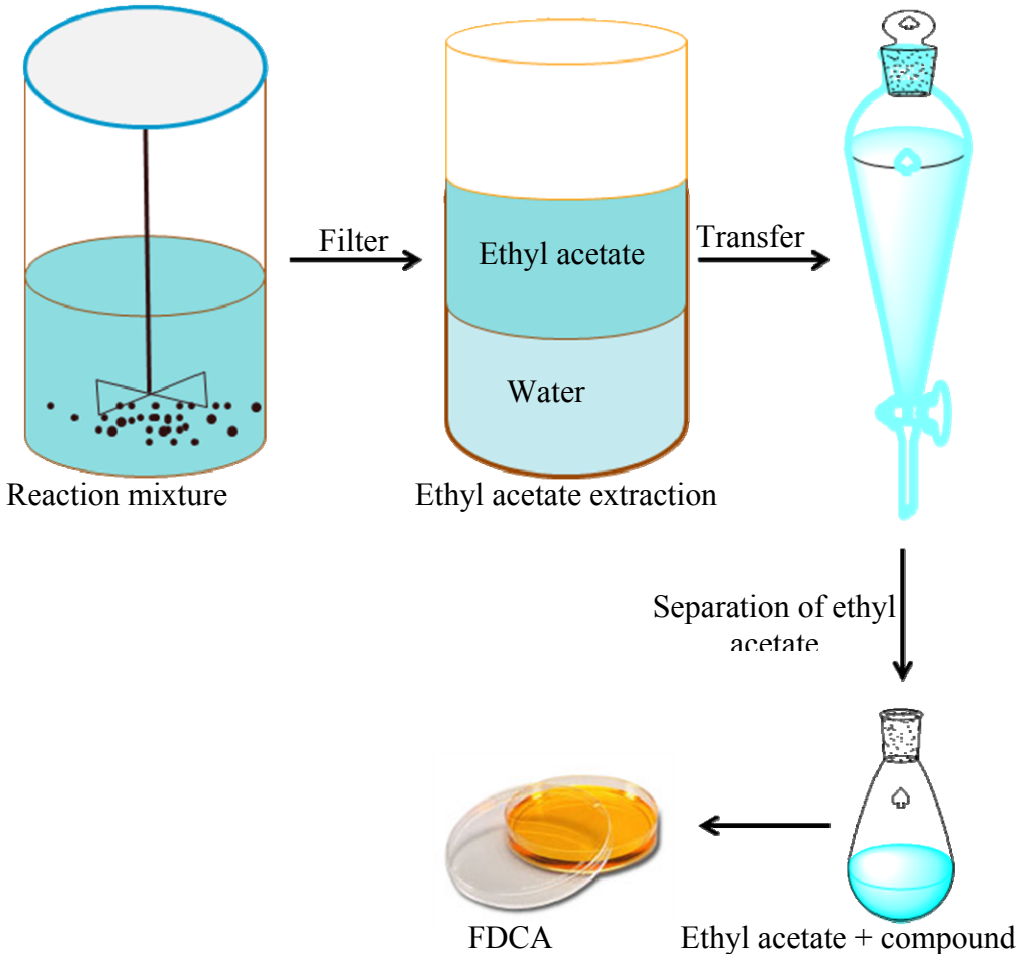

Fig. 5.12. Isolation of FDCA from the reaction mixture.

5.3.2.1.10. Product Isolation

At the end of the reaction, the catalyst was separated by centrifugation. The reaction mixture was acidified with 6 N HCl (pH ~ 2). It was then extracted with ethyl acetate. Water and ethyl acetate layers were separated using a separating funnel. The organic layer was evaporated using a rota-vapor. Brown coloured solid was recovered along with a minute impurity (Fig. 5.12). At optimum conditions, the isolated yield of FDCA was ~75%. The purity of the product was confirmed by TLC, NMR spectroscopy (^{1}H and ^{13}C), mass spectroscopy and elemental analysis (C, H &N).

5.3.2.2. Characterization of the Product

5.3.2.2.1. Thin Layer Chromatography

Thin layer chromatography (TLC) was performed on a E-Merck pre-coated 60 F_{254} plates. The isolated FDCA was dissolved in methanol and spotted on a TLC plate. Similarly, standard FDCA and HMF were also spotted on the same TLC plate. The TLC plate was run with a solvent composition of dichloromethane, methanol and acetic acid in a volume ratio of 6: 2: 0.5. Then, the spots were rendered visible by exposing to UV light (254 nm; Fig. 5.13). It is observed that acetic acid plays an important role in the separation of these spots due to its influence on the polarity of the medium [21].

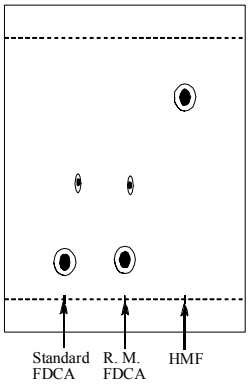

Fig. 5.13. TLC of isolated FDCA.

5.3.2.2.2. ^{1}H & ^{13}C NMR

Nuclear magnetic resonance spectroscopy is the primary characterization tool to get the structural and functional information of organic compounds. The evidence for the successful formation of FDCA and its purity was confirmed primarily from the liquid ^{1}H and ^{13}C nuclear magnetic resonance (NMR) spectral data. Further support

was obtained from the mass spectra and elemental analysis. To get a clear picture about the results obtained from spectral analysis of FDCA, it was compared with the spectral values of computed from the chemdraw software. The DEPT (distortionless enhancement by polarization transfer) technique was used to make an exact assignment to primary, secondary and tertiary carbon atoms. In a DEPT experiment, a sequence of pulses with various delay times were used to create the DEPT spectra where -CH_3 and CH peaks appear as normal and -CH_2- peaks appear inverted. Usually, quaternary carbon is not seen in the spectrum. This way the number of protons attached to carbon can usually be determined. As a general criterion in the DEPT spectrum, the peaks for the carbon atom having an odd number hydrogen atoms normally appear in a positive phase and the peak for the carbon atom having an even number of hydrogen atoms appear with a negative phase. The ^{1}H, ^{13}C and ^{13}C DEPT spectra are shown in Figs. 5.14, 5.15 and 5.16, respectively [20].

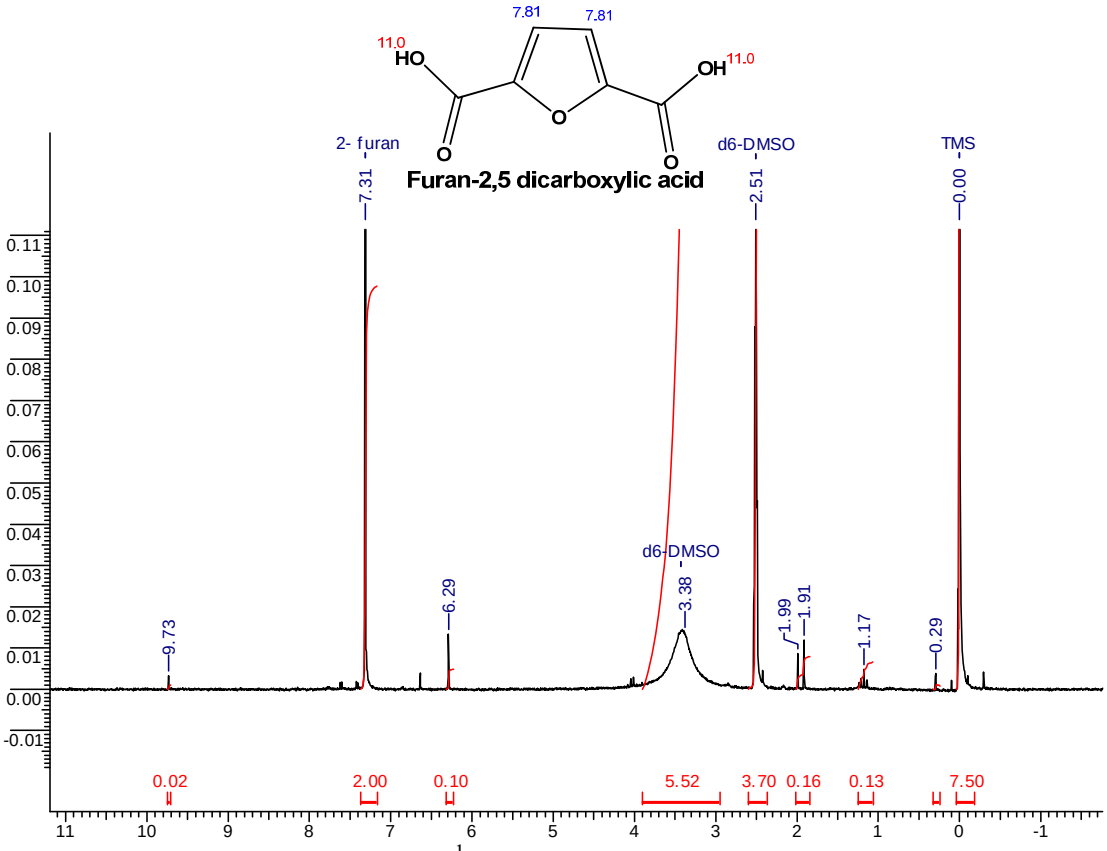

Fig. 5.14. ^{1}H NMR spectrum of FDCA.

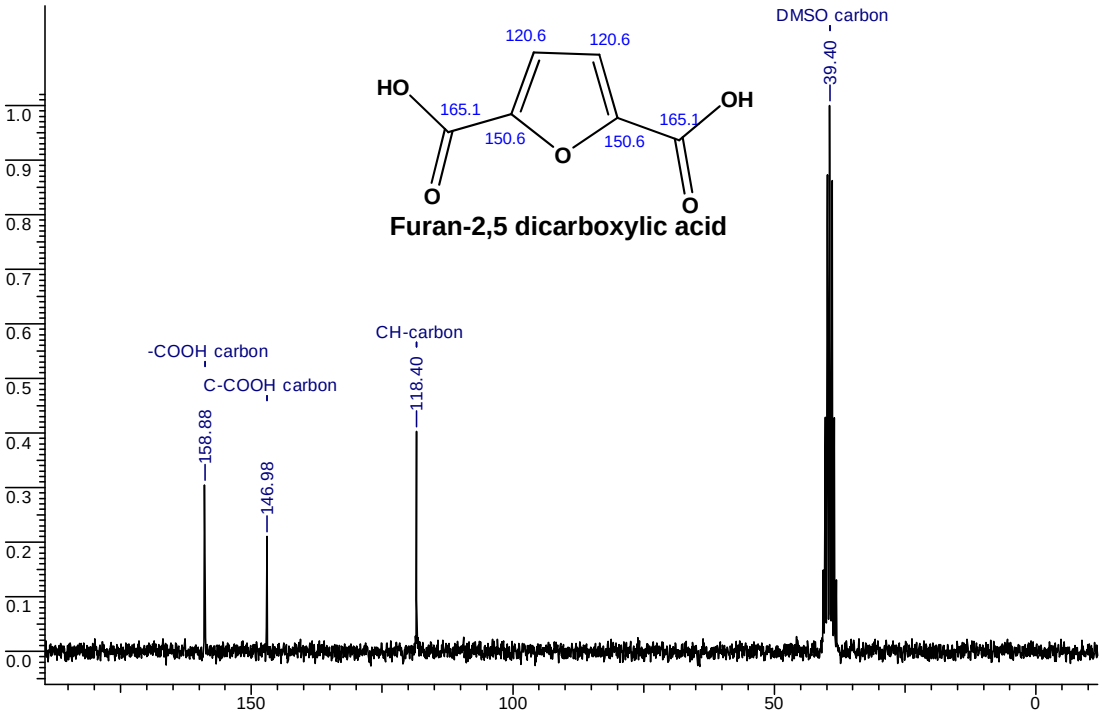

Fig. 5.15. ^{13}C NMR spectrum of FDCA.

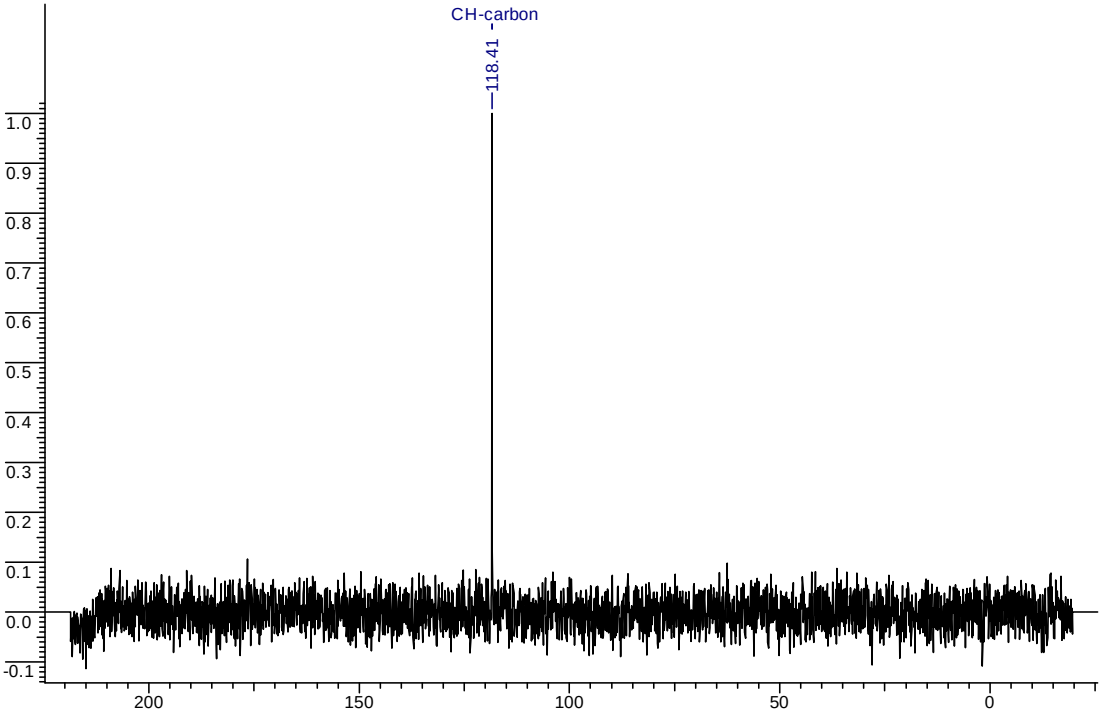

Fig. 5.16. ^{13}C DEPT NMR spectrum of FDCA.

5.3.2.2.3. Mass spectrum and Elemental Analysis

The peaks at M/Z of 157 [M+1] and 179 [M+Na] in the LC-MS profile confirmed the formation of FDCA. The elemental analyses were done with an EA1108 CHN/S Elemental Analyzer (Carlo Erba Instrument) for establishing the presence and exact fraction of elements in the synthesized materials. The percentage C and H contents (Carlo Erba EA1108 CHN/S Elemental Analyzer) were estimated to be 46.53 and 2.6, respectively. These values agree well with the theoretical and reported values (46.16% for C and 2.59% for H) for a pure FDCA compound [22].

A tentative mechanism for the oxidation of HMF over supported Pt catalysts is shown in Fig. 5.17.

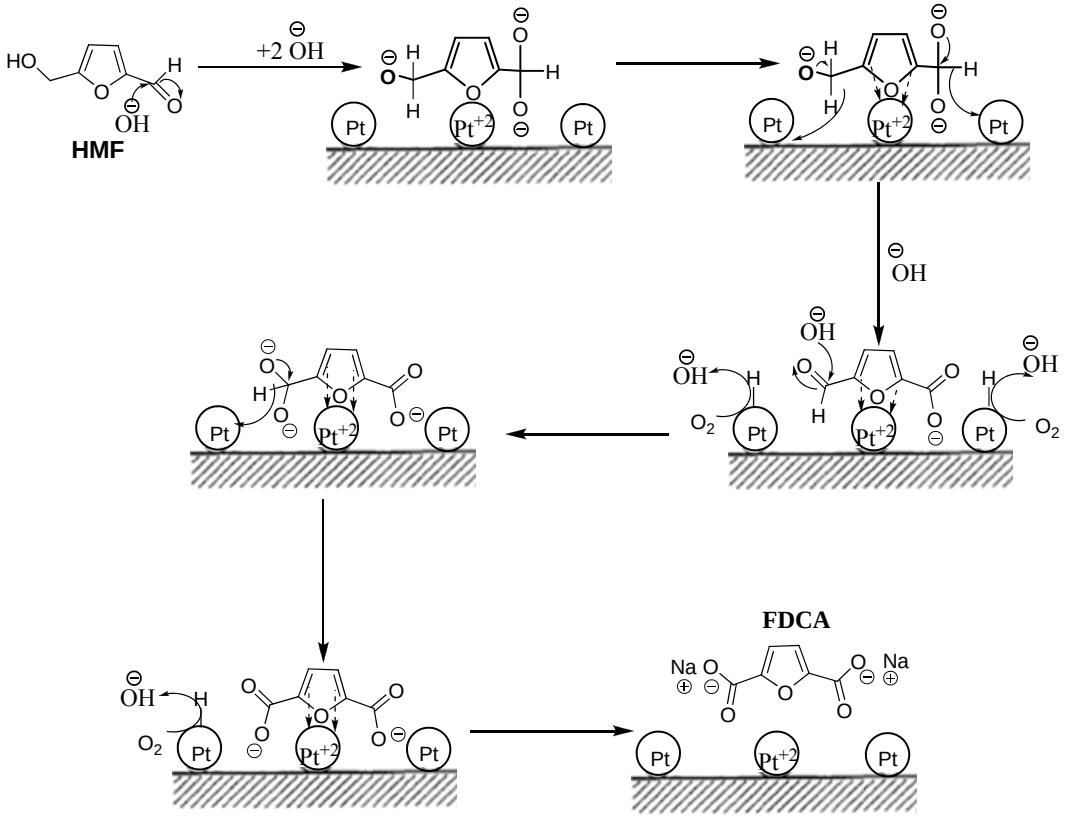

Fig. 5.17. Tentative reaction mechanism for the oxidation of HMF.

5.3.2.3. Oxidation of Furfural

The oxidation reaction of furfural was conducted taking 0.1142 g of furfural, 0.0631 g of Na_2CO_3, 30 g of water and 0.154 g of Pt(3.5 wt%)/γ-Al_2O_3 catalyst. The pH of the reaction mixture was maintained at 11.5. The reactor was purged with oxygen for three times and then, it was closed. The temperature was raised to 75°C and the reaction was conducted for 12 h. Then, the temperature was increased to

140°C and the reaction was continued for another 36 h. The results are represented in Fig. 5.18.

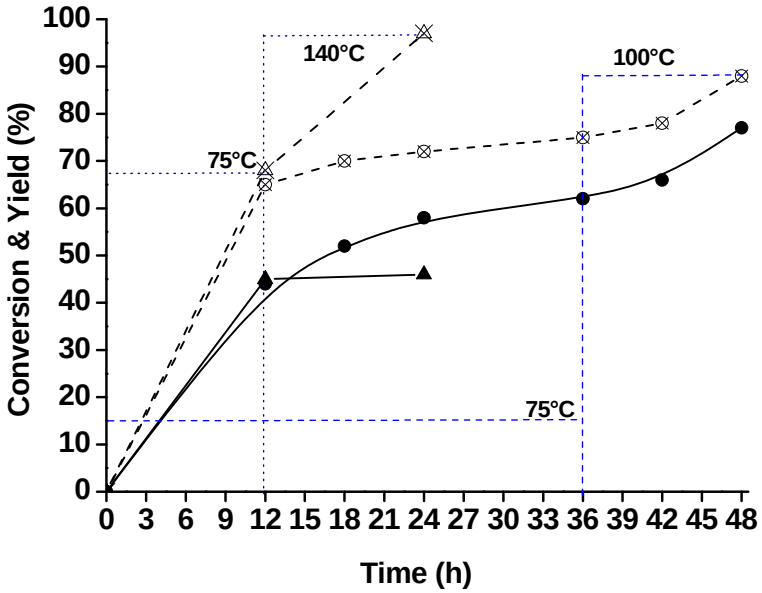

Fig. 5.18. Oxidation of furfural to furoic acid. *Reaction conditions:* Furfural (0.1142 g), water (30 g), catalyst (Pt (3.5 wt%)/γ-Al_2O_3 = 0.15 g), O_2 pressure (1 bar @ RT), two-stage reaction (75°C for 12 h and then at 140°C for another 36 h) and Na_2CO_3 (0.0631 g; 0.5 equivalent of furfural).

As seen from Fig. 5.18, furfural got converted even in the absence of a catalyst. However, furoic acid yield was low. Most of furfural got thermally degraded. In the presence of a catalyst, furfural got selectively oxidized to furoic acid. At the end of 48 hr (in a two stage reaction), furoic acid yield of about 78% was obtained over Pt(3.5 wt%)/γ-Al_2O_3 catalyst. Conversion of furan in the presence catalyst was about 90%.

5.3.3. Characterization of Spent Catalysts

The spent catalysts were characterized by X-Ray powder diffraction (XRD), transmission electron microscopy (TEM), X-Ray photoelectron spectroscopy (XPS), and ICP-OES techniques.

5.3.3.1. X-Ray Powder Diffraction

The fresh catalyst sample (Pt(3.5 wt%)/γ-Al_2O_3) showed characteristic Pt metal peaks at 2θ = 39.7, 46.1, 67.4 and 81.3° which could be assigned to (111), (200), (220) and (311) planes, respectively (Fig. 5.19, trace B) [23]. In the case of a spent catalyst, additional peaks at 18.0, 28.1, 49.0, 64.8 and 71.7° were observed (Fig.

5.19, trace C). While the origin of these peaks is not certain, they have completely disappeared upon activating the catalyst in H_2 atmosphere at 400°C for 2 h (Fig. 5.19, trace D). The catalyst regained its activity and gave FDCA yield similar to that of a fresh catalyst (recyclability experiment). Again upon reuse, the additional peaks have reappeared (Fig. 5.19, trace E). Formation of this additional crystalline phase on the catalyst surface is the cause for catalyst deactivation. It may be noted that the average crystallite size of Pt metal did not change even after its use in catalytic oxidation reactions. Hence, accumulation of organic matter blocking the active sites is the possible cause for catalyst deactivation.

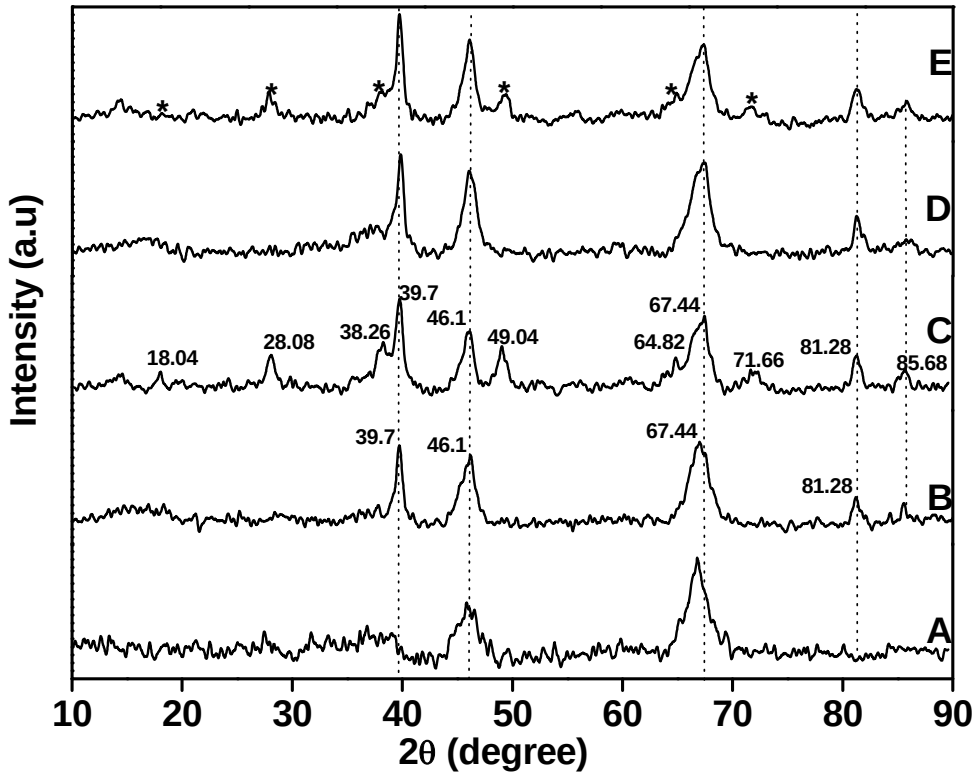

Fig. 5.19. XRD pattern of (A) γ-Al_2O_3, (B) fresh Pt (3.5 wt%)/γ-Al_2O_3, (C) spent Pt/γ-Al_2O_3, (D) regenerated Pt/γ-Al_2O_3 and (E) catalyst after 2nd reuse.

5.3.3.2. Transmission Electron Microscopy

Figs. 5.20, 5.21 and 5.22 show the TEM photographs and metal particle size distributions of the spent catalysts of Pt/γ-Al_2O_3, Pt/AC and Au/γ-Al_2O_3, respectively. The particle sizes of the spent catalysts were found to be 15.0, 10.8 and 13.2 nm, respectively. Sintering of metal particle was not observed during the oxidation reactions (compare Figs. 5.20 - 5.22 with Figs. 5.3 - 5.3). Hence, sintering is not the cause for catalyst deactivation.

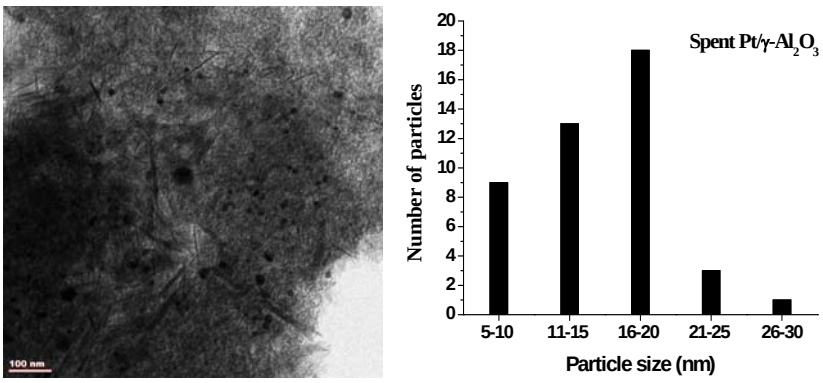

Fig. 5.20. TEM image of spent Pt/γ-Al_2O_3 catalyst and metal particle size distribution.

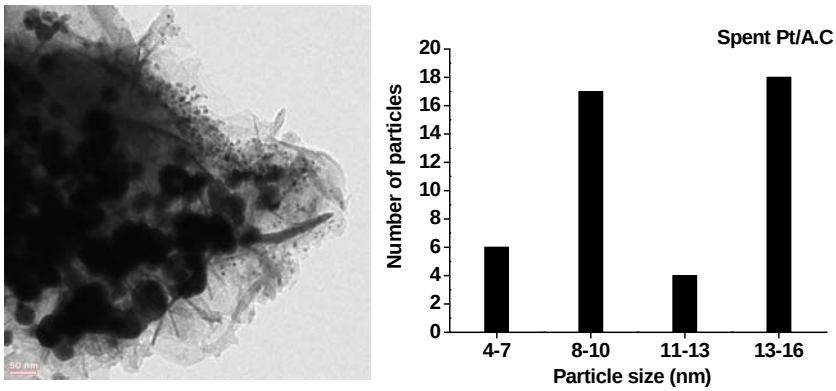

Fig. 5.21. TEM image of spent Pt/AC catalyst and metal particle size distribution.

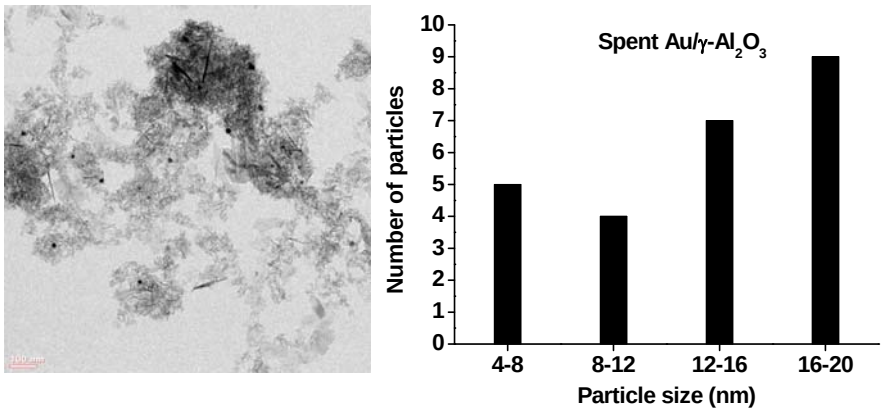

Fig. 5.22. TEM image of fresh spent Au/γ-Al_2O_3 and metal particle size distribution.

5.3.3.3. X-Ray Photoelectron Spectroscopy

XPS was used to determine the oxidation state of the catalysts before and after its use in the oxidation of HMF. Fig. 5.23 presents XPS spectrum of the Pt/AC in the Pt 4f region. The spectra show the doublets containing a low energy band (Pt $4f_{7/2}$) and a high energy band (Pt $4f_{5/2}$). For fresh and spend the catalysts the Pt 4f signal consisted of three pairs of Pt peaks which correspond to Pt^0, Pt^{2+} and Pt^{4+}. The analysis of the Pt 4f peak showed the presence of three different states of Pt with binding energy values being 71.2, 72.6 and 74.4 eV for Pt^0, Pt^{2+} and Pt^{4+}, respectively

[24-26]. The higher the metallic platinum (Pt^0), higher would be the activity of the catalyst. Fresh catalyst contained a higher concentration of Pt^0 compared to the spent catalyst (Fig. 5.23B). This was the reasons for the lower activity of the spent catalysts. Attempts to perform such experiments on Pt(3.5 wt%)/γ-Al_2O_3 were not successful as the peaks of Pt and Al overlapped and no meaningful information was derived.

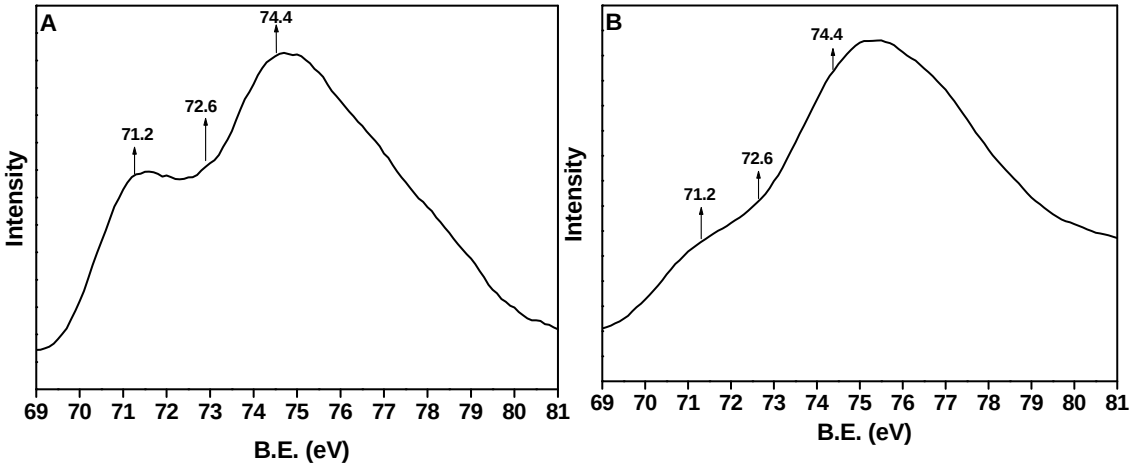

Fig. 5.23. XPS of Pt/AC catalysts: (A) fresh and (B) spent catalysts.

5.3.3.4. Inductively Coupled Plasma-Optical Emission Spectroscopy

The platinum content in fresh and spent Pt(3.5 wt%)/γ-Al_2O_3 catalyst was estimated using the ICP-OES technique. The Pt concentrations were found to be 37 and 33 ppm, respectively. In other words, about 4 ppm of Pt got leached out during the oxidation reactions. However, it was demonstrated (see section 5.3.2.1.9) that the leached Pt was not active in the oxidation of HMF. Only the supported Pt is the active species.

By and large, all these catalyst characterization techniques reveal that the loss in activity upon reuse is due to the following reasons: (1) partial loss in metal content, (2) change in the oxidation state of metal and (3) blocking of active sites by organic matter. Activation of the spent catalyst at high temperatures in hydrogen atmosphere, partly recovers its original catalytic activity.

5.4. Conclusions

The aerial oxidation of HMF and furfural over Pt (3.5 wt%) and Au (2 wt%) supported on γ-Al_2O_3, activated carbon, ZrO_2, TiO_2 and CeO_2 was investigated. The optimum reaction conditions for producing FDCA from HMF in high yields were determined. Pt supported on γ-Al_2O_3 was found to be the best catalyst. A two-stage raise in temperature and 1 bar of oxygen gave higher yields of furan carboxylic acids.

Metal dispersion was found to play an important role on catalytic activity. The catalyst loses its activity upon reuse. However, it can be regenerated by treatment in hydrogen atmosphere at high temperature. Detailed catalyst characterization studies revealed that (1) partial loss of Pt, (2) change in the oxidation state of Pt, and (3) blocking of the active sites by organic matter are the possible causes for catalyst deactivation. The yield (96%) of FDCA obtained in our reaction condition is similar to that reported by others [27-31].

5.5. References

[1] F.W. Lichtenthaler, *Carbohydr. Res*. **1998**, 313, 69.

[2] J. J. Bozell, G. R. Petersen, *Green Chem.* **2010**, 12, 539.

[3] B. Sillion, *High Perform. Poly.* **1999**, 11, 417.

[4] B. M. F. Kuster, *Starch* **1990**, 42, 314.

[5] J. Lewkowski, *Arkivoc* **2001**, 1, 17.

[6] G. W. Huber, J. N. Chheda, C. J. Barrett, J. A. Dumesic, *Science* **2005**, 308, 1446.

[7] A. Corma, S. Iborra, A. Velty, *Chem. Rev.* **2007**, 107, 2411.

[8] A. Gandini, M. N. Belgacem, *Prog. Poly. Sci.* **1997**, 22, 1203.

[9] X. Tong, Y. Ma, Y. Li, *Appl. Catal. A: General* **2010**, 385, 1.

[10] C. Moreaua, M. N. Belgacemb, A. Gandini, *Top. Catal.* **2004**, 27, 11.

[11] K. M. Rapp, *EP 0,230,250* **1988**.

[12] W. F. Hoelderich, F. Kollmer, *Pure Appl. Chem.* **2000**, 72, 1273.

[13] M. Besson, P. Gallezot, *Catal. Today* **2000**, 57, 127.

[14] J. H. J. Kluytmans, A. P. Markusse, B. F. M. Kuster, G. B. Marin, J. C. Schouten, *Catal. Today* **2000**, 57, 143.

[15] T. Mallat, A. Baiker, *Catal. Today* **1994**, 19, 247.

[16] Y. I. Matatov-Meytal, M. Sheintuch, *Ind. Eng. Chem. Res.* **1998**, 37, 309.

[17] M. A. Lilga, R. T. Hallen, M. Gray, *Top. Catal.* **2010**, 53, 1264.

[18] T. Mirura, H. Kakinuma, T. Kawano, H. Matsuhisa, *US 7,411,078* **2008**.

[19] A. N. Grace, K. Pandian, *J. Phys. Chem. Solids* **2007**, 68, 2278.

[20] B. Y. Xia, J. N. Wang, X. X. Wang, *J. Phys. Chem. C* **2009**, 113, 18115

[21] US Biological Technical Data, www.usbio.net/item/F9180

[22] W. Partenheimer, V. V. Grushin, *Adv. Synth. Catal.* **2001**, 343, 102.

[23] A. N. Grace, K. Pandian, *J. Phys. Chem. Solids* **2007**, 68, 2278.

[24] D. Briggs, M. P. Seah, *Practical Surface Analysis,* http// www.lasurface.com

[25] Z. L. Liu, X. Lin, J. Y. Lee, W. Zhang, M. Han, L. M. Gan, *Langmuir* **2002**, 18, 4054.

[26] F. Sen, G. Gökagac, J. Phys. Chem. C 2007**,** 111, 5715.

[27] M. L. Ribeiro, *Catal. Comm.* **2003**, 4, 83.

[28] M. Kroger, U. Prube, K. D. Vorlop, *Top. Catal.* **2000**, 13, 237.

[29] O. Casanova, S. Iborra, A. Corma, *ChemSusChem* **2009**, 2, 1138.

[30] Y. Y. Gorbanev, S. K. Klitgaard, J. M. Woodley, C. H. Christensen, A. Risager, *ChemSusChem* **2009**, 2, 672.

[31] S. E. Davis, L. R. Houk, E. C. Tamargo, A. K. Datye, R. J. Davis, *Catal. Today* **2010**, doi:10.1016/j.cattod.2010.06.004.

CHAPTER-6
SUMMARY AND CONCLUSIONS

SUMMARY AND CONCLUSIONS

The conversion of biomass and biomass-derived compounds into fuels and chemicals is of contemporary importance in view of the issues associated with the use of fossil fuels. The fossil fuels which are used for the synthesis of chemicals will run out one day. Hence, there is an urgent need to look for alternative renewable feedstocks for chemicals and fuels production. However, the technologies based on these alternative feedstocks should be economically competitive and should have the advantage of sustainability by way of not polluting the environment by releasing greenhouse gases. In recently times, it is widely realized that biomass is an ideal renewable alternative feedstock. The lignocellulosic biomass is composed of cellulose, hemicellulose and lignin. While the former two are polymers of sugar molecules, lignin is made up of phenolic compounds. Catalytic conversion of cellulose and hemicellulose leads to a range of platform chemicals including monomeric sugars (glucose, mannose, galactose, xylose, arabinose etc.), sugar alcohols (sorbitol, mannitol, etc.), ethanol, butanol and furan-based compounds (furfural, 5-hydroxymethyl furfural (HMF), etc). Conventionally, the hydrolysis of cellulose, hemicellulose and bagasse is carried out using homogeneous (acid, base or enzyme) catalysts. While the acid/base catalyzed processes are efficient, they are corrosive and the processes involving these catalysts require a special kind of expensive material of construction. Moreover, the homogeneous catalyst-based processes produce significant amount of waste by-products and hard water. The enzyme catalysts are expensive and the reactions using them are very slow. Catalyst recovery and reuse are not possible with these homogeneous catalyst systems. All these disadvantages can be overcome by using solid acid catalysts. Quite often the solid catalysts can be recycled without any loss in activity and product selectivity. Hence, the processes based on solid catalysts are more sustainable and possibly less expensive. While there have been some reports on the hydrolysis of cellulose in the presence of solid catalysts. Similar such reports for hemicellulose and bagasse are not available. The present work probably fills this gap. Several solid acids (zeolites, metal oxides, heteropolyacid and clay) and supported Pt and Au metal catalysts have been screened for the conversion of biomass into value-

added chemicals. The catalysts were characterized by several physicochemical techniques. Reaction conditions were optimized. Structure-activity correlations were made. In general, the thesis was divided into six chapters.

Chapter 1 gave the general introduction of biomass and the various methods of its conversion to chemicals. It also described the scope and objectives of the present work.

Chapter 2 was on material and characterization methods. It provided the synthesis and source of procurement of various catalysts used in the present work. Characterization techniques including chemical analysis (ICP-OES and C, H & N microanalysis), X-Ray powder diffraction, N_2-physisorption, scanning electron and transmission electron microscopies and temperature-programmed desorption of ammonia were discussed.

Chapter 3 described the hydrolysis of hemicellulose over solid-acid catalysts. Several solid acid catalysts including zeolites [HY (Si/Al = 2.6), HUSY (Si/Al = 15), HUSY (Si/Al = 40), HMOR (Si/Al = 10), Hβ (Si/Al = 19), HZSM-5 (Si/Al = 11.5)], Al-incorporated mesoporous silica (Al-MCM-41 and Al-SBA-15), montmorillonite clay (K10), metal oxides (Nb_2O_5 and γ-Al_2O_3) and Cs-exchanged phosphotungstic acid (Cs-HPA), with varying structures and acidic properties were evaluated for the hydrolysis of isolated hemicellulose. Among all these, Hβ (Si/Al = 19) showed the highest catalytic activity and xylose + arabinose yield. HUSY (Si/Al = 15) and HMOR (Si/Al = 10) were found to be the second best catalysts. But the stability of HUSY (Si/Al = 15) in recycling studies was superior to the rest of the solid acid catalysts. Xylose and arabinose were the major products. However, formation of furfural (a product formed via dehydration of the above monomer sugars) was also detected. Experiments were conducted on two types of hemicelluloses: (1) softwood-derived (oat spelt) and (2) hardwood-derived (birch wood) hemicellulases. While the hardwood-derived hemicellulose is more symmetric, the softwood-derived hemicellulose is highly asymmetric. As expected, hydrolysis of the latter was faster than the former. An increase in reaction temperature shortened the reaction time. But prolonged reaction times resulted in loss of selectivity of arabinose + xylose. Detailed structure-activity correlations revealed that in addition to total acidity (strong acid sites), pore structure of the zeolites also contributes to the catalytic activity.

Chapter 4 described the hydrolysis of bagasse over HUSY (Si/Al = 15), Hβ (Si/Al = 19), HMOR (Si/Al =10) and K10 catalysts. At chosen reaction conditions, only the hemicellulose in bagasse got hydrolyzed to its constituent sugars. More severe conditions are needed for the hydrolysis of cellulose in bagasse. However, at those conditions, the C_5-sugars of hemicellulose are prone for degradation (Scheme 6.1). The objective of this chapter was to convert hemicellulose in bagasse and to optimize the reaction conditions. Among the zeolites and clay catalysts, Hβ (Si/Al = 19) gave highest yields of xylose + arabinose. But the stability of HUSY (Si/Al = 15) was found better. Formation of furfural was also detected (Scheme 6.1). An innovative method was developed where the selectivity for the formation of furfural, a value-added chemical could be considerably enhanced. In this novel method, an organic solvent like *p*-xylene, toluene or MIBK was added to the reaction medium. Furfural has higher solubility in the above organic solvents than in water. As soon as it was formed in water medium, it got into the organic layer and hence, was not available to the catalysts for further reaction or degradation. With this method the furfural yield was increased from 28 to 58%. A continuous loss in activity of HUSY was detected in the recycling experiments. Detailed characterization of the spent catalysts revealed that the Na and K ions in bagasse were responsible for zeolite deactivation. The protons of zeolite got exchanged with the alkali ions in bagasse and thereby a reduction in acidity and catalytic activity of the zeolite catalyst was detected.

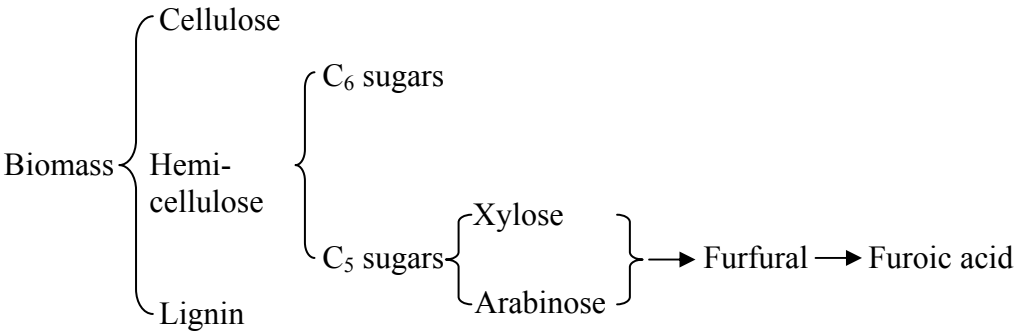

Scheme 6.1. Reaction scheme for the conversion of bagasse to chemicals.

Chapter 5 described the selective oxidation of bio-derived furans (furfural and HMF) with molecular oxygen / air over supported metal catalysts. The furan derivatives are valuable chemicals in the synthesis of polymers with unique properties and pharmaceuticals. The catalytic activities

of Pt (3.5 wt%) supported on γ-Al_2O_3, activated carbon, ZrO_2, TiO_2 and CeO_2 and Au (2 wt%) supported on γ-Al_2O_3 were investigated. Among these, Pt (3.5 wt%)/γ-Al_2O_3 showed superior catalytic performance. Optimization studies revealed that higher yield of carboxylic acid (FDCA from HMF) could be obtained when the reaction was conducted in two-stages first at 75°C and then at 140°C than in a single-stage at 140°C. The catalyst got deactivated during the reaction. Detailed characterization studies of fresh and spent catalysts revealed that the loss in catalytic activity is due to the following reasons: (1) partial loss in metal content, (2) change in the oxidation state of metal, (3) blocking of active sites by organic matter. Catalyst leaching experiments revealed that the oxidation reaction is actually occurring on the heterogeneous catalyst surface, the leached metal is inactive and not contributing to the reaction. The activity could be regained by treating the catalyst in a flow of hydrogen at 400°C. Air is equally efficient to molecular oxygen in oxidizing HMF.

Chapter 6 provided the overall summary and conclusions.

By and large, this study advances the knowledge on the conversion of biomass to value added chemicals. It describes an eco-friendly, sustainable methodology by means of using solid catalysts and greener oxidants (air) for the conversion of biomass. To the best of knowledge, this is the first report on the hydrolysis and conversion of hemicellulose over solid acid catalysts. Although, more research and process optimization is still needed, this study on bagasse conversion is a step forward towards successes. This work contributes to the area of green and sustainable chemistry, in general and biomass to chemicals conversion in particular.

THE FUTURE IS GREEN AND BIOMASS IS THE DREAM OF FUTURE TO USE!

List of Patents and Research Publications

1. Hydrolysis of hemicellulose by heterogeneous catalyst
   P. L. Dhepe and **R. Sahu**
   Patent Application No: 2597/DEL/2008.
2. A one-pot and single-step hydrolytic process for the conversion of lignocellulose into value-added chemicals
   P. L. Dhepe and **R. Sahu**
   Patent Application No: PCT/IN2010/000047.
3. A solid-acid-based process for the conversion of hemicellulose
   P. L. Dhepe and **R. Sahu**, Green Chemistry **2010**, 122, 153.
4. Photocatalytic mineralization of benzene over gold containing titania nanotubes: Role of adsorbed water and nanosize gold crystallites
   S.V. Awate, **R. Sahu**, M.D. Kadgaonkar, S. Malwadkar, R. Kumar and N. M. Gupta, Catalysis Today **2009**, 141, 144.